University of Alberta

Satellite Remote Sensing of Snow Cover and Snowmelt in the Arctic

By

Libo Wang ©

A thesis submitted to the Faculty of Graduate Studies and Research in partial fulfillment of the requirements for the degree of Doctor of Philosophy

Department of Earth and Atmospheric Sciences

Edmonton, Alberta

Fall, 2006

Library and Archives Canada

Published Heritage Branch

395 Wellington Street
Ottawa ON K1A 0N4
Canada

Bibliothèque et Archives Canada

Direction du Patrimoine de l'édition

395, rue Wellington
Ottawa ON K1A 0N4
Canada

Your file Votre référence
ISBN: 978-0-494-23124-1
Our file Notre référence
ISBN: 978-0-494-23124-1

NOTICE:
The author has granted a non-exclusive license allowing Library and Archives Canada to reproduce, publish, archive, preserve, conserve, communicate to the public by telecommunication or on the Internet, loan, distribute and sell theses worldwide, for commercial or non-commercial purposes, in microform, paper, electronic and/or any other formats.

The author retains copyright ownership and moral rights in this thesis. Neither the thesis nor substantial extracts from it may be printed or otherwise reproduced without the author's permission.

AVIS:
L'auteur a accordé une licence non exclusive permettant à la Bibliothèque et Archives Canada de reproduire, publier, archiver, sauvegarder, conserver, transmettre au public par télécommunication ou par l'Internet, prêter, distribuer et vendre des thèses partout dans le monde, à des fins commerciales ou autres, sur support microforme, papier, électronique et/ou autres formats.

L'auteur conserve la propriété du droit d'auteur et des droits moraux qui protège cette thèse. Ni la thèse ni des extraits substantiels de celle-ci ne doivent être imprimés ou autrement reproduits sans son autorisation.

In compliance with the Canadian Privacy Act some supporting forms may have been removed from this thesis.

While these forms may be included in the document page count, their removal does not represent any loss of content from the thesis.

Conformément à la loi canadienne sur la protection de la vie privée, quelques formulaires secondaires ont été enlevés de cette thèse.

Bien que ces formulaires aient inclus dans la pagination, il n'y aura aucun contenu manquant.

Canada

ABSTRACT

In this thesis, satellite remote sensing techniques have been used to detect snow cover and snowmelt in the Arctic from observations made by visible infrared, passive microwave, and active microwave sensors. An evaluation of the NOAA weekly snow cover dataset over the Canadian Arctic was conducted through comparisons with snow cover extent derived from the Advanced Very High Resolution Radiometer, Special Sensor Microwave/Imager, Landsat TM browse images, and surface snow depth observations. The evaluation revealed that the NOAA weekly dataset consistently overestimated snow cover extent during the spring melt period, with delays of up to 4 weeks in melt onset. The most likely causes for the delayed melt onset were frequent cloud cover in the spring melt period, and the low frequency of data coverage over higher latitudes.

The extent and duration of surface melt on the Queen Elizabeth Islands (QEI) ice caps in the Canadian high Arctic and on the Greenland ice sheet were detected from enhanced resolution QuikSCAT (QSCAT) scatterometer images. Based on the sharp changes in microwave backscatter on the appearance/disappearance of liquid water in snow, dates of melt onset and freeze-up across the ice caps and ice sheet were estimated using a dynamic threshold method. Annual melt duration and melt anomaly maps were produced for the 2000 – 2004 period. Over the 5-year period, the mean melt duration ranged from 30.9 to 42.6 days over the QEI, and from 14.3 to 20.5 days over Greenland. Inter-annual changes in the distribution of ice layer formation within the near surface snow and firn on the Greenland ice sheet were also investigated. There was a close

correspondence between melt season duration derived from QSCAT and from temperature measurements at field sites over both the QEI ice caps and the Greenland ice sheet. Systematic mapping of melt season duration on the Arctic ice masses may therefore be an effective and rapid way of detecting the spatial pattern of temperature variability during the summer melt season. In both cases, the relationships between the derived melt patterns and the variability in the local atmospheric circulation were discussed.

ACKNOWLEDGEMENTS

Many thanks to Dr. Martin Sharp for his excellent guidance throughout the completion of this thesis, and especially for his consistent encouragement and help with my English. He has been the first reader for almost all the drafts of my papers, thesis chapters, conference presentations, etc., and he has never complained about the rough English I write as a non-native English speaker. I am very grateful to Dr. Benoit Rivard for his help with remote sensing techniques and his constant encouragement to me during my study.

I would like to thank University of Alberta Department of Earth and Atmospheric Sciences, University of Alberta Institute for Geophysical Research, the Meteorological Service of Canada's CRYSYS program and the Canadian Foundation for Climate and Atmospheric Sciences via the Polar Climate Stability Network for funding my research.

Thanks to Dr. Luke Copland, who shared the office with me during the first 2 years of my abroad graduate career, for helping me get used to the environment of study, and for answering my numerous questions either about some words related to research or anything I didn't hear of before I came to Canada. Thanks also go to every member in Dr. Martin Sharp's research group for their interest and help to my research.

Thanks to my parents and all my sisters and brothers for always supporting me to pursue a higher education. Thanks to my mother for taking care of my daughter both in Edmonton and in China. Finally, I would like to thank my husband, Dr. Shunli Zhang, for coming to Edmonton to join me and for his support and help through my Ph.D. study.

Table of Contents

CHAPTER 1. INTRODUCTION....1

1.1. THESIS GOAL AND OBJECTIVES....1

1.2. BACKGROUND....1

1.3. EVALUATION OF THE NOAA WEEKLY SNOW COVER DATASET OVER NORTHERN CANADA....4

1.4. MICROWAVE REMOTE SENSING OF SNOWMELT OVER POLAR ICE CAPS AND ICE SHEETS....5

1.4.1. Snowmelt over the QEI ice caps....8

1.4.2. Snowmelt and ice layer formation over the Greenland ice sheet....9

1.5. THESIS OUTLINE....11

1.6. REFERENCES....12

CHAPTER 2. EVALUATION OF SPRING SNOW COVERED AREA DEPLETION IN THE CANADIAN ARCTIC FROM NOAA SNOW CHARTS....23

2.1. INTRODUCTION....23

2.2. STUDY AREA....25

2.3. DATA AND METHODS....25

2.3.1. NOAA weekly snow cover dataset....25

2.3.2. AVHRR-derived snow cover extent....26

2.3.3. SSM/I-derived snow cover extent....27

2.3.4. Processing of TM images....29

2.4. RESULTS....30

2.4.1. Comparison between NOAA, AVHRR, and SSM/I....30

2.4.2. Comparison between NOAA, AVHRR, and TM....30

2.4.3. Ground observations....31

2.5. DISCUSSION....31

2.6. CONCLUSIONS....34

2.7. REFERENCES....35

2.8. TABLES....43

2.9. FIGURES.....44
CHAPTER 3. MELT SEASON DURATION ON CANADIAN ARCTIC ICE CAPS, 2000-2004.....52
3.1. INTRUDUCTION.....52
3.2. METHODS.....52
3.2.1. Data.....52
3.2.2. Melt threshold and melt detection.....53
3.3. RESULTS AND DISCUSSION.....55
3.3.1. Melt climatology.....55
3.3.2. Melt anomalies.....55
3.4. SUMMARY AND CONCLUSIONS.....57
3.5. REFERENCES.....58
3.6. TABLES.....60
3.7. FIGURES.....61
CHAPTER 4. MELT SEASON DURATION AND ICE LAYER FORMATION ON THE GREENLAND ICE SHEET, 2000-2004.....65
4.1. INTRODUCTION.....65
4.2. QSCAT ENHANCED RESOLUTION IMAGERY AND IN SITU DATA.....66
4.3. SURFACE FACIES OR ZONES ON THE GREENLAND ICE SHEET.....68
4.4. MELT DETECTION AND RESULTS.....70
4.4.1. QSCAT melt signature.....70
4.4.2. Melt detection.....71
4.4.3. Melt results, 2000 – 2004.....73
4.4.3.1. Melt extent and duration.....73
4.4.3.2. Seasonal melt cycle.....75
4.4.3.3. Regional differences in surface melt.....75
4.4.4. Influence of atmospheric circulation on surface melt patterns.....77
4.5. INTER-ANNUAL CHANGES IN THE DISTRIBUTION OF ICE LAYER FORMATION.....79
4.5.1. Ice layer formation: signature and detection.....79
4.5.2. Changes in the distribution of ice layer formation, 2000 – 2004.....81

4.6. SUMMARY AND CONCLUSIONS.....82
4.7. REFERENCES.....83
4.8. TABLES.....88
4.9. FIGURES.....91
CHAPTER 5. SUMMARY AND CONCLUSIONS.....108
5.1. SUMMARY.....108
5.2. DISCUSSION AND IMPLICATIONS.....111
5.3. FUTURE WORK.....114
5.4. REFERENCES.....117
APPENDIX A.....123

List of Tables

Table 2.1. Percent snow cover calculated from TM images (column 3) from 1997. The dates of the TM images are shown in brackets. The differences between the percent snow cover extracted from the AVHRR and NOAA datasets and those from the TM images are shown in columns 4 and 5.....**43**

Table 3.1. Average melt duration over the whole QEI and each major ice cap, for the summers of 2000-2004. The mean elevation of each ice cap and the correlation between melt duration and July 500 hPa height are also shown.....**60**

Table 4.1. Mean melt extent (%) and mean melt duration (days) over the Greenland ice sheet as a whole during 2000 –2004.....**88**

Table 4.2. Mean melt season duration (days) in the nine regions over the ice sheet. The 5-year mean duration, standard deviation, and the mean elevation (m a.s.l.) in each region are also included.....**89**

Table 4.3. Correlation coefficients of monthly mean melt duration and geopotential height at 700 hPa, 500 hPa, and 300 hPa pressure levels in the nine regions over the ice sheet. The last column is the correlation coefficients of mean daily melt extent and mean daily 300 hPa geopotential height during 2000 – 2004.....**90**

List of Figures

Figure 2.1. Study area (white outline) overlaid on 1000 m resolution Radarsat mosaic downloaded from http://geogratis.cgdi.gc.ca. White dots are snow depth observation stations and black contour stands for forest cover>0 derived from IGBP land cover lassification.....44

Figure 2.2. Weekly snow cover maps derived from AVHRR (a) and NOAA (b) for weeks 23-25 in the spring of 1997. The 9 gray boxes (one at week 23, two at week 24, and 6 at week 25) indicate the locations of the TM images available for each week.....45

Figure 2.3. Two examples of classified Landsat 5 TM browse images. Snow is shown in white. (a) June 11, 1997, 33.1% snow covered; (b) June 15, 1997, 64% snow covered.....46

Figure 2.4. Comparison of weekly snow coverage, in percent of fractional snow covered pixels in the study area from AVHRR (triangle), SSM/I (cross), and NOAA (square) for the six years included in the evaluation. The horizontal axis displays week (e.g. 9811 for year 1998 and week 11).....47

Figure 2.5. Daily mean air temperature (a) and snow depth (b) in May and June of 1997.....48

Figure 2.6. Results of re-mapping 5 km AVHRR-derived snow cover to the 25 km NOAA EASE-grid applying 50%, 30%, and 10% thresholds respectively.....49

Figure 2.7. Daily snow depth network over North America. Station density decreases rapidly north of about 55° N.....50

Figure 2.8. Mean annual cycle of total cloud cover in percent for 3 stations in the study area. Data are from the Canadian Climate Normals for the 1971-2000 period.....51

Figure 3.1. Time series of QSCAT σ^0 and surface air temperature during 2001-2002 for 2 locations on POW Icefield, (a) 78.68° N, 74.96° W, 400m a.s.l., (b) 78.61 N°,78.63° W, 1300 m a.s.l.....61

Figure 3.2. Melt climatology for the QEI for the period 2000-2004, (a) melt onset dates; (b) freeze-up dates; (c) the number of melt days. Areas shown as white in (a) and (b) experienced no melt in at least one year during the 5-year period. Numbers in (b) indicate major ice caps:1~Devon; 2~Manson; 3~Sydkap; 4~POW; 5~Agassiz; 6~Axel Heiberg Island; 7~Northern Ellesmere Island.....62

Figure 3.3. Anomalies in melt duration relative to the 2000-2004 climatology for the summers of (a) 2001 and (b) 2002.....63

Figure 3.4. Variations of melt duration with elevation on POW Icefield in the summers of 2000-2004.....64

Figure 4.1. Average of mean QSCAT backscatter in November over 2000 – 2004. Dashed black contours are elevations, and the locations of nine AWS as well as one cell in the northeast (NE) of the Greenland are labelled.....91

Figure 4.2. Time series of QSCAT σ^0 and air temperature (11:00~20:00) at the (a) Crawford Point1 (CP1), (b) Swiss Camp (ETH), and (c) JAR2 stations on the western flank of the Greenland ice sheet (see locations in Figure 1) during 2000-2003.....92

Figure 4.3. Melt extent and duration (number of days) in 2000 (a), 2001 (b), 2002 (c), 2003 (d), 2004 (e), and the 5-year mean (f). Regions experienced no melt in a particular year are in white.....93

Figure 4.4. Melt duration anomalies in 2000 (a), 2001 (b), 2002 (c), 2003 (d), and 2004 (e), with dashed contours representing regions that experienced no melt in that year.....94

Figure 4.5. Frequency distribution of average melt duration over the Greenland ice sheet, 2000-2004.....95

Figure 4.6. Average melt duration, distribution, and occurrence within each elevation bands. The melt distribution was calculated as the percentage of melt pixels within each elevation band in relation to the total number of melt pixels over the Greenland ice sheet (68181). The melt occurrence was calculated as the percentage of the melt pixels in relation to the total number of pixels within an elevation band.....96

Figure 4.7. Daily melt extent from May to October for the 2000 – 2004 period.....97

Figure 4.8. Melt extent and occurrence (%) from (a) May, (b) June, (c) July, (d) August, (e) September, and (f) October. White represents areas that experienced no melt in that month.....98

Figure 4.9. Nine topographically defined regions on the Greenland ice sheet. The red contours are elevations (m a.s.l.), and the blue lines define the nine regions.....99

Figure 4.10. The percentage of mean daily melt extent in relation to the total area of the region (solid) and the standard deviation (SD, dash) of the daily melt extent over 2000 – 2004. The x axis is day of the year.....100

Figure 4.11. Daily melt extent during 2000 –2004 for each region over the Greenland ice sheet.....101

Figure 4.12. Daily mean geopotential height (m) at 300 hPa on June 25 (a); June 26 (b); June 27 (c); June 28(d); June 29 (e); and June 30 (f) of 2002 (day 176-181).....102

Figure 4.13. 700 hPa isotachs maps on June 26 (a), June 27 (b), June 29 (c), and June 30 (d) of 2002.....103

Figure 4.14. Time series of QSCAT σ^0 at Tunu-N and one cell in the southeastern (SE) corner of Greenland (see locations in Figure 4.1) during 2000-2004.....104

Figure 4.15. Average melt onset dates (a) and melt freeze-up dates (b) during the 2000 –2004 period.....105

Figure 4.16. Changes in the biweekly averaged backscatter between the freeze-up periods in the current and the previous fall in 2000 (a), 2001 (b), 2002 (c), 2003 (d), and 2004 (e). The solid white and black contours represent the upper limits of melt for the current and the previous summers respectively.....106

Figure 3.A.1. Mean and standard deviation of winter QSCAT σ^0 (1999-2003) along a transect over the Devon Ice Cap.....123

Figure 3.A.2. Melt anomalies (onset, freeze-up, and duration) relative to the climatology for 2000-2004 for the Queen Elizabeth Islands ice caps in the summers of 2000-2003: (a) 2000; (b) 2001; (c) 2002; (d) 2003.....124

CHAPTER 1.

INTRODUCTION

1.1. Thesis goal and objectives

The overall goal of this thesis is to retrieve measurements of cryospheric parameters sensitive to climate change in the Arctic from data collected by space-borne sensors. Based on the availability of satellite and field data, the following specific objectives were established to achieve this goal:

(1) to evaluate the National Oceanic and Atmospheric Administration (NOAA) weekly snow cover dataset during the spring melt period for Northern Canada and to investigate the nature and causes of the main differences between the NOAA dataset and other data sources;

(2) to detect the extent and duration of snowmelt on ice caps in the Queen Elizabeth Islands (QEI) in the Canadian Arctic, and to analyze the correlation between the detected melt pattern and the atmospheric circulation;

(3) to detect the extent and duration of snowmelt over the Greenland ice sheet and to analyze the spatial and temporal characteristics of the melt pattern and its relationship with the atmospheric circulation; and

(4) to detect inter-annual changes in the distribution of ice layer formation within the surface snow and firn on the Greenland ice sheet.

1.2. Background

Amplified warming is evident in the Arctic during the 20th century from both historical and paleoclimate data [Overpeck et al., 1997; Jones et al., 1999; Johannessen et al., 2004]. This amplified warming is most likely due to several positive feedbacks, including melting of snow and ice that decreases the surface albedo, shrinking of sea ice that increases sensible heat flux to the atmosphere, the stability of the lower troposphere that traps temperature anomalies near the surface, cloud dynamics that magnify change, and increased moisture availability over the extratropical oceans that increases dynamical heat transports to the Polar regions [Chapman and Walsh, 1993; Curry et al., 1996; Houghton et al., 2001; Solomon 2006]. There is still debate about whether the observed

warming is within the natural variability of the climate system or a response to enhanced anthropogenic forcing by atmosphere greenhouse gases [e.g. Polyakov and Johnson, 2000; Polyakov et al., 2002; Johannessen et al., 2004]. General circulation model (GCM) simulations of climate response to anthropogenic forcing predict that the warming trend will continue and likely increase in the 21st Century, and that the warming will have the largest impact on the arctic region [Houghton et al., 2001; Räisänen, 2001]. Recent studies indicate that changes similar to those predicted by GCM simulations have already occurred in the northern high latitudes [Serreze et al., 2000; Overland et al., 2004]. Changes in the Arctic, in turn, influence the global climate system through impacts on river runoff, thermohaline circulation, atmospheric circulation, and atmospheric greenhouse gas concentrations [Houghton et al., 2001; ACIA, 2005].

However, there are large discrepancies between model simulations. Furthermore the differences in the amplitude of warming simulated by different models are maximized at high latitudes. In addition, the simulated warming tends to be largest in autumn over the Arctic Ocean, whereas observed warming appears to be largest in winter and spring over land [Serreze et al., 2000; Moritz et al., 2002]. Studies indicate that this disagreement most likely stems from differences in model parameterizations of surface albedo, cloud processes, and other feedback mechanisms in the high latitudes, where few observations are available. A recent study [Dethloff et al., 2006] indicates that a global atmosphere-ocean coupled GCM is very sensitive to the parameterization of the Arctic sea ice and snow albedo. An improved Arctic sea ice and snow albedo dataset changes the ice-albedo feedback and the radiative exchange between the atmosphere and the surface, which can then trigger changes in the mid- and high latitude climate by modulating the strength of the mid-latitude westerlies and storm tracks [Dethloff et al., 2006]. Improvements in our knowledge of Arctic snow and ice conditions can therefore advance our understanding of the global climate system and be important for projecting future climate change.

The existence of snow and ice on earth has important effects on the surface energy balance, influencing the planetary albedo, which then feeds back positively to surface temperature [Groisman et al., 1994a; Curry et al., 1995]. This is one reason why studies looking for early indications of global warming focus on the Arctic. The short-wave

incoming solar radiation absorbed by the surface can increase significantly due to small reductions in snow albedo, in particular, for a change from a dry (~0.85) to a melting snow (~0.65) surface. Wet snow absorbs as much as 3 times more incoming solar radiation than dry snow [Steffen, 1995]. The timing of snowmelt in northern Europe was found to be related to the winter Arctic Oscillation [Schaefer et al., 2004], and there is a significant link between the summer snow cover extent and the North Atlantic Oscillation in the following winter [Qian and Saunders, 2003; Saunders et al., 2003]. It is therefore very important to monitor the spatial and temporal variations in snow cover extent and the timing of spring snowmelt at high latitudes.

Melting of glaciers and ice sheets is a major contribution to global sea level rise [Church et al., 2001], but relatively long records of surface mass balance exist for only a small number of glaciers in the world [Dyurgerov, 2002], and there are still major uncertainties in estimates of the mass balance of the Greenland and Antarctic ice sheets [Cazenave and Nerem, 2004; Zwally et al., 2005]. Mass balance of a glacier or ice sheet primarily depends on mass gain through snowfall, and mass loss through meltwater runoff and iceberg calving. Usually it is not easy to directly measure the mass balance, but it is possible to detect changes in the mass input/output processes, such as surface snow accumulation and melting. One can then attempt to relate these changes to changing climatic conditions that will have an effect on the surface mass balance in the long run. Remote sensing of surface melt on the QEI ice caps and the Greenland ice sheet is thus one theme of this thesis.

Satellite remote sensing is a unique tool for change detection, providing spatially continuous data coverage globally with relative consistency. This is especially useful in the Arctic region, where ground observations are sparse and expensive. Since the launch of the first satellite in the early 1960s, various satellite data have been acquired at a global scale. To maximize the scientific potential of these satellite data, unique programs have been designed to reprocess the existing datasets with careful calibration and with consistent projections, making them readily available for global change studies. Two such datasets are used in this research. The first is the AVHRR (Advanced Very High Resolution Radiometer) Polar Pathfinder 5 km EASE-Grid Composites [Fowler et al., 2002]. Based on observations made by the AVHRR sensors aboard a series of NOAA

satellites, the composites consist of twice-daily gridded and calibrated satellite five channel data and derived parameters for both poles from July 1981 through December 2000. In combination with other data sources, this dataset was used to evaluate the NOAA weekly snow cover charts during the spring melt period over northern Canada.

The second dataset is the enhanced resolution backscatter imagery from the Seawinds scatterometer on QuikSCAT (QSCAT) [Long and Hicks, 2005]. These data are available twice daily over the Arctic from July 1999 to present, spanning a period when record melt occurred on the Greenland ice sheet and the Arctic sea ice extent reached its minimum levels since 1978 [Serreze, 2003; Steffen et al., 2004; Steffen and Huff, 2005]. Assisted by near surface air temperature observations in the field, the annual extent and duration of surface melt over the Queen Elizabeth Islands (QEI) ice caps in the Canadian high Arctic and on the Greenland ice sheet were detected from time series of QSCAT data. In both cases, the relationship between the derived melt patterns and the atmospheric circulation was analyzed. An attempt was also made to detect inter-annual changes in the distribution of ice layer formation within the near surface snow and firn on the Greenland ice sheet.

1.3. Evaluation of the NOAA weekly snow cover dataset over northern Canada

The NOAA weekly snow cover dataset consists of digitized weekly charts of snow cover derived from visual interpretation of visible satellite imagery by trained analysts [Dewey and Heim, 1981]. It is the longest time series (1966-present) of spatially continuous snow cover data available for the Northern Hemisphere (NH). This dataset has been widely used to document regional and hemispheric variability in snow cover extent (SCE) [Brown, 2000; Dye, 2002; Easterling et al., 2000; Frei and Robinson, 1999; Iwasaki, 1991; Robinson et al., 1993]. Trends in continental SCE from the NOAA dataset were presented in the Intergovernmental Panel on Climate Change (IPCC) Third Assessment report [Houghton et al., 2001, p124]. Decreases in the spring SCE, as derived from the NOAA dataset, were found to be closely associated with a significant increase in spring surface air temperature over the NH landmass [Groisman et al., 1994a].

In the Canadian Arctic, however, major discrepancies were found between SCE estimates derived from in situ snow depth observations and those from the NOAA dataset

[Brown and Alt, 2001]. To date, the NOAA dataset has received only limited validation [Kukla and Robinson, 1981; Robinson and Kukla, 1988; Wiesnet et al., 1987], especially in the NH high latitudes. In fact, the NOAA product has never been evaluated for the Arctic regions, which are widely believed to be especially sensitive to anthropogenically forced climate change. This is mainly because ground observations in these regions are sparse, making validation of the product more difficult.

In this thesis, the NOAA dataset was evaluated for a study area on the Canadian Arctic mainland north of the tree line during the spring melt period. The evaluation focused on six spring periods from the 1981-2000 period with unusually low (1984, 1988, and 1998) or high (1985, 1995, and 1997) SCE. The spring period was selected because the snow line migration can be tracked over several weeks through the study region, this contrasts with the fall season, when the entire region becomes completely snow covered in a very short period. In addition, the spring is the period when the seasonal snow cover receives the maximum solar radiation and exerts the strongest feedbacks on the climate system [Groisman et al., 1994b]. For the purposes of validation, the NOAA dataset was compared to snow cover extent estimates derived from AVHRR, SSM/I, and Landsat 5 TM browse images, and surface snow observations. A number of variables, including cloud cover, lake ice, and fractional snow cover thresholds, were explored in an attempt to explain the differences observed between the various datasets.

1.5. Microwave remote sensing of snowmelt over polar ice caps and ice sheets

Satellite-borne microwave sensors are well suited to making frequent measurements of polar ice. With year-round, day-night, and all-weather imaging capability, they provide a unique perspective on spatial and temporal variability of surface properties, particularly the surface melt that occurs every summer. These measurements are particularly important in glacier and ice sheet environments where persistent clouds hamper data acquisition by visible sensors and where the polar night imposes a prolonged period of darkness. Passive microwave Scanning Multichannel Microwave Radiometer (SMMR) and Special Sensor Microwave Imager (SSM/I) data have been used to monitor annual snowmelt over the Greenland and the Antarctic ice sheets since 1979 [e.g. Zwally and Fiegles, 1994; Mote and Anderson, 1995; Abdalati and Steffen, 2001; Liu et al., 2006].

These datasets have proven to be very useful in examining the long-term variability of the annual snowmelt over the ice sheets. Due to the large footprints (25-50 km) of the data, however, it is impossible to use the passive microwave dataset to investigate melt processes on glaciers and ice caps other than the large ice sheets. Active microwave synthetic aperture radar (SAR) currently provides high spatial resolution (25 m) imagery data, and has been used to study the temporal and spatial evolution of snowmelt and snow diagenesis on both ice sheets and glaciers [Jezek et al., 1993; Smith et al., 1997; Partington, 1998; Ramage et al., 2000; Rau et al., 2000]. The major limitation to the use of SAR is that the ground swath is usually small (50-500 km), so SAR images generally cover small areas, requiring many scenes to provide complete coverage of large glaciers and ice caps/sheets. In addition, SAR images are typically collected at relatively large time intervals (several days to a week or more), resulting in reduced temporal resolution relative to the passive microwave datasets. Furthermore, the incidence angle of a SAR image is relatively small (less than 40°), making the backscatter more sensitive to surface topography [Jezek et al., 1993]. The incidence angle also varies across a SAR swath, and since the radar backscatter is a function of the incidence angle, this makes comparisons of backscatter within scenes problematic.

A scatterometer is a microwave radar system used to measure the scattering or reflective properties of surfaces and/or volumes [Ulaby et al., 1982]. Satellite-borne scatterometers, such as the Ku-band (~13.4 GHz) Seasat A scatterometer system (SASS), C-band (5.3 GHz) ERS-1 and ERS-2 scatterometers (EScat), Ku-band NASA scatterometer (NSCAT), and Ku-band SeaWinds scatterometer on QuikSCAT (QSCAT) were originally designed to measure the surface backscatter of the ocean in order to retrieve the near surface wind speed and direction [Naderi et al., 1991]. Over the last decade, however, scatterometers have been used to study various surface and subsurface characteristics of the Greenland and Antarctica ice sheets, and especially the snowmelt pattern during summer [e.g. Long and Drinkwater, 1994; Long and Drinkwater, 1999; Wismann 2000; Drinkwater et al., 2001; Nghiem et al., 2001; Steffen et al., 2004; Nghiem et al., 2005]. These studies all exploit the sensitivity of backscatter (σ^0) to surface roughness, snow density, grain size, snow layering and, in particular, liquid water content [Ulaby et al., 1981]. At the microwave frequencies of 5.3 GHz and 13.4 GHz,

volume scattering in the snow and surface scattering from the snow-air interface are the main contributors to radar backscattering from snow-covered surfaces. For dry snow surfaces, the dielectric contrast between snow and air is small, so volume scattering is dominant, surface scattering can be neglected, and snow layering and inhomogeneities inside the snowpack can be important contributors to the radar σ^0. Due to the high dielectric constant of water, a small amount of liquid water in snow causes a large dielectric contrast between the wet snow and air, which greatly reduces volume scattering and decreases radar σ^0. This is the basis of most algorithms used to detect the surface melt on ice sheets [e.g. Long and Drinkwater, 1994; Wismann 2000].

Data from the Ku-band SASS are available from July through early October of 1978, at both vertical (VV) and horizontal (HH) polarizations. This is the oldest available microwave radar dataset and it is very useful for change detection studies [e.g. Long and Drinkwater, 1999; Drinkwater et al., 2001]. SASS data were acquired at a nominal resolution of 50 km over a dual-sided 500 km swath, with a broad range of incidence angles (0°-70°). Two European Remote Sensing Satellites (ERS-1 and ERS-2) have been collecting C-band EScat data continuously since 1992. The σ^0 measurement is made at vertical polarization with a spatial resolution of 50 km over a single 500 km swath [ESA, 1992]. NSCAT was a follow-on mission to SASS. Like SASS, NSCAT only operated for a short period (September 1996 to June 1997) due to a spacecraft power system failure. NSCAT collected 25 km resolution σ^0 data at both VV and HH over two 600 km swaths. The measurement was made at 10° and 16°- 62° incidence angles at three azimuth angles [Naderi et al., 1991].

The SeaWinds scatterometer on QSCAT (Ku-band) was lunched in June 1999 and has been operating until present. Benefiting from a rotating pencil-beam antenna, this scatterometer provides a much wider, more continuous swath than previous instruments. The spatial resolution was improved to 6x25 km [Spencer et al., 2000]. A second SeaWinds scatterometer was lunched aboard the ADEOS-II spacecraft in December 2002, but was lost in October 2003. Unlike the previous scatterometers, which made σ^0 measurements over a broad range of incidence angles, QSCAT makes σ^0 measurements at two constant incidence angles: 46° at HH over a 1400 km swath, and 54.1° at VV over an 1800 km swath. The wide swath enables QSCAT to observe the polar region multiple

times each day. This allows the reconstruction of surface backscatter at finer spatial resolution using algorithms such as the Scatterometer Image Reconstruction (SIR) algorithm developed at Brigham Young University [Long et al., 1993; Long and Hicks, 2005]. Ascending and descending pass images produced with this algorithm are available daily for the Arctic since July 1999. QSCAT σ^0 measurements are reported in two forms: termed "eggs"and "slices" [Perry, 2001]. These differ in their spatial sizes and shapes. Egg-based SIR images have a nominal pixel resolution of 4.45 km with an estimated effective resolution of ~ 8-10 km. Slice-based SIR images have a nominal pixel resolution of 2.225 km with an estimated effective resolution of ~ 5 km [Long and Hicks, 2005].

Although enhanced resolution products are available from the other scatterometers, only QSCAT provides complete single day coverage of the polar region with relatively long time series. In addition, only the slice-based SIR QSCAT images have a spatial resolution sufficiently high for synoptic scale melt mapping of ice caps in the QEI. The enhanced resolution QSCAT scatterometer backscatter time series [Long and Hicks, 2005] were therefore used in this thesis to detect the extent and duration of surface melt over the QEI ice caps and the Greenland ice sheet.

1.4.1. Snowmelt over the QEI ice caps

Nearly 110,000 km^2 of ice exists on land in the QEI in the Canadian high Arctic [Koerner, 2002]. On decadal and century time scales, small glaciers and ice caps are affected more strongly by changes in climate because their response times are typically shorter than those of the large ice sheets [Oerlemans and Fortuin, 1992]. Thus it is important to assess the contribution of these ice masses to global sea level change, especially for the observed and projected amplified climate warming in the Arctic [Johannessen et al., 2004; Houghton, et al., 2001]. Due to the remote and inhospitable environments of these glaciers and ice caps, field measurements are difficult, sparse and usually expensive to implement. Relatively long time series of mass balance observations exist for only a small number of sites [Koerner, 2002]. Airborne laser altimetry [Abdalati et al., 2004] has provided evidence of changes in the thickness of these glaciers and ice caps over the period 1995-2000, but this information is restricted to selected flight lines.

Estimates of changes in the regional ice cover and the resulting sea-level impacts are therefore based either on extrapolation from these measurements [Dyurgerov and Meier, 1997; Meier et al., 2003; Abdalati et al., 2004] or on models that currently lack validation [e.g., Oerlemans and Fortuin 1992; Gregory and Oerlemans 1998].

Due to the low and relatively constant winter accumulation [Koerner, 1979], variations in summer melting are the most significant cause of inter-annual variability in the surface mass balance of glaciers and ice caps in the Canadian high Arctic [Dowdeswell et al., 1997; Koerner, 2002]. Thus, there is a strong interest in monitoring summer melt on ice caps in the QEI. Time series of ERS scatterometer data were used by Smith et al. [2003] to detect melt within single pixels on several Arctic ice caps, but synoptic melt mapping could not be undertaken because of the coarse resolution of the sensor (~25 km). In this thesis, enhanced resolution data from QSCAT [Long and Hicks, 2005] were used to detect the dates of melt onset and freeze-up, and to determine the annual melt extent and duration across all of the major ice caps in the QEI during the 2000-2004 period. Five-year climatology of melt onset/freeze-up dates, melt duration, and annual anomaly patterns were derived, and an attempt was made to explain the observed melt climatology and anomaly patterns in terms of changes in atmospheric circulation and surface air temperature lapse rates.

1.4.2. Snowmelt and ice layer formation over the Greenland ice sheet

As the second largest ice sheet in the world, the Greenland ice sheet plays an important role in regional and global climates. The total ice-covered area on Greenland is 1.71×10^6 km^2 (including surrounding glaciers and small ice caps), and the ice volume is estimated to be 2.85×10^6 km^3, equivalent to a sea level rise of 7.2 m [Church et al., 2001]. Precise knowledge of the mass balance of the ice sheet is required to assess its contribution to global sea level change.

The amount of surface melt is a key component of the surface mass balance, and there is evidence that the rate of flow of some sections of the ice sheet may be influenced by the penetration of surface melt to the ice sheet bed [Zwally et al., 2002]. In addition, due to the gentle slope over most of the Greenland ice sheet, small changes in air temperature can cause large areal changes in the distribution of snowmelt, and thus in the

boundaries between the different snow and ice facies. Assuming an adiabatic lapse rate of 0.6°C/100m [Orvig, 1970], a slope of 0.4° (above the equilibrium line), and a melt area perimeter of 3300 km, a rise of 1°C in air temperature would increase the melt area by 79 000 km^2 [Abdalati and Steffen, 1997]. It is thus clear that melt conditions over the Greenland ice sheet are potentially a useful indicator of the Arctic climate and climate change.

Surface melting is extensive on the Greenland ice sheet, and the extent of melt fluctuates greatly from year to year [Mote and Anderson, 1995; Abdalati and Steffen, 1997; 2001]. Spatial variations in surface melt, together with snow accumulation, result in unique physical properties in the near surface snow and firn on the ice sheet. Based on properties measured in snow pits and cores, Benson [1962] divided the ice sheet into distinct diagenetic facies or zones – dry snow, percolation/saturation, and ablation zone from the summit area to the ice sheet margin. Little or no melt occurs in the dry snow zone, where height changes are mainly due to changes in the rate of snow accumulation and firn densification [Zwally and Li, 2002]. In the ablation zone, all of the annual snow accumulation can be melted during the summer, height changes are related to changes in surface melt and ice dynamics [Thomas et al., 2003]. In the percolation zone, some surface melt occurs and melt water percolates into the snowpack and refreezes, producing numerous ice lenses and pipes, and spatial and temporal variations in snow accumulation and near surface firn density are the main causes of changes in surface height [Braithwaite et al., 1994; McConnell et al., 2000].

Changes in ice sheet thickness have been inferred from airborne laser altimeters [Krabill et al., 2004] and satellite radar altimeters [Zwally et al., 1989; 2005; Davis et al., 1998; 2000; Johannessen et al., 2005]. However, measurements of thickness change alone do not indicate the causes to the observed changes. Using passive microwave data, Steffen et al. [2004] demonstrated that the area of the Greenland ice sheet that experiences summer melt increased by ~16% from 1979 to 2002. Increased melt extent is likely to raise the upper limit of the percolation zone to higher elevations on the ice sheet, and is probably associated with an increase in the near-surface firn density in new areas of ice layer formation. In the absence of increased accumulation, this would probably result in a decrease of surface height in these regions because of the increase in the rate of

snow densification in areas previously unaffected by surface melt and ice layer formation. Nghiem et al. [2005] first attempted to detect the extent of ice layer formation in the percolation zone of the Greenland ice sheet using QSCAT scatterometer data. This study reported a significant increase in the extent of ice layer formation following the record melt summer of 2002.

To better understand the interaction between surface melt and Arctic climate change, it is therefore very important to detect the annual and inter-annual variations in the distribution of surface melt and ice layer formation on the Greenland ice sheet. Such observations will also help to identify areas of the ice sheet where changes in surface elevation might be linked to changes in the rate of snow/firn densification driven by changes in the distribution of summer melting.

1.5. Thesis outline

This thesis is presented in paper format, with each of the three main chapters written as a standalone manuscript. As of May 1st, 2006, Chapters 2 and 3 have been published. Chapter 4 is in preparation for submission to the Journal of Geophysical Research. The full titles and publication details are as follows:

Chapter 2: Wang, L., M. Sharp, R. Brown, C. Derksen, and B. Rivard (2005), Evaluation of spring snow covered area depletion in the Canadian Arctic from NOAA snow charts, Remote Sensing of Environment, 95, 453-463.

Chapter 3: Wang, L., M. J. Sharp, B. Rivard, S. Marshall, and D. Burgess (2005), Melt season duration on Canadian Arctic ice caps, 2000–2004, Geophysical Research Letters, 32, L19502, doi:10.1029/2005GL023962.

Chapter 4: Wang, L., M. J. Sharp, and B. Rivard, Melt season duration and ice layer formation on the Greenland ice sheet, 2000-2004, in preparation for submission to Journal of Geophysical Research.

The thesis summary, conclusions and suggestions for further work are presented in Chapter 5.

The co-authorship of the papers (Chapters 2-4) reflects the fact that:

(1) The work on "Validation of the NOAA weekly snow cover dataset for the Canadian Arctic" presented in chapter 2 resulted from a collaboration with my supervisors and two scientists from Environment Canada. C. Derksen provided data on snow cover extent from the passive microwave SSM/I sensor and he wrote the corresponding section of the paper (2.3.3. SSM/I-derived snow cover extent).

(2) The field data used in chapter 3 were collected as part of a collaborative research project between M. Sharp and S. Marshall, in which D. Burgess was a participant. These data include near surface air temperature measurements on the Prince of Wales Icefield and the Devon Island Ice Cap, and measurements of the physical properties of snow along a transect across the Devon Island Ice Cap.

All co-authors provided critiques and editing of manuscript drafts. However, except for section 2.3.3 of chapter 2, all data processing, analysis and interpretation, and the writing of the chapters/papers, were entirely my own work.

1.6. References

Abadalati W., and K. Steffen (1997), Snowmelt on the Greenland ice sheet as derived from passive microwave satellite data, Journal of Climate, 10, 165–175.

Abdalati, W., and K. Steffen (2001), Greenland ice sheet melt extent: 1979-1999, Journal of Geophysical Research, 106, 33,983-33, 988.

Abdalati, W., W. Krabill, and E. Frederick, et al. (2004), Elevation changes of ice caps in the Canadian Arctic Archipelago, Geophysical Research Letters, 109, F04007, doi:10.1029/2003JF000045.

ACIA (2005), Arctic Climate Impact Assessment, Cambridge Univ. Press, New York, 1042 pp.

Benson, C. S. (1962), Stratigraphic studies in the snow and firn on the Greenland ice sheet, Res. Rep. 70, Snow, Ice, and Permafrost Res. Estab., U.S. Army Corps of Eng., Hanover, N. H.

Braithwaite, R. J., M. Laternser, and T. W. Pfeffer (1994), Variations of near-surface firn density in the lower accumulation area of the Greenland ice sheet, Pakitsoq, West Greenland, Journal of Glaciology, 40, 477–485.

Brown, R. D. (2000), Northern Hemisphere Snow Cover Variability and Change, 1915–97, Journal of Climate, 13, 2339-2355.

Brown, R.D., and B.T. Alt (Eds.) (2001), The state of the Arctic cryosphere during the extreme warm summer of 1998: documenting cryospheric variability in the Canadian Arctic, Unpublished Report, Meteorological Service of Canada, Climate Research Branch, Downsview, Ontario, 33 pp.

Cazenave, A., and R. S. Nerem (2004), Present-day sea level change: observations and causes, Reviews of Geophysics, 42, RG2001/2004.

Chapman, W. L., and J. E. Walsh (1993), Recent variations of sea ice and air temperature in high latitudes, Bulletin of American Meteorology Society, 74, 33-47.

Church, J. A., and 35 others (2001), Changes in sea level, in Climate Change 2001:The Scientific Basis, edited by J. T. Houghton, Y. Ding, D. J. Griggs, M. Noguer, P. J. van der Linden, X. Dai, K. Maskell, and C. A. Johnson, Cambridge Univ. Press, New York, pp. 639–693.

Curry, J. A., J. L. Schramm, and E. E. Ebert (1995), Sea ice-albedo climate feedback mechanism, Journal of Climate, 8, 240– 247.

Curry, J. A., W. B. Rossow, D. Randall, and J. L. Schramm (1996), Overview of arctic cloud and radiation characteristics, Journal of Climate, 9, 1731-1764.

Davis, C. H., C. A. Kluever, and B. J. Haines (1998), Elevation change of the southern Greenland ice sheet, Science, 279, 2086– 2088.

Davis, C. H., C. A. Kluever, B. J. Haines, C. Perez, and Y. T. Yoon (2000), Improved elevation change measurement of the southern Greenland ice sheet from satellite radar altimetry, IEEE Transactions on Geoscience and Remote Sensing, 38, 1367–1378.

Dethloff, K., and 14 others (2006), A dynamical link between the Arctic and the global climate system, Geophysical Research Letters, 33, L03703, doi:10.1029/2005GL025245.

Dewey, K. F., and R. Heim Jr. (1981), Satellite observations of variations in Northern Hemisphere seasonal snow cover. NOAA Technical Report, NESS 87, Washington, D.C., 83 pp.

Dowdeswell, J. A., and others (1997), The mass balance of circum-Arctic glaciers and recent climate change, Quaternary Research, 48, 1 –14.

Drinkwater, M. R., D. G. Long, and A. W. Bingham (2001), Greenland snow accumulation estimates from satellite radar scatteromter data, Journal of Geophysical Research, 106, 33,935–33, 950.

Dye, D. G. (2002), Variability and trends in the annual snow-cover cycle in Northern Hemisphere land areas, 1972–2000, Hydrological Processes, 16, 3065-3077.

Dyurgerov, M. B., and M. F. Meier (1997), Year-to-year fluctuation of global mass balance of small glaciers and their contribution to sea level changes, Arctic and Alpine Research, 29, 392-401.

Dyurgerov, M. (2002), Glacier mass balance and regime: data of measurements and analysis, Occasional Paper No. 55, Institute of Arctic and Alpine Research, University of Colorado, Boulder, 268 pp.

Easterling, D. R., T. R. Karl, K. P. Gallo, and D. A. Robinson (2000), Observed climate variability and change of relevance to the biosphere, Journal of Geophysical Research, 5, 20101- 20114.

"ESA, ERS-1 System," European Space Agency Publication Division, ESTEC, Noordwijk, The Netherlands, ESA SP-1146, 1992.

Fowler, C., J. Maslanik, T. Haran, T. Scambos, J. Key, and W. Emery (2002), AVHRR Polar Pathfinder twice-daily 5 km EASE-Grid composites, Boulder, CO: National Snow and Ice Data Center, Digital media.

Frei, A., and D. A. Robinson (1999), Northern hemisphere snow extent: regional variability 1972–1994, International Journal of Climatology, 19, 1535–1560.

Gregory, J. M., and J. Oerlemans (1998), Simulated future sea level rise due to glacier melt based on regionally and seasonally resolved temperature changes, Nature, 391, 474-476.

Groisman, P. Y., T. R. Karl, and R. W. Knight (1994a), Observed impact of snow cover on the heat balance and the rise of continental spring temperatures, Science, 263, 198–200.

Groisman P.Y., T. R. Karl, R. W. Knight, and G. L. Stenchikov (1994b), Changes of Snow Cover, Temperature, and Radiative Heat Balance over the Northern Hemisphere, Journal of Climate, 7, 1633-1656.

Houghton, J. T., Y. Ding, D. J. Griggs, M. Noguer, P. J. van der Linden, X. Dai, K. Maskell, and C. A. Johnson (Eds.) (2001), Climate Change 2001: The Scientific Basis, Cambridge University Press, New York.

Iwasaki, T. (1991), Year-to-year variation of snow cover area in the Northern Hemisphere, Journal of the Meteorological Society of Japan, 69, 209-217.

Jezek, K. C., M. R. Drinkwater, J. P. Crawford, R. Bindschadler, and R. Kwol (1993), Analysis of Synthetic Aperture Radar Collected over the southwestern Greenland Ice Sheet, Journal of Glaciology, 39, 119-132.

Johannessen, O. M., L. Bengtsson, and M. W. Miles et al. (2004), Arctic climate change: observed and modelled temperature and sea-ice variability, Tellus Series A, Dynamic Meteorology and Oceanography, 56, 328-341.

Johannessen, O. M., K. Khvorostovsky, M. W. Miles, and L. P. Bobylev (2005), Recent ice-sheet growth in the interior of Greenland, Science, 310, 1013-1016.

Jones, P. D., M. New, D. Parker, S. Martin, and I. Rigor (1999), Surface air temperature and its changes over the past 150 years, Reviews of Geophysics, 37, 173-199.

Koerner, R. M. (1979), Accumulation, ablation and oxygen isotope variations in the Queen Elizabeth Island ice caps, Canada, Journal of Glaciology, 22, 25–41.

Koerner, R. M. (2002), Glaciers of Canada: Glaciers of the High Arctic islands, U.S. Geological Survey Professional Paper, 1386-J, 111 –146.

Krabill, W., and 12 others (2004), Greenland ice sheet: Increased coastal thinning, Geophysical Research Letters, 31, L24402, doi:10.1029/2004GL021533.

Kukla, G., and D. A. Robinson (1981), Climatic value of operational snow and ice charts. In Snow Watch 1980, Glaciological Data, Report GD-11, World Data Center-A for Glaciology, University of Colorado, Boulder, pp.103-119.

Liu, H., L. Wang, and K. C. Jezek (2006), Spatiotemporal variations of snowmelt in Antarctica derived from satellite Scanning Multichannel Microwave Radiometer and Special Sensor Microwave Imager data (1978–2004), Journal of Geophysical Research, 111, F01003, doi:10.1029/2005JF000318.

Long, D. G., P. J. Hardin, and P. T. Whiting (1993), Resolution enhancement of spaceborne scatterometer data, IEEE Transactions on Geoscience and Remote Sensing, 32, 700-715.

Long, D. G., and M. R. Drinkwater (1994), Greenland ice-sheet surface properties observed by the Seasat-A scatterometer at enhanced resolution, Journal of Glaciology, 40, 213–230.

Long, D. G., and M. R. Drinkwater (1999), Cryosphere applications of NSCAT data, IEEE Transactions on Geoscience and Remote Sensing, 37, 1671-1684.

Long, D.G., and B. R. Hicks (2005), Standard BYU QuikSCAT/SeaWinds land/ice image products, Report, Brigham Young University, Provo, UT, 30 pp.

McConnell, J. R., R. J. Arthern, E. Mosley-Thompson, C. H. Davis, R. C. Bales, R. Thomas, J. F. Burkhart, and J. D. Kyne (2000), Changes in Greenland ice sheet elevation attributed primarily to snow accumulation variability, Nature, 406, 877–879.

Meier, M. F., M. B. Dyurgerov, and G. J. McCabe (2003), The health of glaciers: recent changes in glacier regime, Climatic Change, 59, 123-135.

Moritz, R. E., C. M. Blitz and E. J. Steig (2002), Dynamics of recent climate change in the Arctic, Science, 297, 1497-1502.

Mote, T. L. and M. R. Anderson (1995), Variations in snowpack melt on the Greenland ice sheet based on passive-microwave measurements, Journal of Glaciology, 41, 51–60.

Naderi, F., M. H. Freilich, and D. G. Long (1991), Spaceborne radar measurement of wind velocity over the ocean - An overview of the NSCAT scatterometer system, Proceedings of the IEEE, 79, 850–866.

Nghiem, S. V., K. Steffen, R. Kwok, and W. Y. Tsai (2001), Detection of snowmelt regions on the Greenland ice sheet using diurnal backscatter change, Journal of Glaciology, 47, 539– 547.

Nghiem, S.V., K. Steffen, G. Neumann, and R. Huff (2005), Mapping of ice layer extent and snow accumulation in the percolation zone of the Greenland ice sheet, Journal of Geophysical Research, 110, F02017, doi:10.1029/2004JF000234

Oerlemans, J., and J. P. F. Fortuin (1992), Sensitivity of glaciers and small ice caps to greenhouse warming, Science, 258, 115-117.

Overland, J. E., M. C. Spillance, and N. N. Soreide (2004), Integrated analysis of physical and biological pan-arctic change, Climatic Change, 63, 291-322.

Overpeck, J., K. Hughen, D. Hardy, R. Bradley, R. Case, M. Douglas, B. Finney, K. Gajewski, G. Jacoby, A. Jennings, S. Lamoureux, A. Lasca, G. MacDonald, J. Moore, M. Retelle, S. Smith, A. Wolfe, and G. Zielinski (1997), Arctic environmental change of the last four centuries, Science, 278, 1251–1256.

Orvig, S. (Eds.) (1970), Climates of the Polar Regions, World Survey of Climatology, 14, Elsevier Publishing Company, 370 pp.

Partington, K. C. (1998), Discrimination of glacier facies using multitemporal SAR Data, Journal of Glaciology, 44, 42-53.

Perry, K.L. (Eds.) (2001), QuikSCAT Science Data Product User's Manual, Jet Propulsion Laboratory, California Institute of Technology, CA.

Pivot, F., C. Duguay, R. Brown, B. Duchiron, and C. Kergomard (2002), Remote sensing of snow cover for climate monitoring in the Canadian subarctic: a comparison between SMMR–SSM/I and NOAA–AVHRR sensors, Proceedings of the Eastern Snow Conference, Stowe, Vermont, USA, pp.15-25.

Polyakov, I. V., and M. A. Johnson (2000), Arctic decadal and interdecadal variability, Geophysical Research Letters, 27, 4097–4100.

Polyakov, I. V., and nine others (2002), Observationally based assessment of polar amplification of global warming, Geophysical Research Letters, 29, 1878, doi:10.1029/2001GL011111.

Qian, B., and M. A. Saunders (2003), Seasonal predictability of wintertime storminess over the North Atlantic, Geophysical Research Letters, 30, 1698, doi:10.1029/2003GL017401

Räisänen, J. (2001), CO2-induced climate change in CMIP2 experiments: Quantification of agreement and role of internal variability, Journal of Climate, 14, 2088-2104.

Ramage R. M., B. L. Isacks, and M. M. Miller (2000), Radar glacier zones in southeast Alaska,U.S.A. : field and satellite observations, Journal of Glaciology, 146, 287-296.

Rau, F., M. Braun, H. Saurer, H. Goßmann, G. Kothe, F. Weber, M. Ebel, and D. Beppler (2000), Monitoring multi-year snow cover dynamics on the Antarctic Peninsula using SAR imagery, Polarforschung, 67, 27-40.

Robinson, D. A., K. F. Dewey, and R. R. Heim (1993), Global snow cover monitoring: An update, Bulletin of American Meteorology Society, 74, 1689–1696.

Robinson, D. A, and G. Kukla (1988), Comments on "Comparison of Northern Hemisphere snow cover datasets", Journal of Climate, 1, 435-440.

Saunders, M. A., B. Qian, and B. Lloyd-Hughes (2003), Summer snow extent heralding of the winter North Atlantic Oscillation, Geophysical Research Letters, 30, 1378, doi:10.1029/2002GL016832.

Schaefer, K., A. S. Denning, and O. Leonard (2004), The winter Arctic Oscillation and the timing of snowmelt in Europe, Geophysical Research Letters, 31, L22205, doi:10.1029/2004GL021035.

Serreze, M.C., J. E. Walsh, F. S. Chapin III, T. Osterkamp, M. Dyurgerov, V. Romanovsky, W. C. Oechel, J. Morison, T. Zhang, and R. G. Barry (2000), Observational evidence of recent change in the northern high latitude environment, Climatic Change, 46, 159-207.

Serreze, M. C., J. A. Maslanik, T. A. Scambos, F. Fetterer, J. Stroeve, K. Knowles, C. Fowler, S. Drobot, R. G. Barry, and T. M. Haran (2003), A record minimum arctic sea ice extent and area in 2002, Geophysical Research Letters, 30, 1110, doi:10.1029/2002GL016406.

Smith, L. C., R. R. Forster, B. L. Isacks, and D. K. Hall (1997), Seasonal Climatic Forcings on Alpine Glaciers revealed using Orbital Synthetic Aperture Radar, Journal of Glaciology, 43, 480- 488.

Smith, L. C., Y. Sheng, R. R. Forster, and K. Steffen, et al. (2003), Melting of small Arctic ice caps observed from ERS scatterometer time series, Geophysical Research Letters, 30, 2034, doi:10.1029/2003GL017641

Solomon, A. (2006), Impact of latent heat release on polar climate, Geophysical Research Letters, 33, L07716, doi:10.1029/2005GL025607.

Spencer, M. W., C. Wu, and D. G. Long (2000), Improved resolution backscatter measurements with the SeaWinds pencil-beam scatterometer, IEEE Transactions on Geoscience and Remote Sensing, 38, 89–104.

Steffen, K. (1995), Surface energy exchange at the equilibrium line on the Greenland ice sheet during onset of melt, Annals of Glaciology, 21, 13–18.

Steffen, K., S. V. Nghiem, R. Huff, and G. Neumann (2004), The melt anomaly of 2002 on the Greenland ice sheet from active and passive microwave satellite observations, Geophysical Research Letters, 31, L20402, doi:10.1029/2004GL020444.

Steffen, K., and R., Huff (2005), Greenland melt extent, 2005, http://cires.colorado.edu/science/groups/steffen/greenland/melt2005/

Thomas, R. H., A. Abdalati, E. Frederick, W. B. Krabill, s. Manizade, and K. Steffen (2003), Investigation of surface melting and dynamic thinning on Jakobshavn Isbrae, Greenland, Journal of Glaciology, 49, 231–239.

Ulaby, F. T., and W. H. Stiles (1981), Microwave response of snow, Advances in Space Research, 1, 131-149.

Ulaby, F. T., R. K. Moore, and A. K. Fung (1982), Microwave remote sensing: Active and Passive, Volume II: Radar remote sensing and surface scattering and emission theory, Addison-Wesley publishing company, Reading, Massachusetts, 746 pp.

Wiesnet, D. R., C. F. Ropelewski, G. J. Kukla, and D. A. Robinson (1987), A discussion of the accuracy of NOAA satellite-derived global seasonal snow cover measurements. Proceedings, Symposium On Large Scale Effects of Seasonal Snow Cover, Vancouver, BC, Canada, IAHS, pp. 291–304.

Wismann, V. R. (2000), Monitoring of seasonal snowmelt in Greenland with ERS scatterometer data, IEEE Transactions on Geoscience and Remote Sensing, 38, 1821–1826.

Zwally, H. J., A. C. Brenner, J. A. Major, R. A. Bindschadler, and J. G. Marsh (1989), Growth of Greenland ice sheet: Measurement, Science, 246, 1587–1589.

Zwally, H. J., and S. Fiegles (1994), Extent and duration of Antarctic surface melting, Journal of Glaciology, 40, 463–476.

Zwally, H. J., and J. Li (2002), Seasonal and interannual variations of firn densification and ice sheet surface elevation at the Greenland summit, Journal of Glaciology, 48, 199–207.

Zwally, H. J., W. Abdalati, T. Herring, K. Larson, J. Saba, and K. Steffen (2002), Surface melt-induced acceleration of Greenland ice-sheet flow, Science, 297, 218-222.

Zwally, H. J., M. B. Giovinetto, J. Li, H. G. Cornejo, M. A. Beckley, A. C. Brenner, J. L. Saba, and D. Yi (2005), Mass changes of the Greenland and Antarctic ice sheets and shelves and contributions to sea-level rise: 1992–2002, Journal of Glaciology, 51, 509-527.

CHAPTER 2.

EVALUATION OF SPRING SNOW COVERED AREA DEPLETION IN THE CANADIAN ARCTIC FROM NOAA SNOW CHARTS

2.1. Introduction

Snow cover extent (SCE) over the northern hemisphere (NH) landmass has been continuously monitored by the National Oceanic and Atmospheric Administration (NOAA) since 1966 (Dewey and Heim, 1981). The NOAA weekly snow cover product is the longest time series of spatially continuous snow cover data available for the NH. It consists of digitized weekly charts of snow cover derived from the visual interpretation of visible satellite imagery by trained analysts. This dataset has been widely used to document regional and hemispheric variability in snow cover extent (Brown, 2000; Dye, 2002; Easterling et al., 2000; Frei and Robinson, 1999; Iwasaki, 1991; Robinson et al., 1993). Trends in continental SCE from the NOAA dataset were presented in the latest Intergovernmental Panel on Climate Change (IPCC) assessment report (IPCC, 2001, p124). A global decrease in spring SCE derived from the NOAA dataset partially explains the significant increase in spring surface air temperature over the NH landmass during the past century (Groisman et al., 1994a). In addition, Saunders et al. (2003) used the NOAA dataset to demonstrate a statistically significant linkage between summer NH SCE and the North Atlantic Oscillation pattern in the following winter.

Brown and Alt (2001), however, found major discrepancies between SCE estimates derived from in situ snow depth observations and those from the NOAA dataset over the Canadian Arctic (the area contributing much of the summer season variability in NH SCE). To date, the NOAA dataset has received only limited validation (Kukla and Robinson, 1981; Robinson and Kukla, 1988; Wiesnet et al., 1987), especially in the NH high latitudes. Kukla and Robinson (1981) performed the most detailed evaluation of the NOAA snow charts. They reproduced an independent set of snow maps for selected blocks of the United States and Asia by re-charting satellite imagery with the assistance of ground observations. Snow coverage, in percent of total area derived from the NOAA weekly charts, was compared to daily snow coverage for selected weeks in November,

January, February, and March. The average differences were found to be less than 10% of the area of the block. The best match was obtained for the last or the penultimate day of the week. However, large discrepancies were often found in the NOAA charts for autumn, especially for Asia. Robinson et al. (1993) concluded that the accuracy of the winter and spring charts was sufficient for continental or hemispheric scale climate-related studies. Nevertheless, the NOAA dataset has never been evaluated for the Arctic regions, which are widely believed to be especially sensitive to anthropogenic climate change. This is mainly because ground observations in these regions are sparse, making validation of the NOAA dataset more difficult.

The NOAA dataset has frequently been compared to other snow cover products. These include passive microwave derived snow products (Special Sensor Microwave/Imager - SSM/I, operational 1987 to present; Scanning Multichannel Microwave Radiometer - SMMR, operational 1978-1987), the U.S. Air Force daily global snow cover dataset, and the National Operational Hydrological Remote Sensing Center snow cover dataset (Armstrong and Brodzik, 2001; Basist et al., 1996; Pivot et al., 2002; Scialdone and Robock, 1987). In most cases, however, the NOAA dataset has been taken more or less as the standard during these comparisons. In this paper, the NOAA dataset was evaluated for the region of the Canadian Arctic mainland north of the tree line (Figure 2.1) during the spring melt period. This particular study area was selected to minimize forest-masking effects, and to avoid problems related to the coarse resolution of the NOAA product over the Canadian Arctic Archipelago. The evaluation focused on six spring periods from the 1981-2000 period with unusually low (1984, 1988, and 1998) or high (1985, 1995, and 1997) SCE over North America. The spring period was selected because the snow line migration can be tracked for several weeks through the study region, unlike the fall season when the entire region becomes completely snow covered in a very short period. There was also an interest in looking at the spring melt period from a snow cover-climate feedback perspective since this is the period when snow cover exhibits the strongest feedbacks to the climate system (Groisman et al., 1994b). The NOAA dataset was compared to snow cover extents derived from AVHRR, SSM/I, and Landsat 5 TM browse images, and surface snow observations. A number of variables

including cloud cover, lake ice, and fractional snow cover thresholds were explored in an attempt to explain differences between the various datasets.

2.2. Study Area

The study area is located on the northwest side of Hudson Bay (Figure 2.1), between latitudes 58° N ~ 70° N, and longitudes 85° W ~ 122° W. This area is located above the tree line and is dominated by barren tundra according to the IGBP land cover classification (Loveland et al., 2000). The study area is relatively flat, with elevations generally below 500 m. This area experiences the longest period of seasonal snow cover on the North American mainland and contributes a large fraction of the NH SCE in spring/summer. Ten snow depth observation stations are located in the study area (Figure 2.1), although the number that were operational varied from year to year. There are also a few snow survey observations in the study area, but none are available during May or June when the NOAA dataset exhibits the largest difference from the other datasets.

2.3. Data and Methods

2.3.1. NOAA weekly snow cover dataset

From November 1966 to May 1999, the National Oceanic and Atmospheric Administration produced weekly snow cover charts for the northern hemisphere land areas based on visual interpretation of visible satellite imagery. The primary data source was NOAA Polar Operational Environmental Satellites (POES). The nadir resolution of the imagery acquired prior to 1972 was about 4 km. The Very High Resolution Radiometer (VHRR) launched in 1972 provided imagery with a spatial resolution of 1.0 km, and from November 1978 the Advanced VHRR (AVHRR) provided 1.1 km resolution data. Secondary data sources used to produce the charts included geostationary imagery, US Air Force snow analyses, and surface observations (Ramsay, 1998). Geostationary data have been used from the NOAA Geostationary Operational Environmental Satellites (GOES) over North America since 1975, from the European Geostationary Meteorological Satellite (METEOSAT) over Europe since 1988, and from the Japanese Geostationary Meteorological Satellite (GMS) over Asia since 1989.

Weekly charts show snow cover boundaries for the latest day of the chart week during which the surface in a region was visible in the imagery. The charts were then digitized to an 89 by 89 polar stereographic grid with 190 km resolution. In this process, a cell was considered to be snow-covered in a given week if it was interpreted to be at least 50% snow covered; otherwise it was considered to be snow free. Recently, the digital NOAA dataset was re-gridded to the Northern Hemisphere 25-km EASE (Equal-Area Scalable Earth) Grid (Armstrong and Brodzik, 2002). The re-gridded data were used in this study to facilitate comparisons with other datasets.

The automated Interactive Multi-sensor snow and ice mapping System (IMS) replaced the manual snow cover analysis in April 1999. The IMS provides a daily snow and ice cover map for the NH with a resolution of 23 km (Ramsay, 1998), and a pseudo-weekly chart has been created to maintain the continuity of the previous database. It is unclear what impact this has had on the homogeneity of the data so the evaluation carried out in this study was restricted to the period when manual charting procedures were in use.

2.3.2. AVHRR-derived snow cover extent

Since the 1980s, several algorithms have been developed for snow monitoring from optical sensors, including the multispectral thresholds classification method (Allen,1990; Gesell, 1989; Harrison and Lucas, 1989; Liu et al., 1999; Romanov et al., 2000). Other approaches for snow extent estimation include linear spectral unmixing for sub-pixel snow mapping (Appel and Salomonson, 2002; Romanov, et al., 2003; and Rosenthal and Dozier, 1996), and Normalized Difference Snow Index (NDSI) algorithm (Dozier, 1989; Hall et al., 1995, 2002). Considering the weekly availability and the coarse resolution of the NOAA dataset (originally 190 km) to be evaluated, the multispectral thresholds algorithm was chosen in this study to derive weekly snow cover extent from the AVHRR Polar Pathfinder twice-daily 5 km EASE-Grid composites (Fowler et al., 2002). Daily AVHRR/2 (NOAA, 2003) calibrated 5-channel data are available in the EASE-Grid composites.

The greatest difficulty in mapping snow cover from AVHRR imagery is the detection of cloud contamination. Snow and clouds both have high reflectance in the VIS

and low brightness temperature in the IR bands. The high reflectance of snow drops quickly from VIS to MIR, however, while the reflectance of water clouds remains high (Dozier 1989; Kidder and Wu, 1984). This feature has been used extensively in AVHRR snow/cloud discrimination and detection (for example, Allen, 1990; Gesell, 1989).

The signal received by AVHRR/2 channel 3 (3.55~3.99 μm) during the day includes two parts: reflected solar radiation and the emitted thermal radiation. In this study, the difference in brightness temperature between channel 3 and 4 (10.3~11.3 μm) was used to approximate the reflective component of channel 3 (Liu et al., 1999; Harrison and Lucas, 1989) and to separate snow from water clouds. AVHRR/2 channel 1 (0.58~0.68 μm) and channel 2 (0.725~1.05 μm) were used mainly to identify snow/clouds from other land cover types, such as bare land and water bodies. The brightness temperature of channel 4 was mainly used to discriminate between snow and ice clouds, which are usually colder than snow in the polar region (Raschke et al., 1992). A number of AVHRR/2 images were selected from which the main surface types (snow, clouds, bare land, and water bodies) can easily be determined visually. Surface snow depth and snow survey observations were used to assist in discriminating between snow and clouds. Many samples of each of the surface types were taken from the AVHRR/2 images. Thresholds for discrimination were then determined by averaging the spectral values of the surface types at each of the 4 AVHRR/2 channels. The thresholds were then adjusted according to snow depth and snow survey observations. A pixel was classified as snow covered if it passed all the thresholds on any day from a 7-day period in a NOAA chart week.

Calibrated AVHRR/2 data were obtained for the six selected springs from the AVHRR Polar Pathfinder twice-daily 5 km EASE-Grid composites (Fowler et al., 2002) available from the National Snow and Ice Data Center (NSIDC). Weekly snow cover extents for the period March through June were derived using the 1400 daytime data for the study area. The AVHRR-derived snow cover extent was found to be consistently less than that shown in the NOAA charts, for example, weeks 23~25 of 1997 are shown in Figure 2.2.

2.3.3. SSM/I-derived snow cover extent

Passive microwave data have been used extensively to map snow cover parameters, for example, snow extent (Grody and Basist, 1996), snow depth (Chang et al., 1990; Kelly et al., 2003) and snow water equivalent (Goita et al., 2003; Josberger et al., 1998; Pulliainen and Hallikainen, 2001; Tait, 1998). The main advantage for high latitude snow cover monitoring is an all-weather sensing capability, while the 25 km resolution and wide swath width are well-suited for regional snow cover monitoring in non-mountainous terrain. The retrieval of snow cover information from passive microwave brightness temperatures is theoretically straightforward: as the depth and density of snow increase, so too does the amount of volume scatter of naturally emitted microwave energy. Shorter wavelength energy (i.e. 37 GHz) is more readily scattered by snow grains than longer wavelength energy (i.e. 19 GHz), so the difference in scatter between these two satellite-measured frequencies can be exploited to estimate snow water equivalent (SWE).

In reality, the relationships between snow depth, density, and microwave scatter are complicated by the physical structure of the snowpack (for example, ice lenses and snow grain size variability) and the microwave emission and scattering characteristics of overlying vegetation. There are limitations in dense forest (not an issue for our study area) and wet snow, although Walker and Goodison (1993) developed a wet snow indicator that can be used to map the spatial extent of wet snow in open prairie environments. The imaging footprint for spaceborne passive microwave data is large (resampling produces grid cell dimensions of 25 km) so these complicating factors are compounded by considerable within-grid cell variability in snowpack structure and vegetative cover.

The Climate Research Branch of the Meteorological Service of Canada (MSC) has an ongoing program to develop the retrieval of snow cover information from spaceborne passive microwave brightness temperatures for major Canadian landscape regions. This research has yielded a suite of land-cover sensitive SWE retrieval algorithms for open (Goodison and Walker, 1995) and forested (Goita et al., 2003) environments (for an overview, see Walker and Goodison, 2000). Evaluation studies have shown that SWE retrievals in open prairie environments are typically within +/-15 mm of in situ snow surveys (Derksen et al., 2002; 2003). Systematic SWE underestimation is, however, a

problem in densely forested areas because vegetation effects can mask the passive microwave signal (Derksen et al., 2003; Walker and Silis, 2002).

To date, evaluation of passive microwave SWE retrievals using the MSC open environments algorithm in tundra areas has been limited (Woo, 1998). A recently completed (March 2004) regional snow surveying campaign across approximately 500 km of northern Manitoba included a number of open tundra sites. Passive microwave derived SWE in these regions was systematically low, potentially due to the unique microwave emission and scattering characteristics of frozen lakes which comprise a high proportion of the tundra surface cover (Derksen and Walker, 2004).

In this study, SSM/I derived SWE retrievals were converted to snow extent to facilitate comparison with the NOAA snow charts, mitigating tundra SWE underestimation issues. SSM/I EASE-Grid brightness temperatures from cold overpass times (0600 LST) were utilized to increase the frequency of monitoring of a cold and dry snowpack – conditions which optimize algorithm performance. SCE was determined by classifying each grid cell with SWE greater than 1 mm as snow covered. The 1 mm SWE threshold for determining SCE was validated through a comparison of passive microwave derived data and NOAA snow charts in the Canadian prairies (Derksen et al., 2004) This "aggressive" threshold was used because passive microwave derived data tend to underestimate snow extent relative to optical data (Armstrong and Brodzik, 2001) due to problems detecting a thin and discontinuous snow cover. The absolute SWE retrievals at these low values are suspect in the context of a meaningful water equivalent, but as a proxy for snow extent, this threshold produces patterns that compare well with optically derived data (Derksen et al., 2004).

2.3.4. Processing of TM images

In situ snow depth observations in the study area are sparse and biased to costal regions (Figure 2.1), and may not be representative of the much larger areas encompassed by pixels from the NOAA and AVHRR datasets. Therefore Landsat 5 TM browse images were used as ground truth in this study, as in Hall et al. (2002). Nine clear sky TM browse images (Figure 2.2) acquired for the study area during the spring of 1997 (the year with the most clear sky TM browse images) were classified to estimate the fraction

of snow-covered pixels (Figure 2.3; Table 2.1). The resolution of the images is approximately 480 m. The TM images were classified to snow/no snow using a threshold visually determined from a trial and error separation of snow (including frozen lakes) from bare ground. The 4 corner coordinates (latitude/longitude) of the browse images were assessed against National Topographic Data Base (NTDB) map sheets and adjusted when necessary.

2.4. Results

2.4.1. Comparison between NOAA, AVHRR, and SSM/I

The NOAA, AVHRR and SSM/I datasets were all in the EASE-Grid projection, facilitating inter-comparison. Weekly snow coverage (the fraction of snow covered pixels in the study area) was calculated from the three datasets for each of the 6 springs (Figure 2.4). Before the onset of melt, the snow cover percentages from the 3 datasets are generally consistent with each other. The only exception is in week 15, 1984, when the NOAA snow cover percentage shows a sudden drop. Examining the original NOAA snow chart for that week, we found that the analyst mapped a large area as patchy snow cover. It seems that patchy snow cover was not interpreted as snow during the digitizing process. This was deduced by comparing the manual charts to the digitized datasets, as no information was found in the references. The AVHRR- and SSM/I-derived datasets produce very similar results for the timing of melt onset and the progression of melt in the study area. Compared to the AVHRR- and the SSM/I-derived datasets, the onset of melt in the NOAA dataset is delayed in all 6 years. The delay ranges from about 1 week (1984 and 1988) to 2 to 4 weeks (other years).

2.4.2. Comparison between NOAA, AVHRR, and TM

We compared the snow cover fraction estimated from TM browse images (480 m) to that estimated from all the NOAA (originally 190 km) and AVHRR (5 km) pixels with center latitude/longitude falling within the TM coverage (Table 2.1). The area covered by the NOAA and AVHRR pixels was within 10% of the TM coverage for each of the nine browse images. Compared to the TM images, the AVHRR-derived dataset consistently underestimates snow cover. The underestimate ranges from 10.5% to 22.5%, with an

average of 13.5%. This is not surprising, because the multi-spectral thresholds algorithm used in this study does not take account of mixed pixels in the AVHRR data. One threshold for a pixel to be classified as snow is that its brightness temperature is below freezing point. Bare ground is clearly present within the snow-covered area in all the TM images. Thus there are many snow-ground mixed pixels in the 5 km AVHRR data, which are not recognized as snow covered if their overall brightness temperatures are well above the freezing point. Relative to the TM dataset, the NOAA dataset consistently overestimates snow cover by 58.9% to 87.4%, with an average of 71.5%. This is consistent with the delay in the onset and progression of melt identified in Figure 2.4.

2.4.3. Ground observations

Except for Lupin A and Baker Lake stations, which are located inland, all ground observation stations in the area are located along the coast. Only 8 sets of in situ snow depth observations (locations are shown in Figure 2.1) are available for the spring of 1997 (MSC, 2000). The daily mean air temperature for 4 of the 8 stations was obtained from the Canadian Daily Climate Data CD-ROM (Environment Canada, 2002). Daily mean air temperature and snow depth observations for May and June 1997 are plotted in Figure 2.5. The stations along the coast show very similar trends to the 2 inland stations. Around May 16 (in week 20), the air temperature rose above the freezing point and the snow depth decreased rapidly thereafter at most stations. The timing of these events is consistent with that of melt onset as detected by the AVHRR and SSM/I datasets, but 3 weeks earlier than the onset of melt in the NOAA dataset (Figure 2.4).

2.5. Discussion

Compared to the AVHRR- and SSM/I-derived snow cover extent, the NOAA dataset shows a delay in the onset of melt in all 6 springs. One possible explanation may lie in the different grid resolutions of the three datasets, and in the use of a 50% threshold value to differentiate between snow-covered and snow-free areas in the NOAA dataset. When considering hemispheric and continental scales, the effects of using this 50% threshold may average out and have little influence on estimates of SCE. For the smaller area investigated here, however, the 50% threshold approach would be expected to cause an

apparent delay in the onset and progression of melt while snow cover is in the 100 - 50% range. On the other hand, the NOAA snow cover estimate would be expected to "catch-up" with the other estimates once the snow cover falls below 50%. This is not, however, observed. Experience with trying to recreate the NOAA weekly snow product from the higher resolution NOAA daily IMS product (Bruce Brasnett, pers. comm.) has revealed that a 30% snow cover fraction threshold gave the best agreement with the manual charts. This finding suggests a bias to overestimating snow cover extent in the gridded NOAA charts.

To test this hypothesis, the AVHRR-derived 5 km EASE-Grid snow dataset was remapped to the NOAA 25 km EASE-Grid using 10%, 30%, and 50% thresholds to define snow cover. As expected, the choice of a lower threshold value does reduce the difference between the NOAA and the AVHRR-derived SCE estimates (Figure 2.6). Even the use of a 10% threshold, however, does not account for the whole difference. This suggests that the apparent melt delay in the NOAA dataset is not attributable solely to differences in grid resolution and the use of a 50% threshold to define snow cover.

Another possible explanation for the apparent melt delay is cloud contamination in the visible imagery used to produce the NOAA product, a problem that may be exacerbated by the reduced range of datasets available to assist in the production of the NOAA dataset at higher latitudes. For lower latitudes of North America, NOAA GOES imagery is used in addition to NOAA POES imagery to produce the snow charts. Although the NOAA GOES imagery theoretically has coverage as far as 70° N, the quality of the imagery near the margin is often not good enough to discriminate snow from clouds. The ground observing network is also concentrated below latitude 55° N over the more populated areas of North America (Figure 2.7). Therefore, for higher latitudes, fewer in situ observations are available to verify the NOAA snow charts, which increases the chance of misclassifying clouds as snow.

Surface cloud observations for 3 stations in the study area are available from the Canadian Climate Normal (1971~2000) dataset (Allsopp and Morris, 2004). Monthly cloud coverage, was calculated as the percent of time in a month with cloud opacity 3 to 10 tenths of the sky (Figure 2.8). All 3 stations show a similar seasonal cycle – cloud cover increases in spring, remains high in summer, and reaches its maximum in autumn.

This is consistent with the surface cloud climatology for the Arctic (Curry et al., 1996). In May and June, when the NOAA dataset shows the largest difference in snow extent from the other datasets, the study area is typically more than 75% cloud covered. According to Huschke (1969), the increase of cloud amount in spring is mainly due to the increase of low cloud. The annual cycle of low cloud amount ranges from ~20% in the winter to ~70% in the summer. The use of 3.7 μm data in the multi-spectral thresholds snow detection algorithm is likely to have effectively separated snow from low level liquid clouds, although the fraction of liquid cloud in the total low cloud is unknown. Such separation would be difficult to achieve using visible images alone (as would be the case for the NOAA dataset). This has also been demonstrated in several other snow/cloud discrimination studies (Key and Barry, 1989; Romanov et al., 2000).

In addition, there are many lakes in the study area. Usually water bodies remain frozen long after the snow melts on land. Robinson et al. (1993) indicated that there might be an overestimation of summer continental snow cover in the NOAA product due to difficulties in distinguishing between frozen water bodies and snow free land in the Arctic regions. This may also contribute to the melt delay in the NOAA dataset. Available Landsat 5 TM browse images from both 1997 and 1998 were used to examine this possibility. It seems that lake ice is not the cause of the melt delay in the NOAA dataset. After week 25, many lakes were still ice-covered, but the NOAA dataset did not indicate those areas as snow covered.

The extent of the melt delay in the NOAA dataset is different for each year – about one week delay in 1984 and 1988, and two to four weeks delay in the other years. Studying the original manual NOAA snow charts for weeks 20 to 26 in all 6 years, we found large areas were depicted as patchy snow cover in charts for 1984 and 1988 in the study area. No patchy snow cover was, however, mapped in the years in which there are large differences between the NOAA dataset and the other datasets. In the case of patchy snow cover, numerical weather prediction models make larger errors if the snow cover is underestimated rather than overestimated. NOAA analysts were therefore instructed to aggressively classify snow-covered area (Peter Romanov, pers. comm.). Changes in the patchy snow cover strategy were most likely during the late 1980s and early 1990s, and there is no guarantee that the strategy was followed consistently due to the different

experience levels of the analysts, and quality of the imagery used (Thomas Baldwin, pers. comm.). This indicates that the NOAA dataset may not always be consistent from year to year, which may account for the differences in melt delay in the NOAA dataset over the 6 springs.

If the observed spring bias applied equally across the entire period of the NOAA dataset (and this may not be the case), trends in snow disappearance date would not be affected, but it would affect trend analysis of SCE carried out on a monthly basis (e.g. trends attributed to April may actually be happening in March). The timing error would also affect correlations of monthly snow cover with other variables such as temperature (e.g. Groisman et al., 1994) or atmospheric circulation indices (e.g. Qian and Saunders, 2003).

2.6. Conclusions

Comparisons with AVHRR- and SSM/I-derived estimates of snow cover extent in the Canadian Arctic show that the NOAA weekly snow cover dataset is late in detecting the onset of melt and overestimates snow cover during the melt period in all of the 6 selected springs. Further investigations using Landsat TM images, near surface air temperatures, and in situ snow depth observations confirm that the NOAA dataset greatly overestimates snow cover extent in the study area during the spring melt period. Caution is therefore needed when using this dataset in any study where the timing of snowmelt is involved.

A number of factors are likely contributing to the delay in snow cover depletion in the NOAA dataset documented in this study. These include the reduced availability of satellite data at higher latitudes, frequent spring cloud cover (which is not readily differentiated from snow in visible imagery), and the limited availability of surface observations. A change in the interpretation strategy for noting patchy snow cover may account for differences between years in the magnitude of melt delay. These conclusions are also likely to apply to other regions of NH high latitudes. At lower latitudes, the NOAA GOES, European METEOSAT, and Japanese GMS imagery are available in addition to NOAA POES imagery, and there is a more extensive network of the ground

observations. Further validation of the NOAA snow dataset over other high latitude regions of the NH is needed to finalize these conclusions.

2.7. References

Allen, R. C., P. A. Durkee, and C. H. Wash (1990), Snow/cloud discrimination with multi-spectral satellite measurements, Journal of Applied Meteorology, 29, 994-1004.

Allsopp, D., and R. Morris (2004), Calculation of the 1971-2000 climate normals for Canada, 14th Conference on Applied Climatology, January 10-15, 2004, Seattle, WA.

Appel, I., and V. V. Salomonson (2002), Estimate of fractional snow cover using MODIS data, Geoscience and Remote Sensing Symposium, IGARSS'02. International Geoscience and Remote Sensing Society, Toronto, Ontario, Canada, 24–28 June 2002.

Armstrong, R. L., and M. J. Brodzik (2001), Recent Northern Hemisphere snow extent: A comparison of data derived from visible and microwave satellite sensors, Geophysical Research Letters, 28, 3673-3676.

Armstrong, R. L., and M. J. Brodzik (2002), Northern Hemisphere EASE-Grid weekly snow cover and sea ice extent version 2, Boulder, CO, USA: National Snow and Ice Data Center, CD-ROM.

Basist, A., D. Garrett, R. Ferraro, N. Grody, & K. Mitchell (1996), A comparison of snow cover products derived from visible and microwave satellite observations, Journal of Applied Meteorology, 35, 163–177.

Brown, R.D. (2000), Northern Hemisphere snow cover variability and change, 1915–97, Journal of Climate, 13, 2339-2355.

Brown, R., and B. Alt (2001), The state of the Arctic cryosphere during the extreme warm summer of 1998: documenting cryospheric variability in the Canadian Arctic,

Unpublished Report, Meteorological Service of Canada, Climate Research Branch, Downsview, Ontario, 33 pp.

Chang, A., J. Foster, and D. Hall (1990), Satellite sensor estimates of northern hemisphere snow volume, International Journal of Remote Sensing, 11, 167-171.

Curry, J. A., W. B. Rossow, D. Randall, and J. L. Schramm (1996), Overview of Arctic cloud and radiation characteristics, Journal of Climate, 9, 1731-1764.

Derksen, C., A. Walker, E. LeDrew, and B. Goodison (2002), Time series analysis of passive microwave derived central North American snow water equivalent imagery, Annals of Glaciology, 34, 1-7.

Derksen, C., A. Walker, and B. Goodison (2003), A comparison of 18 winter seasons of in situ and passive microwave derived snow water equivalent estimates in Western Canada, Remote Sensing of Environment, 88, 271-282.

Derksen, C., and A. Walker (2004), Evaluating spaceborne passive microwave snow water equivalent retrievals across the Canadian northern boreal – tundra ecotone. CD-ROM Proceedings, International Geoscience and Remote Sensing Symposium, Anchorage, Alaska, September, 2004.

Derksen, C., R. Brown, and A. Walker (2004), Merging conventional (1915-92) and passive microwave (1978-2002) estimates of snow extent and snow water equivalent over central North America, Journal of Hydrometeorology, 5, 850-861.

Dewey, K. F., and R. Jr. Heim (1981), Satellite observations of variations in Northern Hemisphere seasonal snow cover, NOAA Technical Report, NESS 87, Washington, D. C., 83 pp.

Dozier, J. (1989), Spectral signature of alpine snow cover from the Landsat Thematic Mapper, Remote Sensing of Environment, 28, 9–22.

Dye, D. G. (2002), Variability and trends in the annual snow-cover cycle in Northern Hemisphere land areas, 1972–2000, Hydrological Processes, 16, 3065-3077.

Easterling, D. R., T. R. Karl, K. P. Gallo, and D. A. Robinson (2000), Observed climate variability and change of relevance to the biosphere, Journal of Geophysical Research, 5, 20101- 20114.

Environment Canada (2002), CD of Canadian Daily Climate Data, Meteorological Service of Canada, Downsview, Ontario.

Fowler, C., J. Maslanik, T. Haran, T. Scambos, J. Key, and W. Emery (2002), AVHRR Polar Pathfinder twice-daily 5 km EASE-Grid composites, Boulder, CO: National Snow and Ice Data Center, Digital media.

Frei, A., and D. A. Robinson (1999), Northern hemisphere snow extent: regional variability 1972–1994, International Journal of Climatology, 19, 1535–1560.

Gesell, G. (1989), An algorithm for snow and ice detection using AVHRR data. An extension to the APOLLO software package, International Journal of Remote Sensing, 10, 897–905.

Goita, K., A. Walker, B. Goodison, and A. Chang (1997), Estimation of snow water equivalent in the boreal forest using passive microwave data, CD-ROM Proceedings, Geomatics in the Era of Radarsat, Ottawa, Ontario, May, 1997.

Goita, K., A. Walker, and B. Goodison (2003), Algorithm development for the estimation of snow water equivalent in the boreal forest using passive microwave data, International Journal of Remote Sensing, 24, 1097-1102.

Goodison, B., and A. Walker (1995), Canadian development and use of snow cover information from passive microwave satellite data, In Choudhury, B., Y. Kerr, E.Njoku, and P. Pampaloni (eds.), Passive Microwave Remote Sensing of Land-Atmosphere Interactions, pp. 245-262, Utrecht, Netherlands: VSP.

Grody, N., and A. Basist (1996), Global identification of snowcover using SSM/I measurements, IEEE Transactions on Geoscience and Remote Sensing, 34, 237-249.

Groisman, P. Y., T. R. Karl, and R. W. Knight (1994a), Observed impact of snow cover on the heat balance and the rise of continental spring temperatures, Science, 263, 198–200.

Groisman P. Y., T. R. Karl, R. W. Knight, and G. L. Stenchikov (1994b), Changes of snow cover, temperature, and radiative heat balance over the Northern Hemisphere, Journal of Climate, 7, 1633–1656.

Hall, D. K., G. A. Riggs, V. V. Salomonson (1995), Development of methods for mapping global snow cover using moderate resolution imaging spectroradiometer data, Remote Sensing of Environment, 54, 127–40.

Hall, D. K., R. E. J. Kelly, G. A. Riggs, A. T. C. Chang, and J. L. Foster (2002), Assessment of the relative accuracy of hemispheric-scale snow-cover maps, Annals of Glaciology, 34, 24-30.

Hall, D. K., G. A. Riggs, V. V. Salomonson, N. DiGiromamo, and K. J. Bayr (2002), MODIS snow-cover products, Remote Sensing of Environment, 83, 181–94.

Harrison, A., and R. Lucas (1989), Multi-spectral classification of snow using NOAA AVHRR imagery, International Journal of Remote Sensing, 10, 907-916.

Huschke, R. E. (1969), Arctic cloud statistics from "air-calibrated" surface weather observations, The Rand Corporation, RM-6173_PR, 79 pp.

Intergovernmental Panel on Climate Change (IPCC), Climate Change (2001), The Scientific Basis, Edited by Houghton, J. T., Ding, Y., Griggs, D. J., Noguer, M., van der Linden, P. J., X. Dai, K. Maskell, and C. A. Johnson, Cambridge University Press, 873 pp.

Iwasaki, T. (1991), Year-to-year variation of snow cover area in the Northern Hemisphere, Journal of the Meteorological Society of Japan, 69, 209-217.

Jones, P. D., and A. Moberg (2003), Hemispheric and large-scale surface air temperature variations: an extensive revision and an update to 2001, Journal of Climate, 16, 206-223.

Josberger, E., N. Mognard, B. Lind, R. Matthews, and T. Carroll (1998), Snowpack water-equivalent estimates from satellite and aircraft remote-sensing measurements of the Red River basin, north-central U.S.A., Annals of Glaciology, 26, 119-124

Kelly, R., A. Chang, L. Tsang, and J. Foster (2003), A prototype AMSR-E global snow area and snow depth algorithm, IEEE Transactions on Geoscience and Remote Sensing, 41, 230-242.

Key, J., and R. G. Barry (1989), Cloud cover analysis with Arctic AVHRR data, 1. Cloud detection, Journal of Geophysical Research, 94, 18521–18535.

Kidder, S. Q., and H. T. Wu (1984), Dramatic contrast between low clouds and snow cover in daytime 3.7 mm imagery, Monthly Weather Review, 112, 2345–2346.

Kukla, G., and D. A. Robinson (1981), Climatic value of operational snow and ice charts, In Snow Watch 1980 (pp. 103-119). Glaciological Data, Report GD-11, World Data Center-A for Glaciology, University of Colorado, Boulder.

Liu Y., L. Wang, and S. Yazaki (1999), Snow Cover Monitoring with AVHRR Data, In Recent Progress in Studies of Asian Monsoon Mechanism, pp.92-102, Chinese Meteorological Press, Beijing.

Loveland, T., B. Reed, J. Brown, D. Ohlen, Z. Zhu, L. Yang, and J. Merchant (2000), Development of a global land cover characteristics database and IGBP DISCover from 1 km AVHRR data, International Journal of Remote Sensing, 21, 1303-1330.

Meteorological Service of Canada (2000), Canadian Snow Data CD-ROM. CRYSYS Project, Climate Processes and Earth Observation Division, Meteorological Service of Canada, Downsview, Ontario.

NOAA (2003), http://noaasis.noaa.gov/NOAASIS/ml/avhrr.html.

Pivot, F., C. Duguay, R. Brown, B. Duchiron, and C. Kergomard (2002), Remote sensing of snow cover for climate monitoring in the Canadian subarctic: a comparison between SMMR–SSM/I and NOAA–AVHRR sensors, Proceedings of the Eastern Snow Conference, pp. 15-25, Stowe, Vermont, USA.

Pulliainen, J., and M. Hallikainen (2001), Retrieval of regional snow water equivalent from space-borne passive microwave observations, Remote Sensing of Environment, 75, 76-85.

Qian, B., and M. A. Saunders (2003), Seasonal predictability of wintertime storminess over the North Atlantic, Geophysical Research Letters, 30, 1698, doi:10.1029/2003GL017401

Ramsay, B. (1998), The interactive multisensor snow and ice mapping system, Hydrological Processes, 12, 1537–1546.

Raschke, E., P. Bauer, and H. Lutz (1992), Remote sensing of clouds and surface radiation budget over polar regions, International Journal of Remote Sensing, 13, 13-22.

Robinson, D. A, and G. Kukla (1988), Comments on "Comparison of Northern Hemisphere snow cover datasets", Journal of Climate, 1, 435-440.

Robinson, D. A. (1991), Merging operational satellite and historical station snow cover data to monitor climate change, Palaeogeography, Paleoclimatology, Palaeoecology, 90, 235-240.

Robinson, D. A., K. F. Dewey, and R. Jr. Heim (1993), Global snow cover monitoring: An update, Bulletin of American Meteorological Society, 74, 1689–1696.

Romanov, P., G. Gutman, and I. Csiszar (2000), Automated monitoring of snow cover over North America with multispectral satellite data, Journal of Applied Meteorology, 39, 1866 – 880.

Rosenthal, W., and J. Dozier (1996), Automated mapping of montane snow cover at a subpixel resolution from the Landsat Thematic Mapper, Water Resources Research, 32, 115– 130.

Saunders, M. A., B. Qian, and B. Lloyd-Hughes (2003), Summer snow extent heralding of the winter North Atlantic Oscillation, Geophysical Research Letters, 30, 1378, doi:10.1029/2002GL016832.

Scialdone, J., and A. Robock (1987), Comparison of Northern Hemisphere snow cover datasets, Journal of Applied Meteorology, 26, 53–68.

Tait, A. (1998), Estimation of snow water equivalent using passive microwave radiation data, Remote Sensing of Environment, 64, 286-291.

Wagner, A. J. (1973), The influence of average snow depth on monthly mean temperature anomaly, Monthly Weather Review, 101, 624-626.

Walker, A., and B. Goodison (1993), Discrimination of a wet snow cover using passive microwave satellite data, Annals of Glaciology, 17, 307-311.

Walker, A., and B. Goodison (2000), Challenges in determining snow water equivalent over Canada using microwave radiometry, Proceedings, International Geoscience and Remote Sensing Symposium, pp. 1551-1554, Honolulu.

Walker, A., and A. Silis (2002), Snow cover variations over the Mackenzie river basin from SSM/I passive microwave satellite data, Annals of Glaciology, 34, 8-14.

Wiesnet, D. R., C. F. Ropelewski, G. J. Kukla, and D. A. Robinson (1987), A discussion of the accuracy of NOAA satellite-derived global seasonal snow cover measurements, Proceedings, Symposium On Large Scale Effects of Seasonal Snow Cover, pp. 291–304, Vancouver, BC, Canada, IAHS.

Woo, M-K. (1998), Arctic snow cover information for hydrological investigations at various scales, Nordic Hydrology, 29, 245-266.

2.8. Tables

Table 2.1. Percent snow cover calculated from TM images (column 3) from 1997. The dates of the TM images are shown in brackets. The differences between the percent snow cover extracted from the AVHRR and NOAA datasets and those from the TM images are shown in columns 4 and 5.

Week	Centre Lat & Long	TM (%)	AVHRR-TM (%)	NOAA-TM (%)
9723 (6/2-8)	61.46° N, 103.56° W	22.7 (June 4)	-13.1	69.8
9724 (6/9-15)	65.57° N, 101.67° W	33.1 (June 11)	-11.5	66.9
9724 (6/9-15)	68.25° N, 92.60° W	64.0 (June 15)	-9.8	36.0
9725 (6/16-22)	64.20° N, 93.65° W	10.9 (June 17)	-5.7	82.1
9725 (6/16-22)	65.57° N, 92.40° W	12.6 (June 17)	-10.5	87.4
9725 (6/16-22)	66.92° N, 91.02° W	26.4 (June 17)	-21.6	75.6
9725 (6/16-22)	65.57° N, 103.21° W	14.5 (June 18)	-13.4	85.5
9725 (6/16-22)	66.92° N, 87.93° W	30.0 (June 19)	-22.5	58.9
9725 (6/16-22)	66.91° N, 98.75° W	18.5 (June 20)	-13.1	81.5
Mean			**-13.5**	**71.5**

2.9. Figures

Figure 2.1. Study area (white outline) overlaid on 1000 m resolution Radarsat mosaic downloaded from http://geogratis.cgdi.gc.ca. White dots are snow depth observation stations and black contour stands for forest cover>0 derived from IGBP land cover classification.

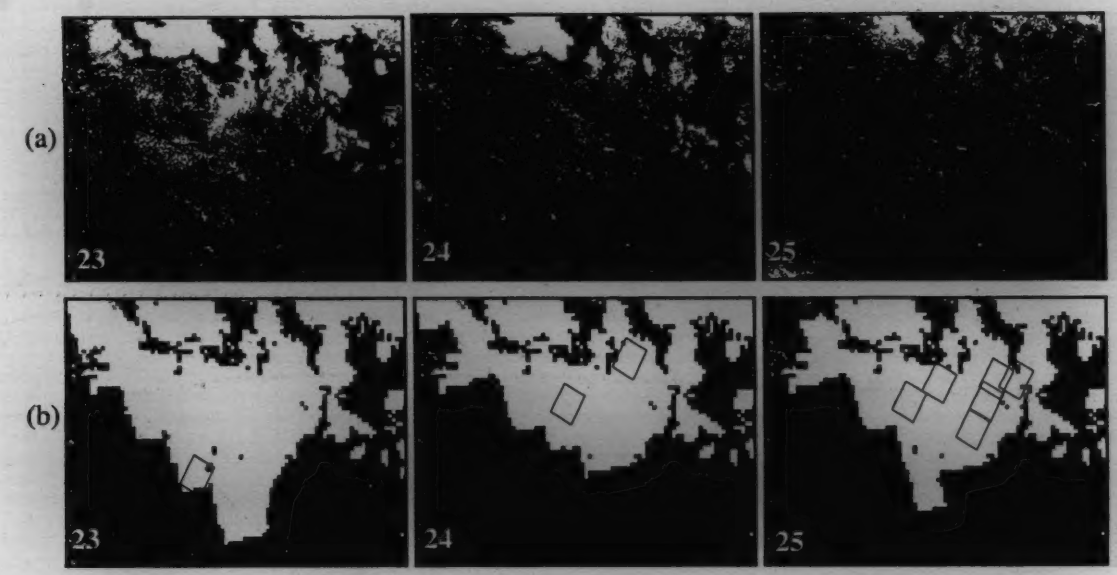

Figure 2.2. Weekly snow cover maps derived from AVHRR (a) and NOAA (b) for weeks 23-25 in the spring of 1997. The 9 gray boxes (one at week 23, two at week 24, and 6 at week 25) indicate the locations of the TM images available for each week.

(a) June 11, 1997, 33.1%

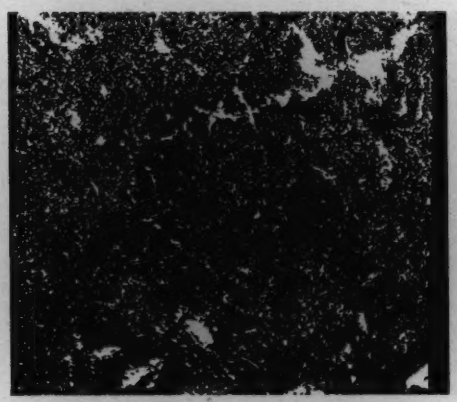

(b) June 15, 1997, 64%

Figure 2.3. Two examples of classified Landsat 5 TM browse images. Snow is shown in white. (a) June 11, 1997, 33.1% snow covered; (b) June 15, 1997, 64% snow covered.

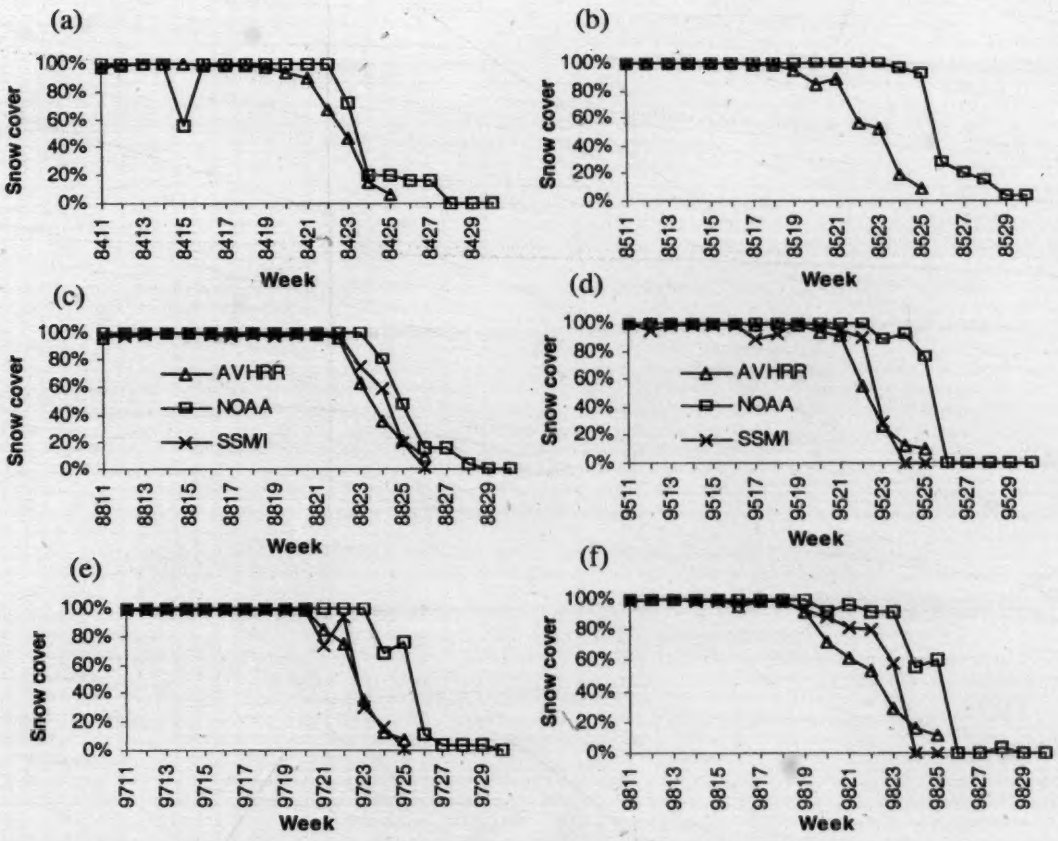

Figure 2.4. Comparison of weekly snow coverage, in percent of fractional snow covered pixels in the study area from AVHRR (triangle), SSM/I (cross), and NOAA (square) for the six years included in the evaluation. The horizontal axis displays week (e.g. 9811 for year 1998 and week 11).

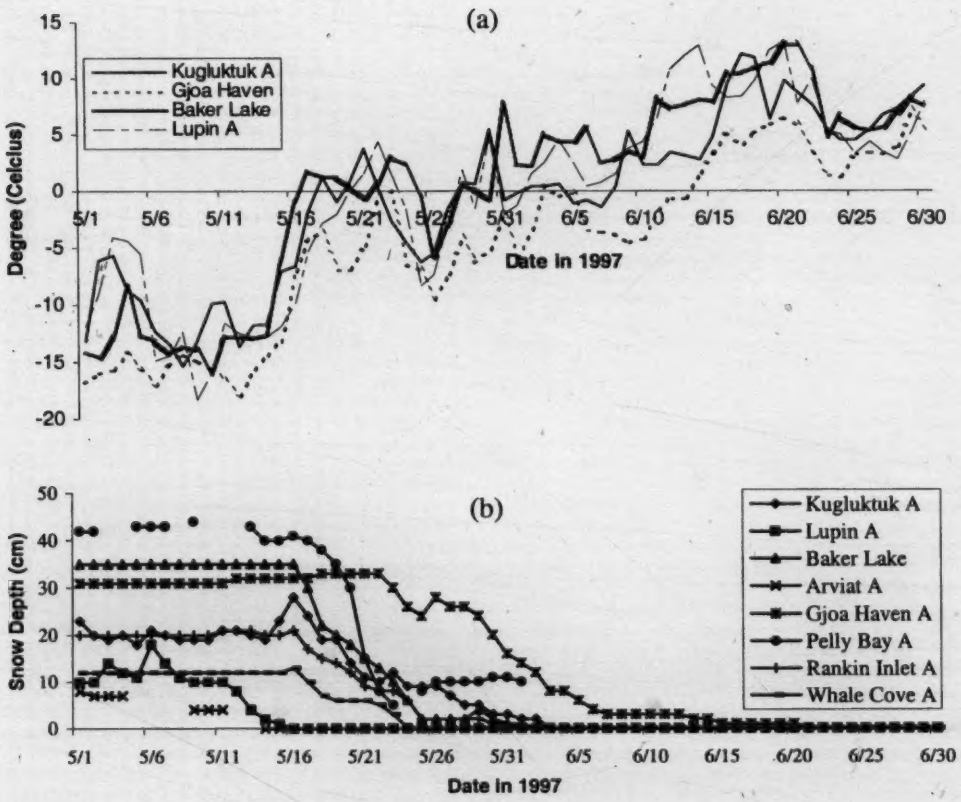

Figure 2.5. Daily mean air temperature (a) and snow depth (b) in May and June of 1997.

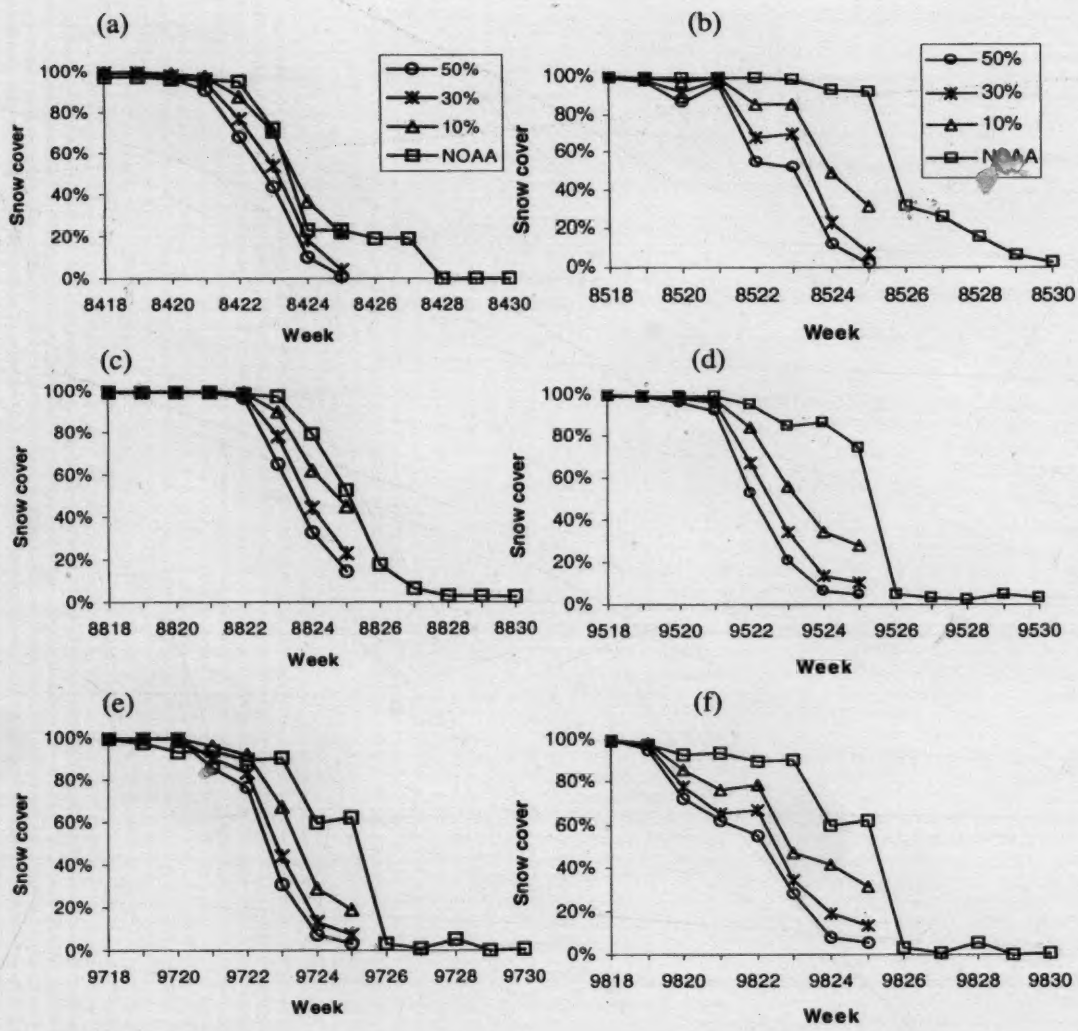

Figure 2.6. Results of re-mapping 5 km AVHRR-derived snow cover to the 25 km NOAA EASE-grid applying 50%, 30%, and 10% thresholds respectively.

Figure 2.7. Daily snow depth network over North America. Station density decreases rapidly north of about 55° N.

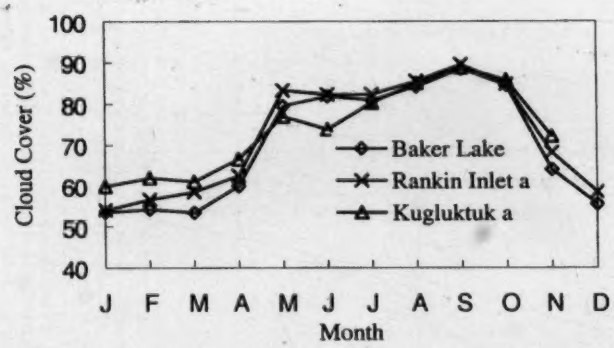

Figure 2.8. Mean annual cycle of total cloud cover in percent for 3 stations in the study area. Data are from the Canadian Climate Normals for the 1971-2000 period.

CHAPTER 3.

MELT SEASON DURATION ON CANADIAN ARCTIC ICE CAPS, 2000-2004

3.1. Introduction

Melting of all glaciers and ice caps (excluding the Antarctic and Greenland ice sheets) would raise sea level by ~0.5 m [Church et al., 2001]. 46% of the area of these glaciers and ice caps is in the Arctic [Dyurgerov, 2002], where there was strong warming in the 20th century [Johannessen et al., 2004]. General Circulation Model simulations predict that this trend will continue and likely increase in the 21st Century due to anthropogenic forcing [Houghton et al., 2001]. It is therefore important to understand how and why the extent and volume of glacier ice in the Arctic have changed in the recent past.

There is over 110,000 km^2 of glacier ice in Canada's Queen Elizabeth Islands (QEI) [Koerner, 2002]. Variations in summer melt drive the inter-annual variability in glacier mass balance in the QEI [Koerner, 2002], so there is a strong interest in monitoring summer melt across the region. Satellite-borne Ku- and C-band radar scatterometers have been used to detect melt on the Greenland Ice Sheet [Wismann, 2000; Nghiem et al., 2001; Steffen et al., 2004]. Smith et al. [2003] used this method to detect melt within single pixels on several small Arctic ice caps, but could not undertake synoptic melt mapping because of the coarse resolution of the sensors (~25 km). In this study, enhanced resolution data from QSCAT [Long and Hicks, 2005] were used to detect the dates of melt onset and freeze-up, and determine annual melt extent and duration across all major ice caps in the QEI for the period 2000-2004. The results provide a measure of variability in summer climate over ice-covered areas remote from long-term weather stations and may prove useful in the development of methodologies for up-scaling site-specific measurements of glacier mass balance [Koerner, 2002] to the regional ice cover.

3.2. Methods

3.2.1. Data

The SeaWinds scatterometer on QSCAT makes measurements at Ku-band frequency with two constant incidence angles: 46° at H-pol over a 1400 km swath, and 54° at V-pol over an 1800 km swath. The resolution of the original data is low. Due to its wide swath and orbit geometry, however, QSCAT observes the Polar Regions multiple times each day, allowing reconstruction of surface backscatter at finer spatial resolution using the Scatterometer Image Reconstruction (SIR) algorithm [Long and Hicks, 2005]. Ascending and descending pass images produced with this algorithm are available daily for the Arctic since July 1999. These images have a nominal pixel spacing of 2.225 km and an estimated effective resolution of 5 km [Long and Hicks, 2005]. Due to ascending-to-descending swath overlap and day boundary effects in the Polar Regions, there is large temporal variability in the measurements used to construct each (ascending/descending) image [Hicks and Long, 2005]. The majority of effective measurement times (local) over the QEI are 22:00 for descending pass images, and 2:00 for ascending pass images. Since ice caps are more likely to be melting at 22:00, descending pass images (H-pol) were used to detect melt in this study.

1:250,000 NTDB (National Topographic Data Base) shapefiles of permanent ice were used to extract ice pixels from the QSCAT data. These shapefiles are based on aerial photographs taken in 1959/1960, and many glaciers and ice caps have changed significantly since then. The ice mask thus includes many mixed pixels along the ice margins and in areas surrounding nunataks. Landsat7 ETM+ (30m) or MODIS (250m) images from 1999 to 2002 were used to identify these mixed pixels and remove them from the ice mask.

To validate the use of QSCAT images for detecting surface melt, 25 air temperature loggers (either Onset HOBO H8-PRO loggers or Veriteq SP2000 temperature-relative humidity loggers with an accuracy of +/- 0.25° C) were deployed at elevations from 130-2010 m on the Prince of Wales (POW) Icefield, Ellesmere Island, from 2001-2003. Sensors were installed in Onset radiation shields (without ventilation) and recorded near-surface (1-1.5m) air temperatures at 30-minute intervals [Marshall et al., in review].

3.2.2. Melt threshold and melt detection

The basis for melt mapping is the reduction in Ku-band radar backscatter (σ^0) that occurs during the melt season. Liquid water in snow dramatically increases microwave absorption and masks out subsurface scattering, resulting in decreased σ^0 at the onset of snowmelt [Ulaby et al., 1981]. Transient increases in σ^0 occur during subsequent periods of refreezing, but σ^0 falls again if snowmelt resumes. At low elevations, the snow pack may be removed completely in summer, exposing glacier ice. Backscatter may then increase over time due to the relative roughness of the ice surface, but detailed comparisons of σ^0 and air temperature records from POW indicate that these increases are significantly less than those associated with refreezing.

During winter (December to February), mean σ^0 values (W_{mn}) increase with elevation, while the standard deviations (W_{sd}) decrease (Figure 3.A.1). Since dry snow is almost transparent at Ku-band frequency [Ulaby et al., 1981], this is mainly due to elevation dependent differences in the physical properties (grain size, surface roughness, density, ice layers) of near surface snow and firn at the end of the previous summer. Nevertheless, this result implies that the magnitude of σ^0 that indicates melting during the following summer will vary with W_{mn} and W_{sd}. Two dynamic thresholds were therefore used to detect melt in each pixel:

$$M_1 = W_{mn} - a\,(W_{sd})^{-b} \qquad (1)$$

$$M_2 = cM_1 \qquad (2)$$

Here a, b, and c are user defined constants. Using trial and error and the air temperature records, optimal values for a, b, and c were identified as: a = c = 1.3, b = -1.1. For each pixel, all periods when either (A) σ^0 remained below M_1 for 3 or more consecutive days, or (B) σ^0 dropped below M_2 for 1 day, were categorized as melt days. Step (A) eliminates possible "false starts" in melt onset; and step (B) makes it possible to capture short periods of melt at high elevations on the ice caps. The first melt day and last melt day plus one were used as melt onset and freeze-up dates respectively. The number of melt days in each pixel was determined as the time period between melt onset and freeze-up minus the duration of any periods without melt within the melt season.

At all elevations on POW, there is a close correspondence between the periods of decreased σ^0 (MD_{QS}) and positive air temperatures (MD_T) in the 20:00 – 23:00 time

window (Figure 3.1). Linear regression gives MD_{QS} = 0.9 MD_T + 9 days (r^2 = 0.78, P<0.001, standard error of the estimate = 10.1 days). There is also a good relationship between MD_{QS} and the annual positive degree-day total (ΣPDD = 0.11+ 0.6036 MD_{QS} + 0.01430 MD_{QS}^2, r^2 = 0.74, p<0.001, standard error of the estimate = 20 PDD).

3.3. Results and Discussion

3.3.1. Melt Climatology

Average melt onset dates range from late May to mid-July (Figure 3.2a), and freeze-up dates range from mid-July to early September (Figure 3.2b). Melt duration ranges from 1 day or less at high elevations to 100 days at low elevations in areas facing Baffin Bay in the southeast QEI (Figure 3.2c). For the whole QEI, the average is 37.7 days (standard deviation (s.d.) = 4.9 days, Table 3.1). Ice cap margins facing either Baffin Bay to the southeast or the Arctic Ocean to the northwest have significantly longer melt seasons than margins facing the interior of the QEI. Areas with longer melt seasons tend to have both earlier melt onset and later freeze-up dates.

The spatial pattern of melt duration can be well explained in terms of surface elevation and distance from Baffin Bay (measured relative to 74.010° N, 75.042° W) – a source of warm maritime air masses. Multiple regression gives: MD_{QS} = 87.98 - 0.0346h - 0.0461x (r^2 = 0.69, p< 0.001), where h is surface elevation (m) and x is distance from Baffin Bay (m). The correlation with distance from Baffin Bay alone is -0.44, while that with elevation is -0.80, so surface elevation is the main influence on melt duration in the QEI. MD_{QS} ranges from 26.3 days (s.d. = 6.7 days) on the Agassiz Ice Cap to 61.7 days (s.d. = 2.4) on the Manson Icefield (Table 3.1). This is consistent with the mean elevations of the ice caps: 1286 m for Agassiz and 585 m for Manson.

3.3.2. Melt Anomalies

For the whole QEI, the longest melt season was 2001 (42.6 days) and the shortest 2002 (30.9 days) (Table 3.1). The pattern for individual ice caps was similar (Table 3.1), although 2003 was the longest melt season on the Northern Ellesmere and Axel Heiberg Island ice caps, and the shortest season on the Manson Icefield. 2004 was the shortest

melt season on the Devon Ice Cap. In relatively cool years, like 2002 and 2004, no melt was detected in some high elevation areas of Ellesmere Island and Axel Heiberg Island (Figure 3.2).

In the southeast QEI, the melt duration anomalies in 2001 and 2002 were of opposite sign at high and low elevations (Figure 3.3, Figure 3.A.2). At low elevations, the anomalies were extremely negative in 2001 and extremely positive in 2002 (i.e. the low elevation anomalies were of opposite sign to the anomalies for the ice caps as a whole). On POW, the decrease in melt duration with increasing elevation was almost linear in 2001 (Figure 3.4). In 2002 the melt duration decreased abruptly between 700m (68 days) and 1100m (29 days), resulting in a much steeper average rate of decrease of melt duration with increasing elevation. Consistent with this, lapse rates in daily mean surface air temperature in June-August were -3.7°C km^{-1} in 2001 and -5.1° C km^{-1} in 2002 [Marshall et al., in review]. In 2001, the melt duration at elevations below 700m was less than in the generally shorter melt season of 2002. This suggests that in some years, like 2002, the temperature regimes of the high and low elevation regions of the Icefield are partially decoupled, while in other years, like 2001, they are more closely related. The correlation coefficient between the June-August daily mean air temperatures at stations at 130m and 1300m was 0.74 in 2001, but only 0.56 in 2002.

Alt [1987] found that high melt years on QEI ice caps were associated with the intrusion of a ridge into the QEI at all levels in the troposphere, while low melt years were associated with the maintenance of a deep cold trough across Ellesmere Island and down Baffin Bay, which resulted in northwest flow off the Polar Ocean. In addition, on POW, less negative vertical gradients in daily mean surface air temperature (2001) are associated with high pressure and anticyclonic flow, while more negative gradients (2002) are associated with low pressure and generally cyclonic flow [Marshall et al., in review]. It was thus hypothesized that melt season duration would vary systematically with geopotential height over the QEI. Indeed, the correlation between the mean melt season duration over the QEI and the mean July 500 hPa height over the region 74-83°N, 70-92°W (as derived from the NCEP-CDAS Reanalysis [Kalnay et al., 1996]) was +0.96 (Table 3.1). Similar relationships were found for all the individual ice caps except the Manson Icefield and, possibly, Sydkap, which have low mean surface elevations and

relatively small areas above 1000m (Table 3.1). Although these results are based on only 5 years of data, they suggest that the less negative surface air temperature gradients associated with high mean geopotential heights result in longer than average melt seasons at higher elevations on the QEI ice caps, and in longer melt seasons overall. In contrast, lower mean geopotential heights are associated with more negative surface air temperature gradients, shorter melt seasons at high elevations, and shorter melt seasons overall.

In the QEI, 2002 was the shortest melt season in the period 2000-2004. On the Greenland Ice Sheet, however, unusually extensive melt in northeast Greenland made 2002 the year with the most extensive melt in the period 1979-2003 [Steffen et al., 2004]. NCEP-CDAS Reanalysis data reveal a positive 500 hPa geopotential height anomaly over northeast Greenland in June and July 2002, while the anomaly was negative over the QEI. This suggests that changes in melt extent and duration in the QEI and northern Greenland may have a common relationship to changes in the distribution of atmospheric mass.

3.4. Summary and Conclusions

The extent and duration of summer melt on the QEI ice caps from 2000-2004 were mapped using enhanced resolution QSCAT backscatter time-series. The 5-year mean melt duration pattern was largely a function of surface elevation, with shorter melt seasons at higher elevations. No melt was detected over some high-elevation regions in 2002 and 2004. For monitoring sites on the POW Icefield, QSCAT derived melt durations correspond well with those derived from air temperature measurements, and are well correlated with the annual positive degree-day total. This suggests that it may be possible to use maps of melt duration to derive positive degree-day fields that could be used to compute summer melt volume using temperature index melt models.

The annual mean melt duration over the larger ice caps is positively correlated with the local 500 hPa height. In a given year, however, the sign of melt duration anomalies may be opposite at high and low elevations on an ice cap. This phenomenon appears to be linked to pressure-related variations in the vertical gradient of surface air temperature over the ice caps, which is more negative in years with relatively low pressure. Thus, in

high-pressure years, ice caps with relatively large areas at high elevations experience longer than average melt seasons, which increases the mean melt duration over the whole ice cap. The mean melt duration over these ice caps can therefore be inversely correlated to the duration at elevations near sea level.

3.5. References

Alt, B.T. (1987), Developing synoptic analogues for extreme mass balance conditions on Queen Elizabeth Island ice caps, Journal of Climate and Applied Meterology, 26, 1605-1623.

Church, J., and 35 others (2001), Changes in sea level, in Climate Change 2001: The Scientific Basis, edited by J. T. Houghton et al., pp. 639–693, Cambridge Univ. Press, New York.

Dyurgerov, M. (2002), Glacier Mass Balance and Regime: Data of Measurements and Analysis, Occasional Paper 55, University of Colorado, Boulder, Colorado.

Hicks, B. R., and D. G. Long (2005), Improving temporal resolution of SIR images for QuikSCAT in the polar regions, Report, Brigham Young University, Provo, UT.

Houghton, J. T., Y. Ding, D. J. Griggs, M. Noguer, P. J. van der Linden, X. Dai, K. Maskell, and C. A. Johnson (Eds.) (2001), Climate Change 2001: The Scientific Basis, Cambridge Univ. Press, New York.

Johannessen, O. M., and 11 others (2004), Arctic climate change: observed and modelled temperature and sea-ice variability, Tellus, Sereris A, 56, 328-341.

Kalnay, E., and 21 others (1996), The NCEP/NCAR 40-year reanalysis project. Bulletin of American Meteorology Society, 77, 437-471.

Koerner, R.M. (2002), Glaciers of the High Arctic Islands, in Satellite Image Atlas of Glaciers of the World. Glaciers of North America - Glaciers of Canada, edited by: R.S. Williams, Jr. and J.G. Ferrigno, U.S. Geological Survey Professional Paper, 1386-J-1, 111-146.

Long, D.G., and B. R. Hicks (2005), Standard BYU QuikSCAT/SeaWinds land/ice image products, Report, Brigham Young University, Provo, UT.

Marshall S. J., M. J. Sharp, D. O. Burgess, and F. S. Anslow (2005), Surface temperature lapse rate variability on the Prince of Wales Icefield, Ellesmere Island, Canada: Implications for regional-scale downscaling of temperature, submitted to International Journal of Climatology.

Nghiem, S. V., K. Steffen, R. Kwok, and W. Y. Tsai (2001), Detection of snowmelt regions on the Greenland ice sheet using diurnal backscatter change, Journal of Glaciology, 47, 539– 547.

Smith, L. C., Y. Sheng, R. R. Forster, K. Steffen, K. E. Frey, and D. E. Alsdorf (2003), Melting of small Arctic ice caps observed from ERS scatterometer time series, Geophysical Research Letters, 30, 2034, doi:10.1029/2003GL017641.

Steffen, K., S.V. Nghiem, R. Huff, and G. Neumann (2004), The melt anomaly of 2002 on the Greenland Ice Sheet from active and passive microwave satellite observations, Geophysical Research Letters, 31, L20402, doi:10.1029/2004GL020444.

Wismann, V. (2000), Monitoring of seasonal snowmelt in Greenland with ERS scatterometer data, IEEE Transactions on Geoscience and Remote Sensing, 38, 1821-1826.

Ulaby, F. T., R. K. Moore and A. K. Fung (1981), Microwave remote sensing: fundamentals and radiometry, Addison-Wesley Publishing Co., Reading, MA.

3.6. Tables

Table 3.1. Average melt duration over the whole QEI and each major ice cap, for the summers of 2000-2004. The mean elevation of each ice cap and the correlation between melt duration and July 500 hPa height are also shown.

	Melt Duration (days)							*Mean*	*Correlation*
Ice cap	2000	2001	2002	2003	2004	Mean	S.D.	*Elevation (m)*	*with 500 hPa*
QEI	39.1	42.6	30.9	41.4	34.7	37.7	4.9	998	0.96
Devon	40.8	50.9	37.5	45.7	35.4	42.1	6.3	1080	0.93
Manson	61.6	63.4	62.4	57.6	63.4	61.7	2.4	585	-0.2
Sydkap	49.0	49.2	32.7	44.1	45.1	44.0	6.7	827	0.77
POW	47.6	53.9	40.1	51.0	44.7	47.4	5.4	967	0.95
Agassiz	29.8	32.6	16.2	29.8	22.9	26.3	6.7	1286	0.92
Axel	40.4	39.0	31.8	40.4	36.0	37.5	3.7	1073	0.93
N. Ellesmere	31.4	32.7	23.9	37.1	26.6	30.3	5.2	1171	0.97

3.7. Figures

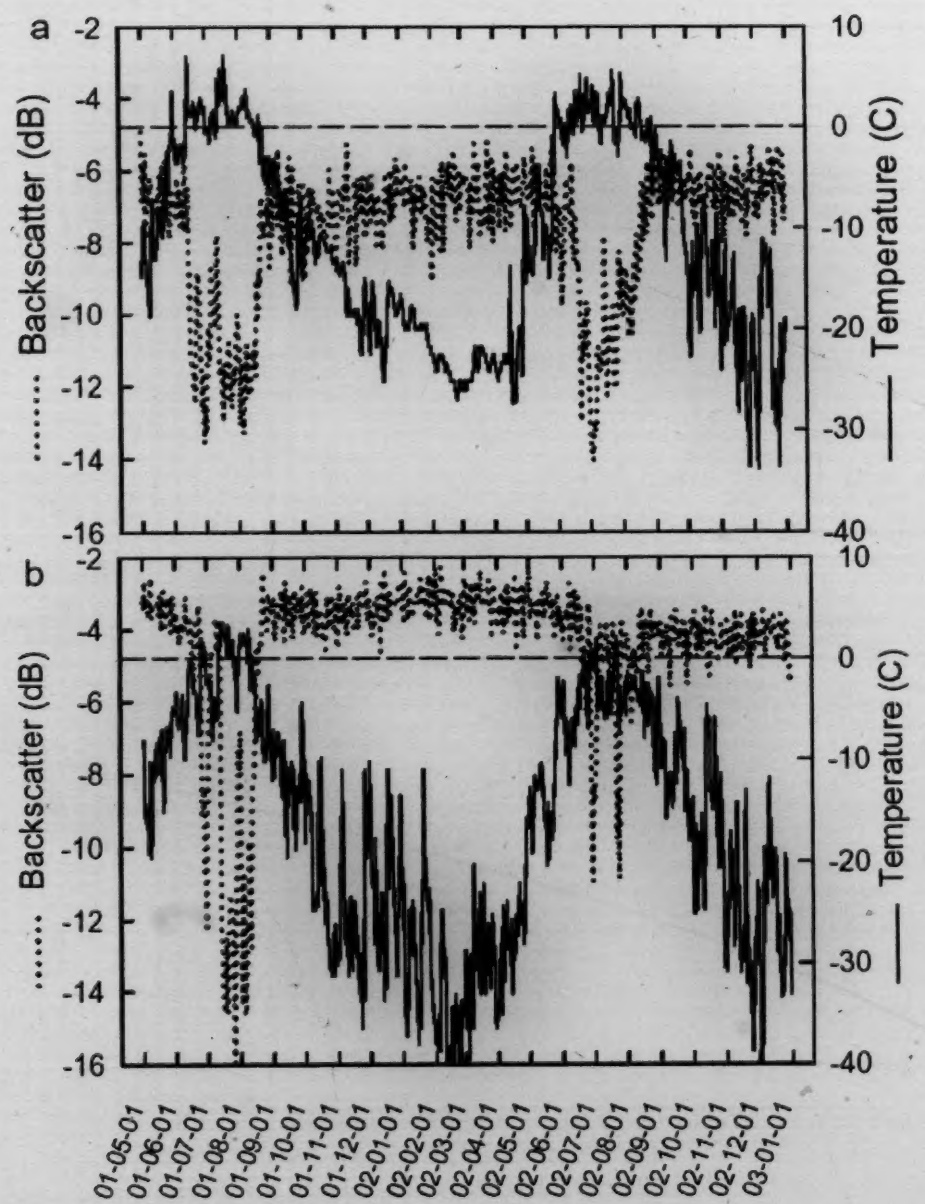

Figure 3.1. Time series of QSCAT σ^0 and surface air temperature during 2001-2002 for 2 locations on POW Icefield, (a) 78.68° N, 74.96° W, 400m a.s.l., (b) 78.61 N°,78.63° W, 1300 m a.s.l.

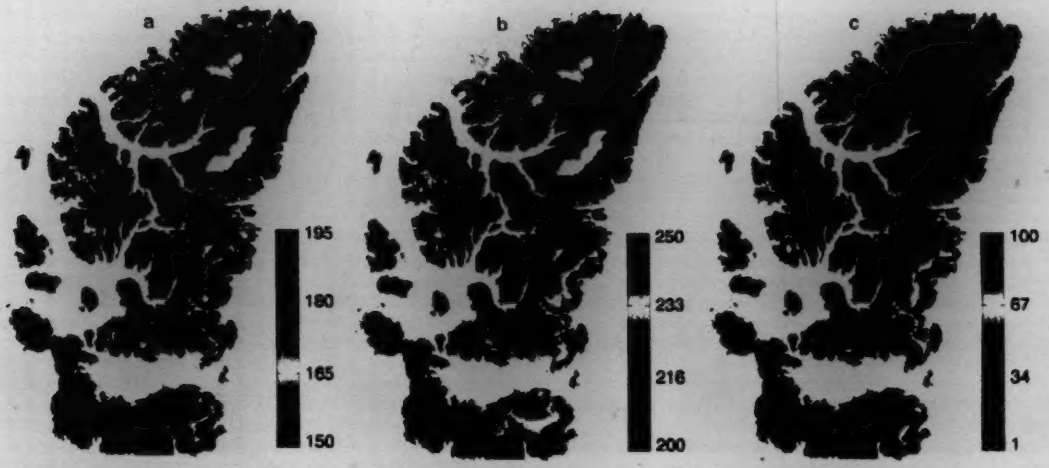

Figure 3.2. Melt climatology for the QEI for the period 2000-2004, (a) melt onset dates; (b) freeze-up dates; (c) the number of melt days. Areas shown as white in (a) and (b) experienced no melt in at least one year during the 5-year period. Numbers in (b) indicate major ice caps:1~Devon; 2~Manson; 3~Sydkap; 4~POW; 5~Agassiz; 6~Axel Heiberg Island; 7~Northern Ellesmere Island.

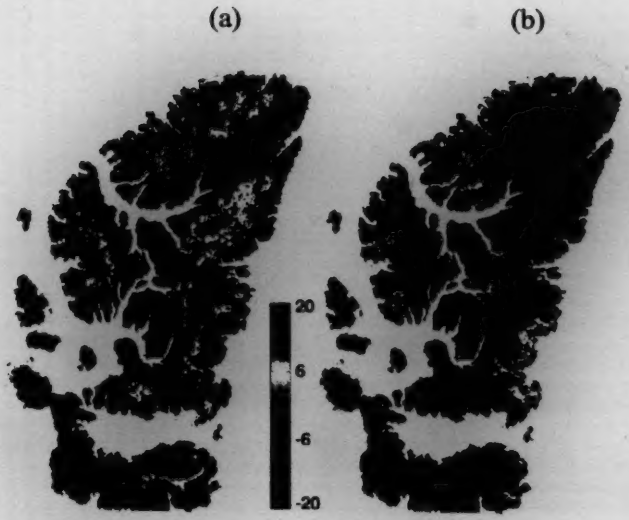

Figure 3.3. Anomalies in melt duration relative to the 2000-2004 climatology for the summers of (a) 2001 and (b) 2002.

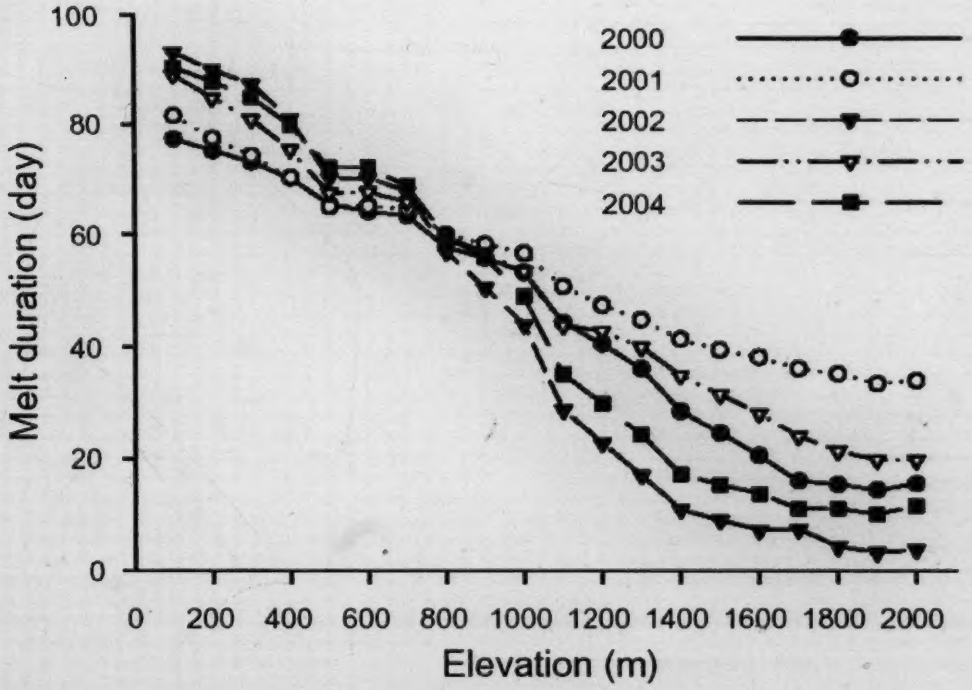

Figure 3.4. Variations of melt duration with elevation on POW Icefield in the summers of 2000-2004.

CHAPTER 4.

MELT SEASON DURATION AND ICE LAYER FORMATION ON THE GREENLAND ICE SHEET, 2000-2004

4.1. Introduction

The Greenland ice sheet plays an important role in regional and global climate due to its high elevation and large fresh water content. Precise knowledge of its mass balance is required to assess its contribution to global sea level change. Due to the gentle slope of the ice sheet surface, the extent of seasonal snowmelt on the ice sheet is a good indicator of climate change [Bindschadler, 1998]. In addition, the amount of melt is potentially an important component of mass balance. Although airborne laser altimeters [Krabill et al., 2004] and satellite radar altimeters [Zwally et al., 1989; 2005; Davis et al., 1998; 2000] have been used to infer changes in ice sheet thickness, they do not by themselves indicate whether the changes observed are due to changes in the rates of snow accumulation or densification in the accumulation zone [McConnell et al., 2000; Zwally and Li, 2002], or to changes in surface melt or ice dynamics in the ablation zone [Thomas et al., 2003]. Field observations in the lower accumulation area of western Greenland show that variations of near-surface firn density can cause annual surface elevation changes of the order of ± 10-20 cm [Braithwaite et al., 1994]. In those parts of the ice sheet accumulation zone where melt occurs, the density of the near-surface firn is mainly controlled by the formation of ice layers by refreezing of meltwater in the cold snow pack. Even small changes in the annual melt and/or annual accumulation can have a noticeable effect on firn-density profiles.

The extent of surface melt on the Greenland ice sheet has been studied with both passive [e.g. Mote and Anderson, 1995; Abdalati and Steffen, 1995] and active microwave sensors [e.g. Jezek et al., 1994; Wismann, 2000; Nghiem et al., 2001] at relatively coarse spatial resolutions (25~50km). These studies revealed large variations in melt extent from year to year, which are related to the surface climatology [Steffen and Box, 2001] and changing atmospheric circulation patterns [Mote, 1998a; 1998b]. Based on passive microwave satellite data, Steffen et al. [2004] demonstrated that the area of the

Greenland ice sheet that experiences summer melt increased by ~16% from 1979 to 2002. Increased melt extent is likely to be associated with a shift to higher elevations in the area of ice layer formation in the percolation zone of the ice sheet, and probably also with an increase in the near-surface firn density in new areas of ice layer formation. In the absence of increased accumulation, this would probably result in a decrease of surface height in these regions. Nghiem et al. [2005] first attempted to detect the extent of ice layer formation in the percolation zone of the Greenland ice sheet using QuikSCAT (QSCAT) scatterometer data. Their study indicated that there was extensive ice layer formation during the record melt year of 2002. Monitoring of annual melt and ice layer formation on the Greenland ice sheet is therefore potentially very useful for identifying the contribution of firn densification to changes in surface height and to accurate estimation of ice sheet mass balance from altimeter measurements.

In the present study, enhanced resolution QSCAT images [Long and Hicks, 2005] were used to detect surface melt on the Greenland ice sheet in the period 2000 – 2004, at a higher spatial resolution than was possible in previous studies. Dates of melt onset and freeze-up and thus melt season duration in each grid cell were determined using a dynamic threshold method. Based on the derived freeze-up dates at each location, a different approach was used to identify inter-annual changes in the distribution of ice layer formation on the ice sheet than the Nghiem et al [2005] approach (hereafter simplified as the Nghiem approach), in which fixed dates were used to indicate the start and the end of melt seasons over the whole ice sheet. The potential for mapping the different snow facies/zones over the Greenland ice sheet from the QSCAT data was also explored, and a bare ice mask was generated to define the maximum bare ice extent during the 2000 – 2004 period.

4.2. QSCAT Enhanced resolution imagery and in situ data

The SeaWinds scatterometer on QSCAT makes measurements at 13.4 GHz Ku-band frequency with two constant incidence angles: 46° at horizontal polarization over a 1400 km swath, and 54° at vertical polarization over an 1800 km swath. The resolution of the original data is 6*25 km [Spencer et al., 2000]. Due to its wide swath and orbit geometry, however, QSCAT observes the Polar Regions multiple times each day, allowing

reconstruction of surface backscatter (σ^0) at finer spatial resolution using the Scatterometer Image Reconstruction (SIR) algorithm [Long, et al., 1993; Long and Hicks, 2005]. Ascending and descending pass images produced with this algorithm are available daily for the Arctic since July 1999. QSCAT σ^0 measurements are available in two forms: termed "eggs"and "slices" [Perry, 2001]. These differ in their spatial sizes and shapes. Egg-based SIR images have a nominal pixel resolution of 4.45 km with an estimated effective resolution of ~ 8-10 km. Slice-based SIR images have a nominal pixel resolution of 2.225 km with an estimated effective resolution of ~ 5 km [Long and Hicks, 2005]. Although lower resolution, the egg measurements have less noise and are less sensitive to calibration errors.

Due to ascending-to-descending swath overlap and day boundary effects in the Polar Regions, there is large temporal variability in the measurements used to construct each (ascending/descending) image [Hicks and Long, 2005]. The effective measurement times (local) over the Greenland ice sheet are 11:00 to 20:00 for descending pass images, and 2:00 to 5:00 for ascending pass images. Since ice surfaces are more likely to be melting during the day than in the early morning, descending pass images were used for melt detection. In addition, Ku-band backscatter of snow is stronger at horizontal polarization than that at vertical polarization because of the lower incidence angle at horizontal polarization [Ulaby and Stiles, 1981]. Egg-based descending pass horizontal polarization images were therefore used to detect melt and changes in ice layer formation in this study.

Near surface air temperatures recorded at 9 automatic weather stations (AWS, see locations in Figure 4.1) in the Greenland Climate Network [Steffen and Box, 2001] were used to assist in the interpretation of the QSCAT σ^0 data and to develop algorithms to detect melt and ice layer formation on the ice sheet. Three of these stations (JAR1, JAR2, and JAR3) are in the ablation zone, one station (Swiss Camp (ETH)) is located at the mean ice sheet equilibrium line altitude (ELA), and another (Summit) is at the ice sheet summit in the dry snow region. The other four stations are located in the percolation zone. Shape files of the Greenland ice sheet taken from the Circum-Arctic map of permafrost and ground ice conditions dataset [Brown et al., 1998] were used as an ice

mask. Only pixels fully contained within the ice sheet were used in this study so as to minimize mixed-pixel effects on the backscatter.

4.3. Surface facies or zones on the Greenland ice sheet

Based on the unique physical properties of the near surface snow, firn, and ice, the Greenland ice sheet can be divided into four zones or "facies" [Benson, 1962]. The distribution of these zones is closely related to the spatial patterns of surface melt and snow accumulation and can be mapped by air-borne or space-borne microwave sensors [e.g. Fahnestock et al., 1993; Jezek et al., 1994; Long and Drinkwater, 1994; 1999]. This is because microwaves can penetrate several meters into the snow and are thus sensitive to both surface and subsurface characteristics [Ulaby and Stiles, 1981]. Variations in surface characteristics are clearly apparent in early winter QSCAT images. Figure 4.1 shows the average November backscatter for the 2000 – 2004 period. The high interior of Greenland exhibits very low backscatter (yellow to blue colors) because little or no melt occurs there during the summer. As a result, the snow has a low density and relatively small grain size. The fine grains produce little volume scattering at the Ku-band frequency. However, the σ^0 is much lower in the southwest interior (blue areas) than in the northeast interior (yellow to light blue areas) of Greenland. This is probably related to the accumulation patterns over the ice sheet. The northeast is located in the precipitation shadow of the main ice sheet topographic barrier and receives minimum snow accumulation [Ohmura and Reeh, 1991; Bales et al., 2001]. Thus the snow grains are probably larger in the northeast than in the southwest because they are exposed longer at the surface. In addition, model simulations suggest that the small-scale surface roughness associated with wind-scouring of the previous summer surface or wind-slab may become significant where there is relatively low accumulation [Long and Drinkwater, 1994]. A rougher surface and a relatively larger contribution from the previous summer surface or wind-slab that is not deeply buried, are the most likely causes of the higher backscatter in the northeast.

At lower elevations outside the interior dry snow zone, there is a region with maximum backscatter (red colors). This is the percolation zone, where some surface melt occurs and melt water percolates into the snowpack and refreezes, producing ice lenses

and pipes that cause the strongest backscattering of the Ku-band signal. Below this region is a narrow zone of intermediate backscatter – the saturation zone (roughly the yellow color band around the lower limits of the percolation zone). Here the entire snow pack reaches the melting point in summer as a result of latent heat release by refreezing of melt water. The firn in the saturation zone is usually denser than in the percolation zone because enhanced compaction occurs under higher temperatures [Benson, 1962], and a solid ice layer can also be formed within the surface firn in some years. Although ice lenses can still be present in this zone, they are probably less effective backscatterers because of the reduced penetration of the microwave energy into the higher density firn or ice. Since the saturation zone is so narrow, it is not easily distinguished from the percolation zone with the 4.45 km pixel spacing in the QSCAT images.

At the lowest elevations, all the annual snow accumulation is melted in the summer, exposing glacier ice. In this zone, surface backscatter dominates and surface roughness determines the magnitude of the backscatter. In the early winter image (Figure 4.1), this region exhibits relatively low backscatter (green to blue margins) compared to the firn at higher elevations. This is probably the result of less surface backscattering from a relatively smooth surface in the bare ice zone and more volume scattering in the saturation/percolation zones.

The locations of the boundaries between the surface zones vary from year-to-year depending on the extent of maximum melt conditions during the summer. Although it is possible to map the annual distribution of the zones using QSCAT data, this is beyond the scope of this study. Because of difficulties in detecting melt onset/freeze-up in the bare ice zone of the ice sheet, which are discussed in the next section, a bare ice mask that defines the inferred maximum extent of bare ice during the 2000 – 2004 period was generated as follows. First, the mean November backscatter was mapped for each year. Then the minimum mean November backscatter recorded at each grid cell over the 5-year period was used to outline the bare ice region. The strong gradient between low values of σ^0 in the bare ice zone and high values of σ^0 in the saturation/percolation zone was used as an indicator, and a backscatter of -6.9 dB was chosen to define the upper limit of the bare ice zone. Using this approach, stations JAR1 and JAR2 are found to lie in the bare ice zone, while ETH station is located in the saturation/percolation zone. This is

consistent with observations [Steffen and Box, 2001] and supports the choice of this threshold.

A total of 78708 cells or 1.58×10^6 km^2 in area were retained for analysis after removing the bare ice and the mixed pixels along the ice sheet margin. The total ice-covered area on Greenland is 1.71×10^6 km^2 (including surrounding glaciers and small ice caps) [Church et al., 2001]. Thus approximately 8% of the ice sheet area along the perimeter was excluded from the analysis in this study.

4.4. Melt detection and results

4.4.1. QSCAT melt signature

The basis for melt mapping is the reduction in Ku-band σ^0 that occurs during the melt season. Liquid water in snow dramatically increases microwave absorption and masks out subsurface scattering, resulting in decreased σ^0 at the onset of snowmelt [Ulaby and Stiles, 1981]. Figure 4.2 shows 4-year time series of QSCAT σ^0 and air temperature (11:00~20:00) at the Crawford Point1 (CP1, Figure 4.2a), Swiss Camp (ETH, Figure 4.2b), and JAR2 (Figure 4.2c) stations on the western flank of the Greenland ice sheet (see locations in Figure 4.1). CP1 is located in the percolation zone at 2022 m a.s.l., ETH is located at the mean ice sheet equilibrium line altitude, i.e., at 1150 m a.s.l., and JAR2 is located in the ablation zone at 568 m a.s.l. [Steffen and Box, 2001]. JAR2 is close to the ice sheet margin, but still within the pure ice mask. QSCAT σ^0 decreases dramatically as the air temperature approaches the melting point at the beginning of each melt season. As the melt season progresses, however, σ^0 exhibits very different patterns of variation at different stations. At CP1 and ETH, the period of decreased σ^0 is closely associated with the occurrence of positive air temperatures throughout the melt season; intermittent cold periods with air temperatures below freezing point correspond to periods when σ^0 returns all or part-way to its winter value. At JAR2, however, σ^0 increases again within a few days of melt onset, even though air temperatures remain positive. Above the ELA (CP1 and ETH), the winter snow accumulation is not completely removed during the summer, and the wet snow pack greatly reduces the σ^0. Below the ELA (JAR2), however, all the winter snow is melted

during the summer, exposing bare glacier ice, which may have a rough surface and exhibits higher σ^0. The timing of the increase of σ^0 depends on the amount of snow accumulation in the previous winter and the melt rate of the snow. As a result, freeze-up dates and melt season duration cannot be determined reliably for the bare ice zone. Grid cells in the bare ice zone were therefore removed from the following analysis by applying the bare ice mask described in section 3.

4.4.2. Melt detection

Wang et al. [2005] used enhanced resolution slice-based QSCAT images to detect melt on ice caps in the Queen Elizabeth Islands (QEI) over the Canadian high Arctic. In this region, the mean values of the winter σ^0 (W_{mn}) increased with elevation, while the standard deviations of σ^0 decreased from the ice margin to the summit areas of the ice caps. These features were used to establish the σ^0 thresholds used to detect melt over the QEI. Similar behaviour was found on the Greenland ice sheet, except that the highest values of W_{mn} were found in the percolation zone, rather than over the highest elevation regions of the ice sheet. This is because the dry snow zone is extensive on the Greenland ice sheet but very limited in most years on the QEI ice caps. In the percolation zone of the Greenland ice sheet, σ^0 can decrease noticeably over the winter at a single location, e.g. Figure 4.2 (a), while σ^0 changes relatively little over the winter on the QEI ice caps [Wang et al., 2005, their Figure 1]. This is because high rates of snow accumulation occur in some regions of the Greenland ice sheet [Ohmura and Reeh, 1991; Bales et al., 2001], and the backscatter from ice lenses and pipes in the snow pack decreases as snow accumulates on the surface [Nghiem et al., 2005]. On the QEI ice caps, however, winter snow accumulation rates are relatively low [Koerner, 1979] and this effect is less marked. A slightly different threshold-based melt detection technique was therefore used to map melt on the Greenland ice sheet:

$$M_1 = W_{mn} - a \quad (1)$$

$$M_2 = W_{mn} - b \quad (2)$$

Here a and b are user defined constants. Using trial and error and the available air temperature records, two sets of optimal values for a and b were identified as: a1=2.0, b1=3.0; a2=3.0, b2=3.5. A1 and b1 were used for the majority of pixels, and a2 and b2

were used for pixels experiencing very high winter accumulations (mainly in the south and west of Greenland) so that σ^0 of those pixels usually have large decreases during the winter. Pixels for which the inter-annual variability in W_{mn} was more than 3.9 dB in the 2000 – 2004 period (~2.6% of the total pixels) were optimally chosen for applying a2 and b2. For each pixel, all periods when either (i) σ^0 remained below M_1 for 2 or more consecutive days, or (ii) σ^0 dropped below M_2 for 1 day, were categorized as melt days. Step (i) eliminates possible "false starts" in melt onset; and step (ii) makes it possible to capture short periods of melt at high elevations on the ice sheet. The first melt day and the last melt day plus one were taken as the dates of melt onset and freeze-up respectively. The number of melt days (melt duration) in each pixel was defined as the time period between melt onset and freeze-up minus the duration of any periods without melt within the melt season.

In addition to the observations from ETH and CP1, air temperature records for the period of 2000 – 2003 from Dye-2, NASA-SE, and Tunu-N (all of which are located in the saturation/percolation zone of the ice sheet) were used to validate the estimates of melt duration from QSCAT. There is a close correspondence between the melt durations derived from the QSCAT images (MD_{QS}) and positive air temperatures (MD_T) in the 11:00 – 20:00 time window. A linear regression gives $MD_{QS} = 1.08\ MD_T + 3.7$ days ($r^2 = 0.94$, $P<0.001$, standard error of the estimate = 7.9 days). There is also a good relationship between MD_{QS} and the annual positive degree-day total ($\Sigma PDD = 0.88 + 0.2542\ MD_{QS} + 0.0135\ MD_{QS}^2$, $r^2 = 0.95$, $p<0.001$, standard error of the estimate = 12.8 PDD). This implies that the melt season duration estimated from QSCAT is longer than that derived from the air temperature records. There are three possible reasons: (i) melt occurred under subfreezing near surface air temperature conditions, this is especially likely at high elevations where the atmosphere is thinner and under clear sky conditions when short-wave radiation receipts at the ice surface are high; (ii) QSCAT detects subsurface melting while the ice surface is frozen due to a sudden drop of the near surface air temperature (to below melting point); (iii) The melt thresholds are insufficiently conservative and the melt season duration was overestimated from QSCAT. Since there are no field measurements of snow wetness, it is not possible to directly estimate the accuracy of the melt season duration estimated from QSCAT using the

chosen thresholds. However, the high r^2 values for the above two regression analyses indicate that the estimated melt season duration is in very good correspondence with the air temperature observations. It should therefore be suitable for analyses of the spatial and temporal distributions of surface melt over the ice sheet and their relationship to climatic variability during the study period.

4.4.3. Melt results, 2000 –2004

4.4.3.1. Melt extent and duration

A total of 78708 cells or 1.58×10^6 km^2 in area were retained for analysis after removing the bare ice and mixed pixels along the ice sheet perimeter. There are four days during the study period with missing data: days 132, 133, and 188 in 2001, and day 228 in 2003. The backscatter for these days was calculated by linear interpolation from adjacent days. Figure 4.3 shows the annual and average melt extent and duration during the 2000 – 2004 period. Areas shown in white experienced no melt in that particular year. Over the 5-year period, the maximum melt extent occurred in 2002, and the minimum in 2001. Figure 4.4 shows the melt season duration anomalies in each year relative to the 5-year mean (Figure 4.3f). Over west, east, and northeast of Greenland (north of 66° N), there was an extremely positive melt anomaly in 2002; the most positive melt anomaly in southern Greenland occurred in 2004. In 2001, melt anomalies were negative over most of Greenland except for the northwest corner, where melt extended to higher elevations than in any other year of the 5-year period. The annual percentage of the ice sheet that experienced melt for at least one day was calculated as the melt area divided by the total area (Table 4.1, column 1). The annual mean melt duration for the ice sheet as a whole was calculated in two ways – (i) the sum of melt durations in all cells that experienced melt was divided by the total number of cells (Table 4.1, column 2), and (ii) the sum of melt durations in all cells that experienced melt was divided by the total number of cells that experienced melt in a particular melt season (Table 4.1, column 3). 2002 had the most extensive melt extent within the 5-year period (79.7%), and 2001 the least (44.2%). This is consistent with the mean melt duration (for all cells) that was longest in 2002 (20.5 days) and shortest in 2001 (14.3 days). However, the mean melt duration for melt

cells was shortest in 2002 (25.7 days). This is because the large melt extent in 2002 was mainly due to widespread melt over high elevation areas of west, east, and northeast Greenland that lasted for only a few days (Figure 4.3c). For melt cells, the mean melt duration was longest in 2003, which is consistent with the air temperature observations at the AWS sites (not shown) and the fact that the low elevation regions of the ice sheet had extremely positive melt duration anomalies in 2003 (Figure 4.4d).

Of the 78708 cells 68181 experienced melt for at least one day during the 2000-2004 period. The total area affected by melt was 1,362,045 km^2, or 86.46% of the areas of the ice sheet. This excludes the area of the bare ice mask and mixed pixels, most of which probably did experience melting. The average melt duration is shown in Figure 4.3f. The melt duration decreases rapidly as elevation increases from the ice margin to the high interior. To a first approximation, areas above 2000 m in the north and 2500 m in the central and south dome areas of the ice sheet experienced less than 4 days of melt (grey to purple coloured region in Figure 4.3f). On average, 55% of the melt area experienced melt for less than 1 week each year, and about 76% of the melt area experienced less than 30 days of melt (Figure 4.5). Only 13% of the melt regions experienced more than 60 days of melt.

Figure 4.6 shows the average melt duration, melt distribution and melt occurrence within each elevation band. The melt distribution was calculated as the percentage of the number of all melt pixels that occurred within each elevation band. The melt occurrence was calculated as the percentage of the pixels within an elevation band that experienced melt. The melt duration decreases as the elevation increases, and it decreases more rapidly above 1400 m than at lower elevations. The melt distribution curve shows that there are more melt pixels at high elevations (>1800 m) than at low elevations, this reflects the facts that the central part of the ice sheet lies at 3000 m or more above sea level, and 87% of the ice sheet is above 1,220 m a.s.l. [Putnins, 1970], and that most pixels at low elevations were excluded from the analysis, either because they were mixed pixels or because they were located in the bare ice zone. All pixels within elevation bands below 1800 m experienced melt (melt occurrence=100%). Even for elevation bands as high as 2800-3000 m, nearly 75% pixels experienced melt during the study period.

Stepwise regression indicates that the spatial pattern of mean melt duration can be well explained in terms of surface elevation and latitude: MD_{QS} = 364.69 - 0.0435h – 3.434y (r^2 = 0.76, $p<0.0001$), where h is surface elevation (m), and y is latitude (degrees north). The r^2 only increases by 0.002 when longitude is included in the regression, thus it is only weakly correlated with surface melt duration and was not included in the regression. The correlation with elevation alone is –0.64, while that with longitude is –0.18, and that with latitude is –0.38. Thus, surface elevation and latitude appear to be the main influences on mean melt duration on the Greenland ice sheet.

4.4.3.2. Seasonal melt cycle

To illustrate the seasonal cycle of surface melt, the daily melt extent was calculated for the period May to October each year. The average for the 5-year period was also calculated (Figure 4.7). Figure 4.8 depicts the distribution and occurrence of melt in each summer month. The melt occurrence was calculated as the average percentage of days with melt in each month over the 2000 – 2004 period. On average, melt starts in the middle of May along the west and southeast coasts. In early June melt begins to spread and the melt extent increases rapidly, reaching its peak in late June to mid July. From mid July, refreezing begins to occur on the north and east flanks of the ice sheet and the areal extent of melt begins to decrease. Most of the ice sheet refreezes by the end of September, but there is still some melt in southern Greenland in October, which is largely due to the prolonged melt in 2003. Although the melt extent is similar in June and July (Figures 4.8 b and c), the melt occurrence is much higher in July than in June for low elevation areas.

Figure 4.7 also shows the progression of melt extent in each individual summer. It is noticeable that each melt season is characterised by up to 5 or 6 melt events of a few days duration, during which the melt extent can fluctuate considerably. The timing of these events varies from year to year. This will be further discussed later.

4.4.3.3. Regional differences in surface melt

In order to examine the regional variability of melt extent and duration, the Greenland ice sheet was divided into nine regions defined by topographic barriers. These regions are

similar to those defined by Ohmura and Reeh [1991], although two of their larger regions – Jakobshavn and Angmagssalik were sub-divided into smaller regions to conform with the higher spatial resolution of this study (Figure 4.9). Due to differences in the orientation of the topographic barriers relative to the major stream lines of air flow over the ice sheet and the distribution of warm air sources, these barriers play an important role in dividing the ice sheet surface into different climatic zones [Mote and Anderson, 1995; Ohmura and Reeh, 1991]. The mean melt duration in each of the nine regions was calculated for each summer between 2000-2004 (Table 4.2). In general, the melt duration is longer for regions in west Greenland (regions 1, 2, 3, and 4) than for regions at similar latitudes in east Greenland (regions 6, 7, 8 and 9), and melt duration decreases from south to north. This is consistent with the conclusion of Steffen and Box [2001] that the climate on the eastern side of Greenland is colder than that on the western side at the same latitude. Region1, located in the southwest corner of Greenland, has a relatively low mean elevation (2035m) and the longest mean melt duration (68.2 days) over the 5-year period. Region 7, which includes the highest regions of the ice sheet, has the highest mean elevation (2840m) and the shortest mean melt duration (7.0 days). Although 2002 had the most extensive melt extent and duration for the ice sheet as a whole (Table 4.1), only three regions on the eastern side of the ice sheet (regions 6, 7, and 8) had their obvious maximum melt duration in 2002. Regions in the south and southwest had their maximum melt duration in either 2003 (region 1) or 2004 (regions 2, 3, and 9). Although regions 2, 3, and 6-9 all had their minimum melt durations in 2001, region 5, in the northernmost part of Greenland, had its maximum melt duration in 2001. This demonstrates the highly variable characteristics of surface melt over the different regions of the ice sheet.

The seasonal melt cycle for each region is shown in Figure 4.10 by the mean daily melt extent as a percentage of the total area of the region and the standard deviation (SD) of the daily melt extent over 2000 – 2004. The southern regions (region 1, 2, 3, and 9) have the longest melt seasons, extending from early May to late October. In contrast, the northernmost region (5) and the northeast region (6) have the shortest melt seasons. These regions are the last to show melting, and the earliest to show freezing. The standard deviation curves in Figure 4.10 indicate the inter-annual variability of the daily

melt extent over the 2000 – 2004 period. Region 1, where most pixels experienced melt every summer, has the lowest SD. In contrast, region 6, where most pixels only experienced melt in very warm years, like 2002, has the highest SD.

4.4.4. Influence of atmospheric circulation on surface melt patterns

Based on the daily 700 hPa geopotential height field, Mote [1998b] found that the strength and location of the North American trough and Baffin Bay low were highly related to the extent of surface melt on the Greenland ice sheet. A westward displaced North American trough was associated with increased melt whereas an eastward displaced trough was associated with reduced melt on the ice sheet.

The correlations between the monthly mean melt duration (MD) and the monthly mean geopotential height (as derived from the National Centers for Environmental Prediction/National Center for Atmospheric Research (NCEP/NCAR) Reanalysis 1 [Kalnay et al., 1996]) from May to August during the 2000-2004 period were calculated for each of the nine topographic regions on the Greenland ice sheet. To find the pressure level that correlates most strongly with the surface melt, separate correlation analyses were conducted for the 700 hPa, 500 hPa, and 300 hPa pressure levels (Table 4.3). For comparison, the correlations between mean melt extent (ME) and geopotential height for each region are also included in Table 4.3. Geopotential height at the 300 hPa pressure level – the upper troposphere, correlates most closely with surface melt on the Greenland ice sheet. In general, geopotential height at all three pressure levels is better correlated with MD than with ME. This suggests that MD might be a better index of climatic conditions over the ice sheet than the more widely used parameter, melt extent [e.g. Abdalati and Steffen, 1997; 2001; Mote, 1998a; 1998b]. The correlation coefficients of mean daily melt extent and mean daily 300 hPa geopotential height for each region are reported in the last column of Table 4.3, and are similar to those derived from the monthly analyses.

Figure 4.11 illustrates the daily melt extent for each of the nine regions of the ice sheet. It clearly shows that there was a distinct high melt event from June 28th to July 2nd (day 179 – 183), 2002, for all the regions except Regions 1 and 2, during which melt on the northeast side (Region 6) of the ice sheet reached the highest elevations during the

2000-2004 period. To investigate the causes of this extensive melt event, maps of 300 hPa geopotential height (Figure 4.12) and 700 hPa isotachs (Figure 4.13) were examined.

On June 25th 2002 (Figure 4.12a), the main 300 hPa vortex was centered on the North American side of the Polar Ocean, with an elongated south-north shape across the west and northwest of Greenland, while a less intense 300 hPa low was situated in the Denmark Strait to Norwegian Sea region. A cyclone was located at lower latitude along the east coast of Canada. Under these atmospheric settings, the flow was weak and primarily zonal over the Greenland ice sheet, resulting in little melt in all regions on the ice sheet (Figure 4.11).

By June 26th 2002 (Figure 4.12b), the main 300 hPa polar vortex split into two parts and the main part retreated northward to the Polar Ocean. In the meantime, the cyclone over the east coast of Canada migrated towards the northeast, and merged with the 300 hPa low centered over Davis Strait. The low over Denmark Strait and the Norwegian Sea moved eastward, away from the east coast of Greenland. Under these atmospheric circulation conditions, a ridge was building from the North Atlantic Ocean and extending onto the ice sheet from the area southeast of Greenland. From June 27th to 28th (Figures 4.12 c and d), the 300 hPa lows contracted, and the main center located over the Arctic Ocean was linked to lows centered near Davis Strait and over the Barents Sea region. These likely favored the strengthening of the Atlantic ridge, which reached northern Greenland by June 28th.

From June 26th to 28th, the saddle like atmospheric setting resulted in strong southerly flow over western Greenland (Figure 4.13). Air was forced to rise orographically over the southern Greenland ice sheet, but the flow brought warm air to the west and the north of the ice sheet. According to the melt detection results from QSCAT, the onset of melt over most of the high elevation areas of northeast Greenland where melt occurred in the summer of 2002 (Figure 4.15a) was on June 28th (day 179). During this period, the daily melt extent increased dramatically over most regions of the ice sheet (Figure 4.11). In comparison to the other summers, the increase in the daily melt extent was especially remarkable for regions 6 and 7. However, the daily melt extent was not unusually high for regions 1 and 2 during this period. We suspect that snowfall might

have occurred under the strong orographic forcing in southern Greenland, reducing the occurrence of extensive melt there.

By June 29th (Figure 4.12f), all the 300 hPa lows began to weaken, as did the Atlantic ridge. By June 30th (Figure 4.12e), the low over Davis Strait split into two cyclones, and one of which moved eastward around the southern tip of Greenland, cutting off the already weakened Atlantic ridge. The southerly surface flow over western Greenland was reduced dramatically (Figure 4.13d). After June 30th, the areal extent of daily melt in most regions of the ice sheet decreased until the beginning of the next melt event (Figure 4.11).

Thus, the extensive melt that occurred in the summer of 2002 was due to a single high melt event that lasted for only a few days. The most likely cause of the high melt event was the intrusion of a ridge from the North Atlantic Ocean, bringing warm air to the west and north of the ice sheet.

4.5. Inter-annual changes in the distribution of ice layer formation

4.5.1 Ice layer formation: signature and detection

Figure 4.2 shows 4-year time series of QSCAT σ^0 at three AWS locations. At CP1 (Figure 4.2a) there were obvious jumps in σ^0 between the periods immediately before and after the 2001 and 2002 melt seasons. Nghiem et al. [2005] observed a similar phenomenon at NASA-E weather station (see location in Figure 4.1) in 2002. At NASA-E, field observations confirmed that the main cause of the σ^0 jump was a 2-cm thick ice layer in the snowpack and a number of vertical percolation features. As snow accumulates in the following winter, these ice layers become buried and their contribution to σ^0 becomes weaker because of the two-way attenuation in the snow [Nghiem et al., 2005]. This explains the decrease of σ^0 during the winter (Figure 4.2a), the magnitude of which appears to depend on the amount of snow accumulation. For low accumulation areas, such as the northeast of Greenland [Ohmura and Reeh, 1991; Bales et al., 2001], the over-winter decrease in σ^0 is negligible. For example, at station Tunu-N (Figure 4.14), σ^0 increased from ~-6.0 dB to ~ -3.0 dB over summer 2002 because of ice layer formation during that summer, but it decreased by only about 0.8 dB over the 2002

– 2003 winter. For areas such as the south-eastern corner of Greenland, where the snow accumulation is greatest [Ohmura and Reeh, 1991; Bales et al., 2001], the decrease of σ^0 is much larger (Figure 4.14). The magnitude of the decrease in σ^0 varies noticeably between freezing seasons. It was ~ 2.0 dB over the 2000 – 2001 freezing season, and ~ 5.0 dB over the 2002 – 2003 freezing season.

Nghiem et al. [2005] developed the first algorithm to detect ice layer formation on the Greenland ice sheet. Their approach was to subtract the biweekly averaged backscatter for a period before a melt season from the biweekly averaged backscatter for a period after the same melt season to determine the backscatter change. A possible limitation of this approach is that, in many regions, σ^0 may change between the end of one melt season and the start of the next because of attenuation by winter snow accumulation. Since the magnitude of attenuation is probably a function of the magnitude of over winter snow accumulation, this implies that the magnitude of ice layer formation suggested by the over-summer change in σ^0 will be a function of the end of winter σ^0, and hence of the over-winter snowfall. Another possible limitation of the Nghiem approach is that fixed dates were used to mark the start and the end of the melt season, when these dates can vary considerably in reality. Figure 4.15 shows the average melt onset dates (a) and freeze-up dates (b) over the ice sheet during the 2000 – 2004 period. From the ice sheet margin to the high interior, melt onset dates ranged from ≤ day 150 (~ the end of May) to ≥ day 220 (~ beginning of August). The freeze-up dates ranged from ≤ day 180 (~ the end of June) at the highest elevations to ≥ day 260 (~ mid September) at the lowest elevations. Therefore using fixed melt onset/freeze-up dates to indicate the melt season duration for the whole ice sheet will result in some bias in the derived extent of ice layer formation.

To avoid these problems, a different approach was used to identify changes in the distribution of ice layer formation in this study. This approach compares the magnitude of σ^0 between biweekly periods starting two weeks after the end of successive melt seasons, and assumes that the larger the increase in σ^0 between successive melt seasons, the greater the increase in ice layer formation between the two melt seasons. Where σ^0 decreases between melt seasons, this implies reduced ice layer formation in melt season

2. For the purposes of these calculations, actual freeze-up dates for each grid cell were used instead of fixed dates to determine the timing of the end of each melt season. For pixels that experienced no melt in a given melt season, a fixed date – October 31st was chosen as the reference date, and the biweekly averaged σ^0 was determined for those pixels as well.

4.5.2. Changes in the distribution of ice layer formation, 2000 – 2004

Maps of the changes in the biweekly averaged σ^0 between successive ends of melt season periods for the years 2000 – 2004 at each of the 78708 cells are shown in Figure 4.15. The solid white and black contours represent the upper limits of melt for the current and the previous summers respectively. The yellow to red colors represent regions where there was an increase in backscatter from ice layers in the snowpack relative to the previous fall. The darker the red color, the larger the backscatter increase. Typically, large increases in backscatter occur in regions where the upper limit of melt in the current summer lies inside the limit in the previous summer (for example, the extensive region that encircles much of the northern part of the ice sheet in 2002). The cyan to blue colors represent regions with decreased backscatter. Typically these are regions where the upper limit of melt in the previous summer lies within the upper limit of melt for the current summer (for example, the region that runs north-south along the western side of Greenland in 2001 (Figure 4.15b)). Figure 4.15 reveals significant variations in the extent and distribution of new ice layer formation during the 2000 – 2004 period. Melt duration maps (Figure 4.3) indicate that ice layers can be formed with as little as one day of melt in most areas of the percolation zone except in the northeast region where the accumulation is the lowest and summer melt occurred only in 2002. It appears that obvious ice layer formation in the northeast region is associated with more than 5 days of melt.

Overall 2002 had the most extensive increase in the area of ice layer formation in the west, east, and northeast of Greenland, and 2004 had the most in southern Greenland. 2001 had the largest decrease in the area of ice layer formation over most regions of the ice sheet, but had a considerable increase in the area of ice layer formation in the northwest corner of Greenland where melt occurred only in 2001. In 2003, there were

clear decreases in σ^0 in areas where there had been increases in the area of ice layer formation in 2002. This is consistent with the reduced melt extent in these areas in 2003. These large inter-annual variations in the distribution of regions of ice layer formation could result in significant variations in near surface firn density that should be accounted for in the estimation of mass change from altimeter measurements.

4.6. Summary and conclusion

Time series of enhanced resolution QSCAT backscatter allow the detection of summer melt on the Greenland ice sheet at a higher spatial resolution than was possible in previous studies. The results reveal unique characteristics of melt in nine topographic regions for the 2000-2004 period. The distribution of the mean melt duration was largely a function of surface elevation and latitude, with shorter melt seasons in regions with higher mean elevations and at higher latitudes. In addition, the melt seasons were shorter at a given latitude on the east side of the ice sheet than on the west side, which is consistent with the climatology of Steffen and Box [2001]. Although melt occurred over 86.46% of the ice sheet during the study period, nearly 55% of the melt areas experienced melt for less than 1 week each year. The mean melt extent in each region of the ice sheet was positively correlated with the local 300 hPa geopotential height at both daily and monthly scales. However, the monthly mean melt duration was more strongly correlated with the local geopotential height at all pressure levels than was the melt extent. The extensive melt that occurred in the summer of 2002 was associated with the intrusion of a ridge over the ice sheet from the North Atlantic Ocean. Warm air brought by strong southerly flow associated with the ridge, combined with adiabatic warming on the lee side of the ice sheet, are the most likely causes of the extensive melt on the ice sheet.

Changes in the distribution of ice layers formed by refreezing of melt water in the percolation zone of the ice sheet were mapped using the change of biweekly averaged backscatter between the freeze-up periods in successive falls. Extensive increases in the area of ice layer formation were detected in the summer of 2002, which is consistent with the occurrence of maximum melt conditions at high elevations of the ice sheet in that year. Inter-annual changes in the amount of ice layers formed at a site are probably related to changes in the rate of densification of near surface snow and firn, and may be

associated with changes in surface height that are not indicative of mass balance changes [Braithwaite et al., 1994]. The distribution of ice layers in snow may also be an important influence on the performance of satellite radar altimeters over ice sheets and on the accuracy of surface elevation retrievals [Davis and Ferguson, 2004; Thomas et al., 2006]. A recent study [Thomas et al., 2006] indicated that the rate of thickening estimated from ERS radar altimeter measurements (1992 – 2002/2003) for high elevation regions (> 1500 m) of Greenland was greater than that estimated from ICESat/Airborne Topographic Mapper laser altimeter data (1993/1994 – 2004) over nearly the same time intervals. This is probably a result of increased surface melting in warm summers (e.g. 2002) extending the upper limit of the percolation zone to higher elevations, and a consequent lifting of the radar-reflecting ice layers within near-surface snow [Thomas et al., 2006]. Systematic mapping of ice layer formation over Greenland may therefore have an important role to play in the interpretation of altimeter-derived measurements of changes in the surface elevation of the ice sheet.

4.7. References

Abdalati, W., and K. Steffen (1995), Passive microwave-derived snowmelt regions on the Greenland ice sheet, Geophysical Research Letters, 22, 787–790.

Abdalati, W., and K. Steffen (1997), Snowmelt on the Greenland ice sheet as derived from passive microwave satellite data, Journal of Climate, 10, 165–175.

Abdalati, W., and K. Steffen (2001), Greenland ice sheet melt extent: 1979-1999, Journal of Geophysical Research, 106, 33,983-33, 988.

Bales, R. C., J. R. McConnell, E. Mosley-Thompson, and G. Lamorey (2001), Accumulation map for the Greenland ice sheet: 1971 – 1990, Geophysical Research Letters, 28, 2967-2970.

Benson, C. S. (1962), Stratigraphic studies in the snow and firn on the Greenland ice sheet, Research Report 70, Snow, Ice, and Permafrost Research Establishment, U.S. Army Corps of Engineers, Hanover, N. H.

Bindschadler, R.(1998), Monitoring Ice sheet behavior from space, Reviews of Geophysics, 36, 79 -104.

Braithwaite, R. J., M. Laternser, and T. W. Pfeffer (1994), Variations of near-surface firn density in the lower accumulation area of the Greenland ice sheet, Pakitsoq, West Greenland, Journal of Glaciology, 40, 477 – 485.

Brown, J., O. J. Ferrians, Jr., J.A. Heginbottom, and E.S. Melnikov. (1998), revised February 2001, Circum-arctic map of permafrost and ground ice conditions. Boulder, CO: National Snow and Ice Data Center/World Data Center for Glaciology, Digital media.

Church, J. A., and 35 others (2001), Changes in sea level, in Climate Change 2001:The Scientific Basis, edited by J. T. Houghton, Y. Ding, D. J. Griggs, M. Noguer, P. J. van der Linden, X. Dai, K. Maskell, and C. A. Johnson, Cambridge Univ. Press, New York, pp. 639–693.

Davis, C. H., C. A. Kluever, and B. J. Haines (1998), Elevation change of the southern Greenland ice sheet, Science, 279, 2086 – 2088.

Davis, C. H., C. A. Kluever, B. J. Haines, C. Perez, and Y. T. Yoon (2000), Improved elevation change measurement of the southern Greenland ice sheet from satellite radar altimetry, IEEE Transactions on Geoscience and Remote Sensing, 38, 1367–1378.

Davis, C., and A. Ferguson (2004), Elevation change of the Antarctic Ice Sheet, 1995 – 2000, from ERS-2 satellite radar altimetry, IEEE Transactions on Geoscience and Remote Sensing, 42, 2437–2445.

Drinkwater, M. R., D. G. Long, and A. W. Bingham (2001), Greenland snow accumulation estimates from satellite radar scatterometer data, Journal of Geophysical Research, 106, 33,935 – 33, 950.

Fahnestock, M., R. Bindschadler, R. Kwok, and H. Jezek (1993), Greenland Ice Sheet Surface Properties and Ice dynamics from ERS-1 SAR Imagery. Science, 262, 1530 - 1534.

Hicks, B. R., and D. G. Long (2005), Improving temporal resolution of SIR images for QuikSCAT in the polar regions, Report, Brigham Young University, Provo, UT.

Jezek, K.C., P. Gogineni, and M. Shanableh (1994), Radar measurements of melt zones on the Greenland ice sheet, Geophysical Research Letters, 21, 33-36.

Kalnay, E., and 21 others (1996), The NCEP/NCAR 40-year reanalysis project, Bulletin of American Meteorology Society, 77, 437–471.

Koerner, R. M. (1979), Accumulation, ablation and oxygen isotope variations in the Queen Elizabeth Island ice caps, Canada, Journal of Glaciology, 22, 25–41.

Krabill, W., and 12 others (2004), Greenland ice sheet: Increased coastal thinning, Geophysical Research Letters, 31, L24402, doi:10.1029/2004GL021533.

Long, D. G., P. J. Hardin, and P. T. Whiting (1993), Resolution enhancement of spaceborne scatterometer data, IEEE Transactions on Geoscience and Remote Sensing, 32, 700-715.

Long, D. G., and M. R. Drinkwater (1994), Greenland ice-sheet surface properties observed by the Seasat-A scatterometer at enhanced resolution, Journal of Glaciology, 40, 213–230.

Long, D. G., and M. R. Drinkwater (1999), Cryosphere applications of NSCAT data, IEEE Transactions on Geoscience and Remote Sensing, 37, 1671–1684.

Long, D. G., and B. R. Hicks (2005), Standard BYU QuikSCAT/SeaWinds land/ice image products, report, Brigham Young Univ., Provo, Utah.

McConnell, J. R., R. J. Arthern, E. Mosley-Thompson, C. H. Davis, R. C. Bales, R. Thomas, J. F. Burkhart, and J. D. Kyne (2000), Changes in Greenland ice sheet elevation attributed primarily to snow accumulation variability, Nature, 406, 877–879.

Mote, T. L., and M. R. Anderson (1995), Variations in snowpack melt on the Greenland ice sheet based on passive-microwave measurements, Journal of Glaciology, 41, 51–60.

Mote, T. L. (1998a), Mid-tropospheric circulation and surface melt on the Greenland ice sheet, part I, Atmospheric teleconnections, International Journal of Climatology, 18, 111–130.

Mote, T. L. (1998b), Mid-tropospheric circulation and surface melt on the Greenland ice sheet, part II, Synoptic climatology, International Journal of Climatology, 18, 131–146.

Nghiem, S. V., K. Steffen, R. Kwok, and W. Y. Tsai (2001), Detection of snowmelt regions on the Greenland ice sheet using diurnal backscatter change, Journal of Glaciology, 47, 539– 547.

Nghiem, S.V., K. Steffen, G. Neumann, and R. Huff (2005), Mapping of ice layer extent and snow accumulation in the percolation zone of the Greenland ice sheet, Journal of Geophysical Research, 110, F02017, doi:10.1029/2004JF000234

Ohmura, A., and N. Reeh (1991), New precipitation and accumulation maps for Greenland, Journal of Glaciology, 37, 140–148.

Perry, K.L. (Edt.) (2001), QuikSCAT Science Data Product User's Manual, Jet Propulsion Laboratory, California Institute of Technology, CA.

Putnins, P. 1970, The climate of Greenland, in Climates of Polar Regions, 14, World Survey of Climatology, 3-128.

Spencer, M. W., C. Wu, and D. G. Long (2000), Improved resolution backscatter measurements with the SeaWinds pencil-beam scatterometer, IEEE Transactons on Geoscience and Remote Sensing, 38, 89–104.

Steffen, K., and J. Box (2001), Surface climatology of the Greenland ice sheet: Greenland Climate Network 1995–1999, Journal of Geophysical Research, 106, 33,065-33,982.

Steffen, K., S. V. Nghiem, R. Huff, and G. Neumann (2004), The melt anomaly of 2002 on the Greenland ice sheet from active and passive microwave satellite observations, Geophysical Research Letters, 31, L20402, doi:10.1029/2004GL020444.

Thomas, R. H., W. Abdalati, E. Frederick, W. B. Bribill, S. Manizade, and K. Steffen (2003), Investigation of surface melting and dynamic thinning on Jakobshavn Isbrae, Greenland, Journal of Glaciology, 49, 231–239.

Thomas, R. H., E. Frederick, W. Krabill, S. Manizade, and C. Martin (2006), Progressive increase in ice loss from Greenland, Geophysical Research Letters, 33, L10503, doi:10.1029/2006GL026075.

Ulaby, F.T. and W. H. Stiles (1981), Microwave response of snow, Advances in Space Research, 1, 131-149.

Wang, L., M. J. Sharp, B. Rivard, S. Marshall, and D. Burgess (2005), Melt season duration on Canadian Arctic ice caps, 2000–2004, Geophysical Research Letters, 32, L19502, doi:10.1029/2005GL023962.

Wismann, V. R. (2000), Monitoring of seasonal snowmelt in Greenland with ERS scatterometer data, IEEE Transactions and Geoscience and Remote Sensing, 38, 1821–1826.

Zwally, H. J., A. C. Brenner, J. A. Major, R. A. Bindschadler, and J. G. Marsh (1989), Growth of Greenland ice sheet: Measurement, Science, 246, 1587–1589.

Zwally, H. J., and J. Li (2002), Seasonal and interannual variations of firn densification and ice sheet surface elevation at the Greenland summit, Journal of Glaciology, 48, 199–207.

Zwally, H. J., M. B. Giovinetto, J. Li, H. G. Cornejo, M. A. Beckley, A. C. Brenner, J. L. Saba, and D. Yi (2005), Mass changes of the Greenland and Antarctic ice sheets and shelves and contributions to sea-level rise: 1992–2002, Journal of Glaciology, 51, 509-527.

4.8. Tables

Table 4.1. Mean melt extent (%) and mean melt duration (days) over the Greenland ice sheet as a whole during 2000 –2004.

Year	Melt extent (%)	Melt duration for all cells	Melt duration for melt cells
2000	54.9	16.0	28.8
2001	44.2	14.3	32.1
2002	79.7	20.5	25.7
2003	48.2	18.6	38.1
2004	64.0	19.4	30.0

Table 4.2. Mean melt season duration (days) in the nine regions over the ice sheet. The 5-year mean duration, standard deviation, and the mean elevation (m a.s.l.) in each region are also included.

Region	2000	2001	2002	2003	2004	mean	s.d.	Elevation (m)
1	70.2	61.3	58.1	80.1	71.3	68.2	8.7	2035
2	45.5	33.7	35.2	45.7	49.5	41.9	7.1	2242
3	21.2	16.9	22.4	22.1	27.6	22.0	3.8	2359
4	12.4	13.6	16.8	16.7	15.4	15.0	1.9	2259
5	7.0	13.8	11.3	11.7	8.3	10.4	2.8	1817
6	4.9	4.4	17.0	7.6	6.1	8.0	5.2	2198
7	4.8	3.5	10.8	7.0	8.8	7.0	3.0	2840
8	16.1	9.2	22.7	17.8	20.9	17.3	5.2	2633
9	34.6	28.5	35.2	35.1	40.7	34.8	4.3	2283

Table 4.3. Correlation coefficients of monthly mean melt duration (MD) and melt extent (ME) and geopotential height at the 700 hPa, 500 hPa, and 300 hPa pressure levels in the nine regions of the ice sheet. The last column is the correlation coefficients of mean daily melt extent and mean daily 300 hPa geopotential height during 2000 – 2004.

	700 hPa		500 hPa		300 hPa		300 hPa
Region	MD	ME	MD	ME	MD	ME	Daily ME
1	0.86	0.79	0.93	0.86	0.94	0.86	0.79
2	0.77	0.78	0.87	0.87	0.89	0.89	0.73
3	0.60	0.56	0.76	0.70	0.80	0.73	0.77
4	0.62	0.49	0.81	0.69	0.91	0.81	0.80
5	0.52	0.55	0.68	0.73	0.73	0.78	0.69
6	0.33	0.36	0.53	0.59	0.59	0.66	0.62
7	0.48	0.40	0.70	0.59	0.75	0.62	0.69
8	0.53	0.46	0.71	0.62	0.77	0.67	0.71
9	0.70	0.66	0.79	0.76	0.80	0.79	0.75
Mean	0.60	0.56	0.75	0.71	0.80	0.76	0.73

4.9. Figures

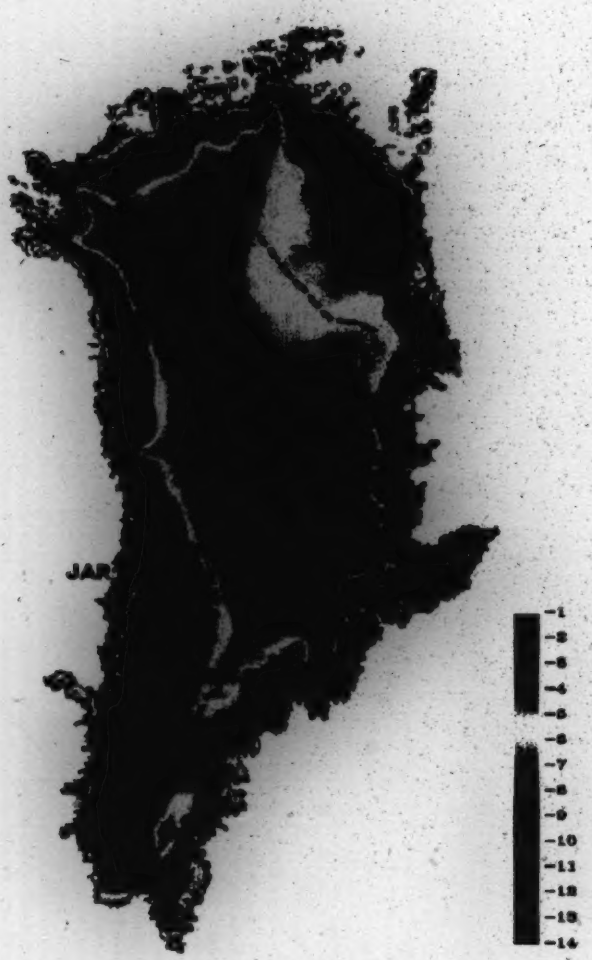

Figure 4.1. Average of mean QSCAT backscatter in November, 2000 – 2004. Dashed black contours are elevations, and the locations of nine AWS as well as one cell in the southeast (SE) of the Greenland are labelled.

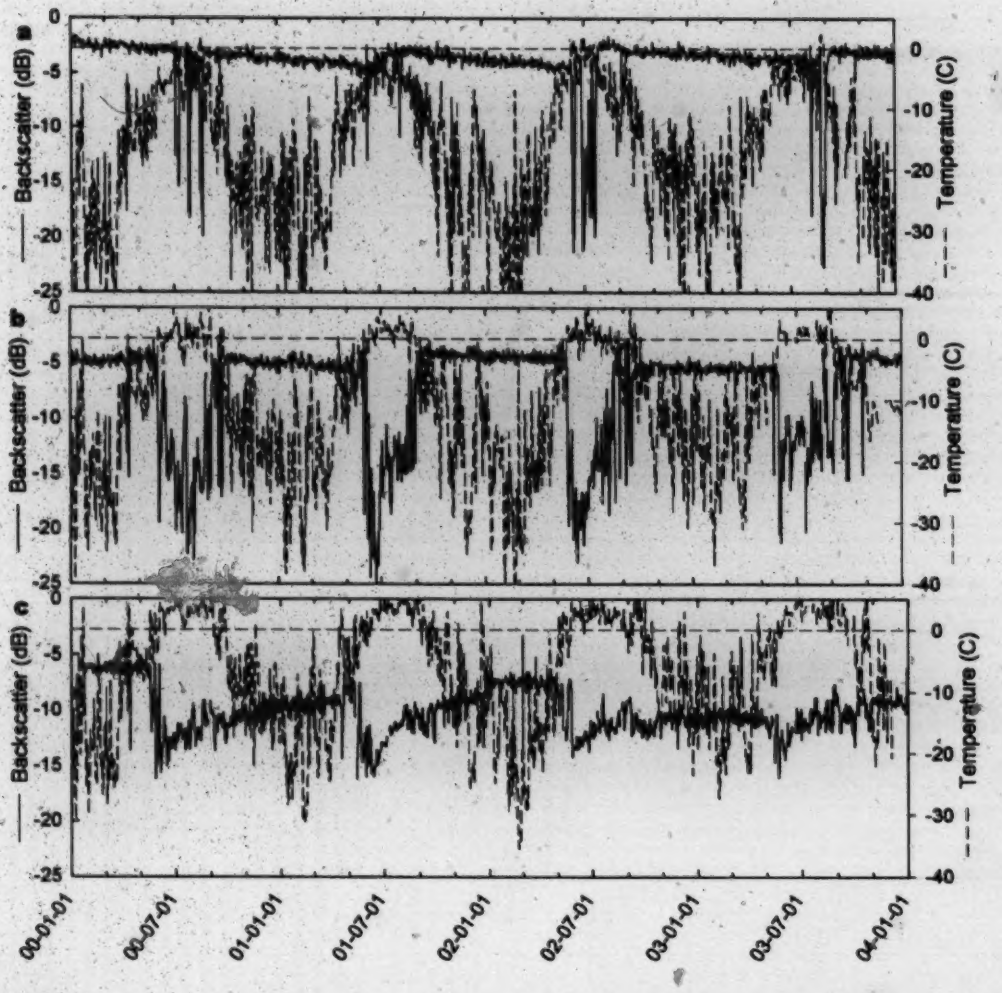

Figure 4.2. Time series of QSCAT σ^0 and air temperature (11:00~20:00) at the (a) Crawford Point1 (CP1), (b) Swiss Camp (ETH), and (c) JAR2 stations on the western flank of the Greenland ice sheet (see locations in Figure 1) during 2000-2003.

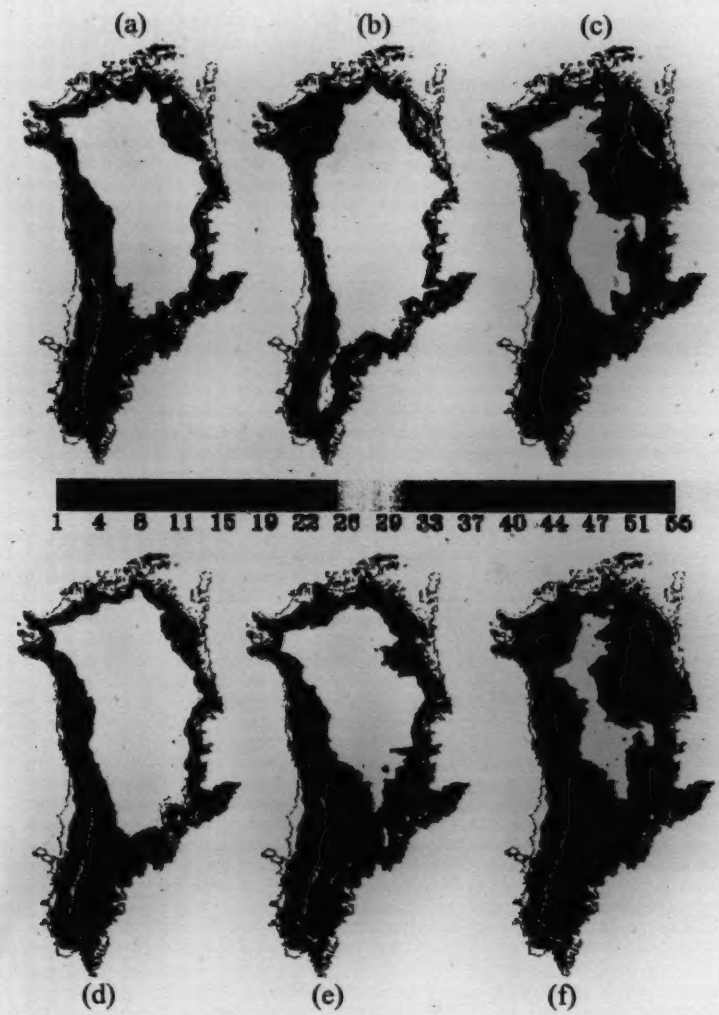

Figure 4.3. Melt extent and duration (number of days) in 2000 (a), 2001 (b), 2002 (c), 2003 (d), 2004 (e), and the 5-year mean (f). Regions which experienced no melt in a particular year are shown in white.

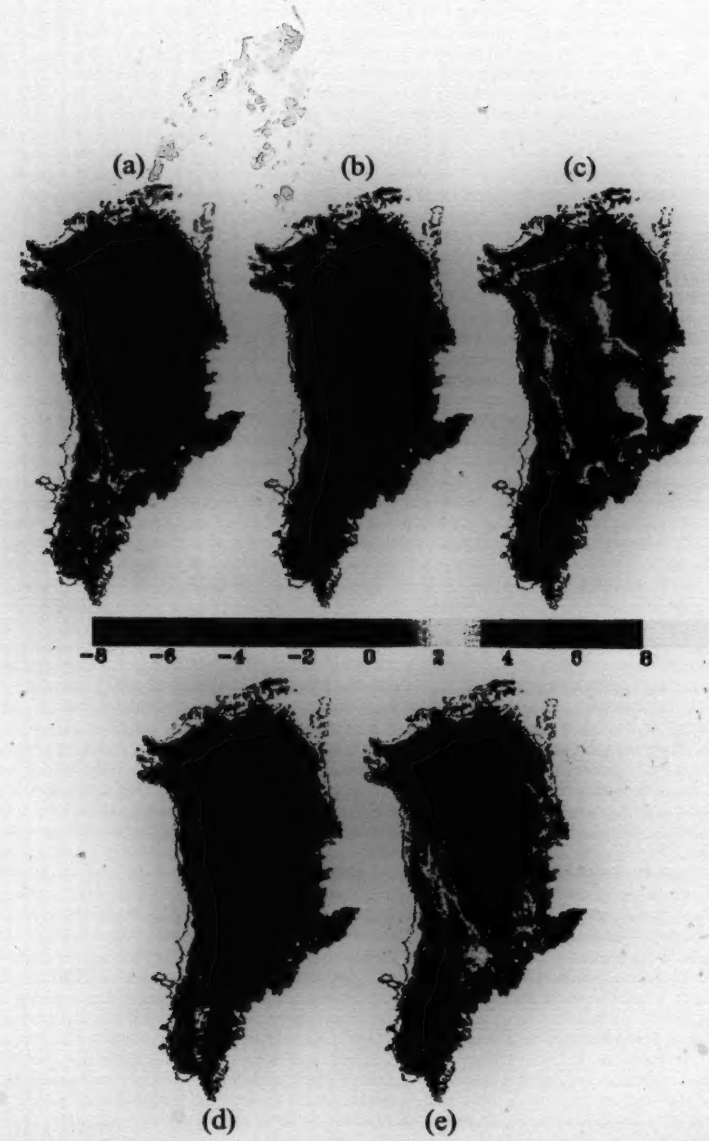

Figure 4.4. Melt duration anomalies in 2000 (a), 2001 (b), 2002 (c), 2003 (d), and 2004 (e), with dashed contours representing regions that experienced no melt in that year.

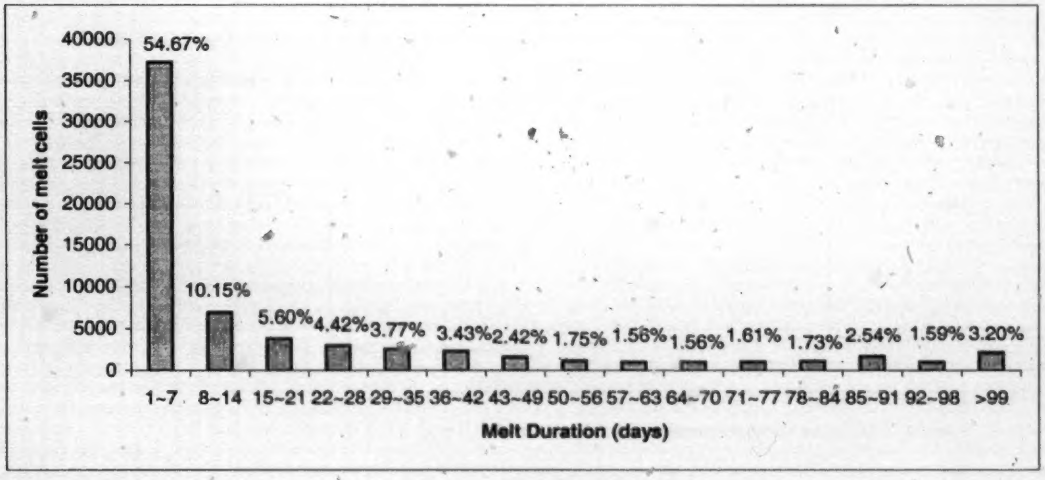

Figure 4.5. Frequency distribution of average melt duration over the Greenland ice sheet, 2000-2004.

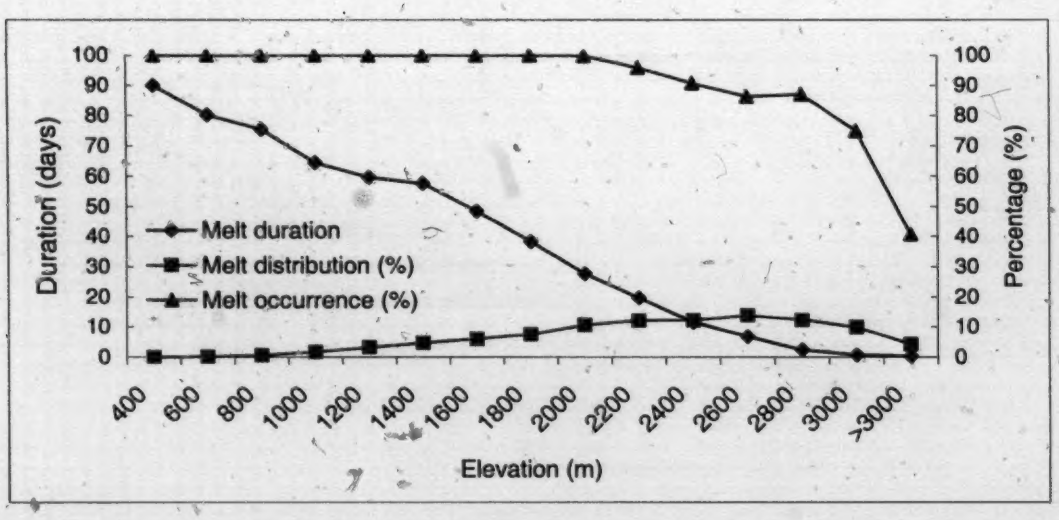

Figure 4.6. Average melt duration, distribution, and occurrence within each elevation bands. The melt distribution was calculated as the percentage of melt pixels within each elevation band in relation to the total number of melt pixels over the Greenland ice sheet (68181). The melt occurrence was calculated as the percentage of the melt pixels in relation to the total number of pixels within an elevation band.

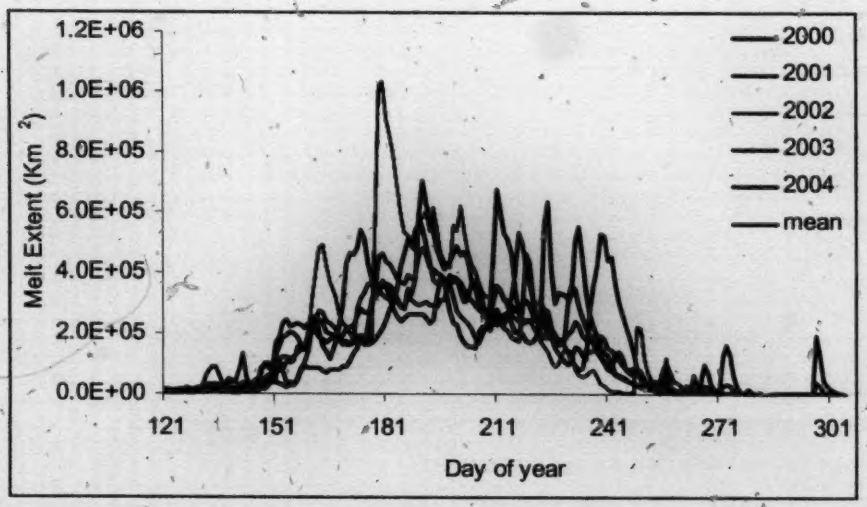

Figure 4.7. Daily melt extent from May to October for the 2000 – 2004 period.

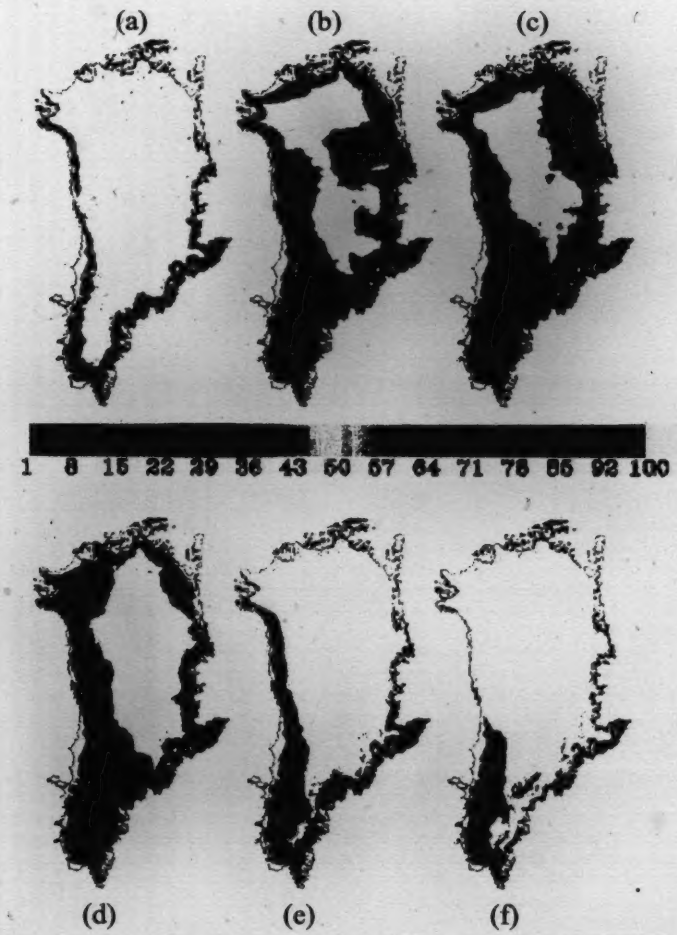

Figure 4.8. Melt extent and occurrence (%) from (a) May, (b) June, (c) July, (d) August, (e) September, and (f) October. White represents areas that experienced no melt in that month.

Figure 4.9. Nine topographically defined regions on the Greenland ice sheet. The red contours are elevations (m a.s.l.), and the blue lines define the nine regions.

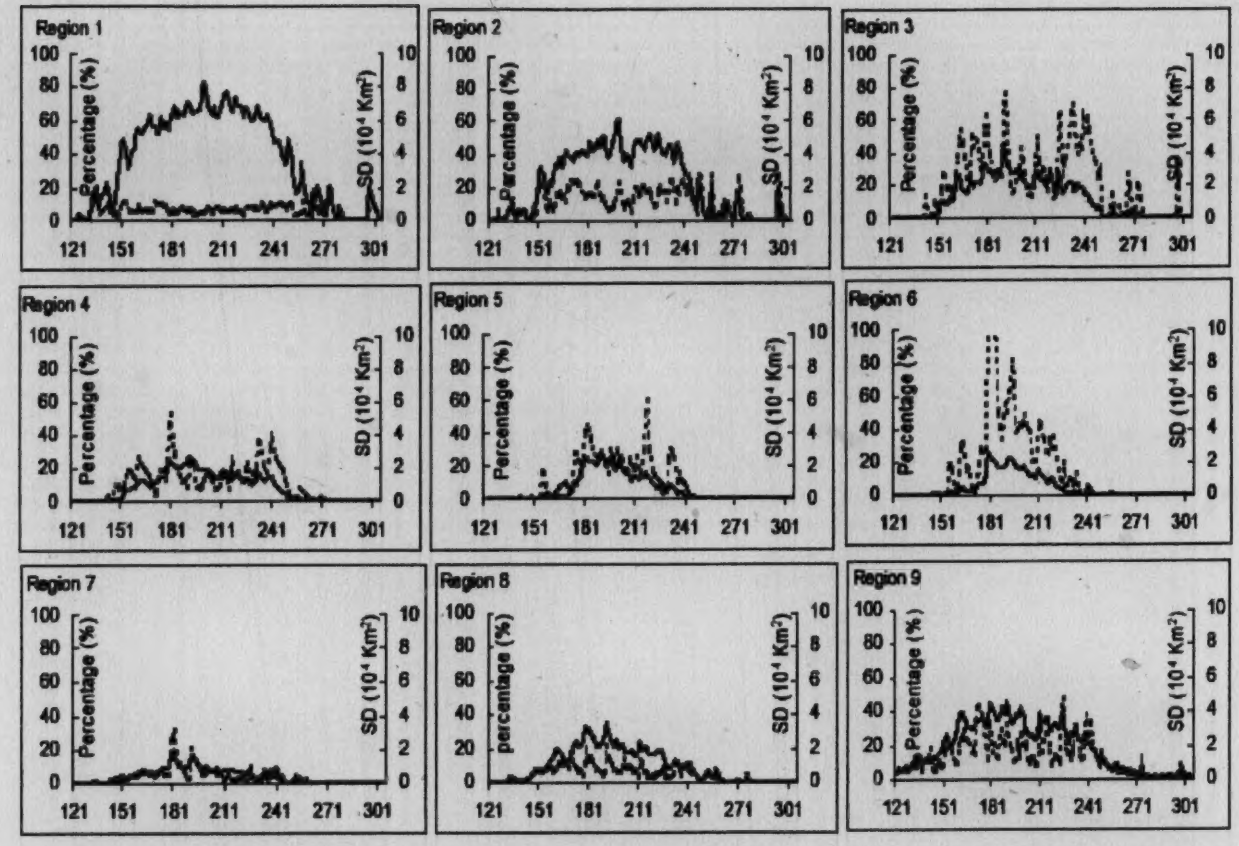

Figure 4.10. The percentage of mean daily melt extent in relation to the total area of the region (solid) and the standard deviation (SD, dash) of the daily melt extent over 2000 – 2004. The x axis is day of the year.

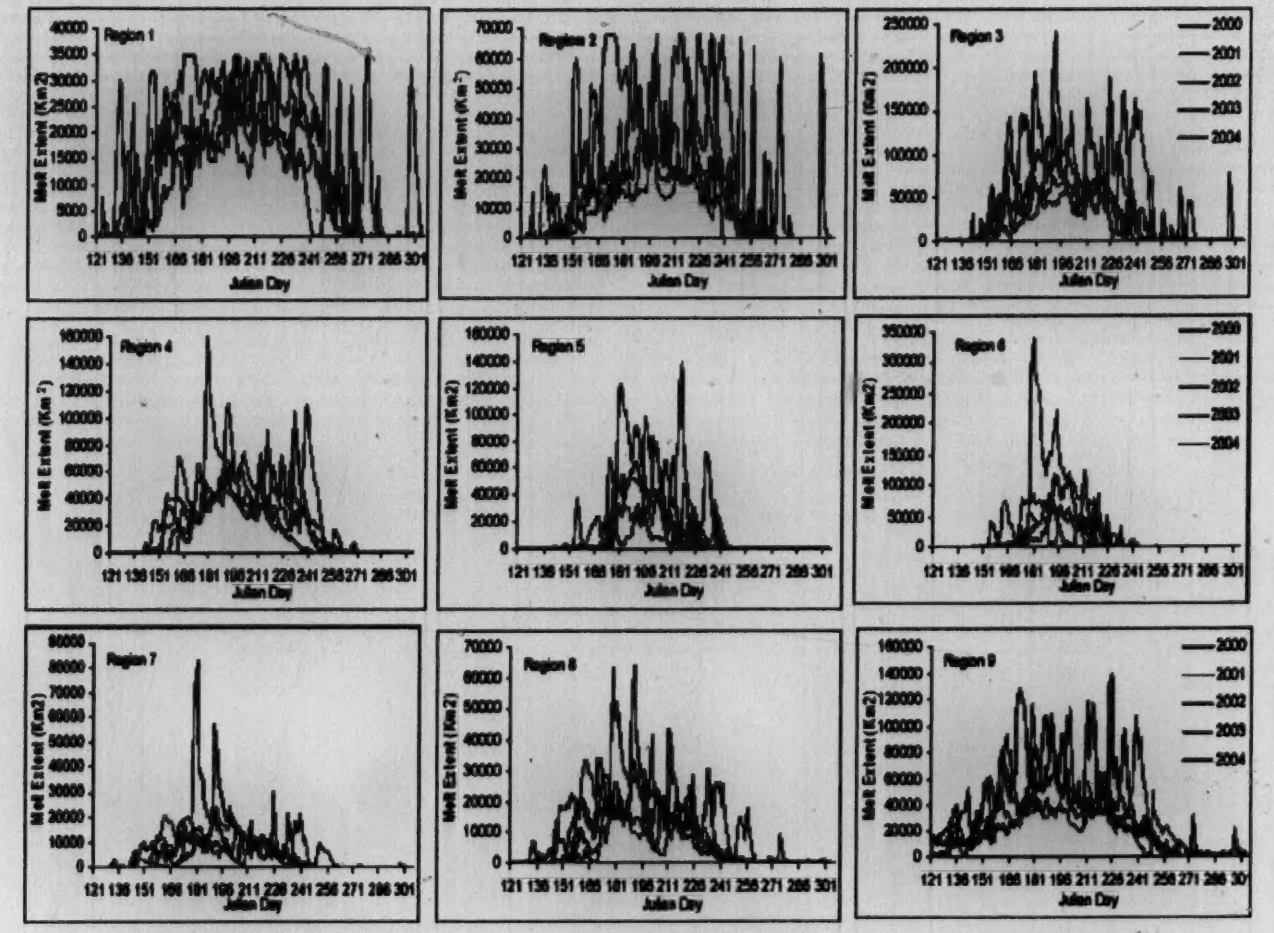

Figure 4.11. Daily melt extent during 2000 –2004 for each region over the Greenland ice sheet.

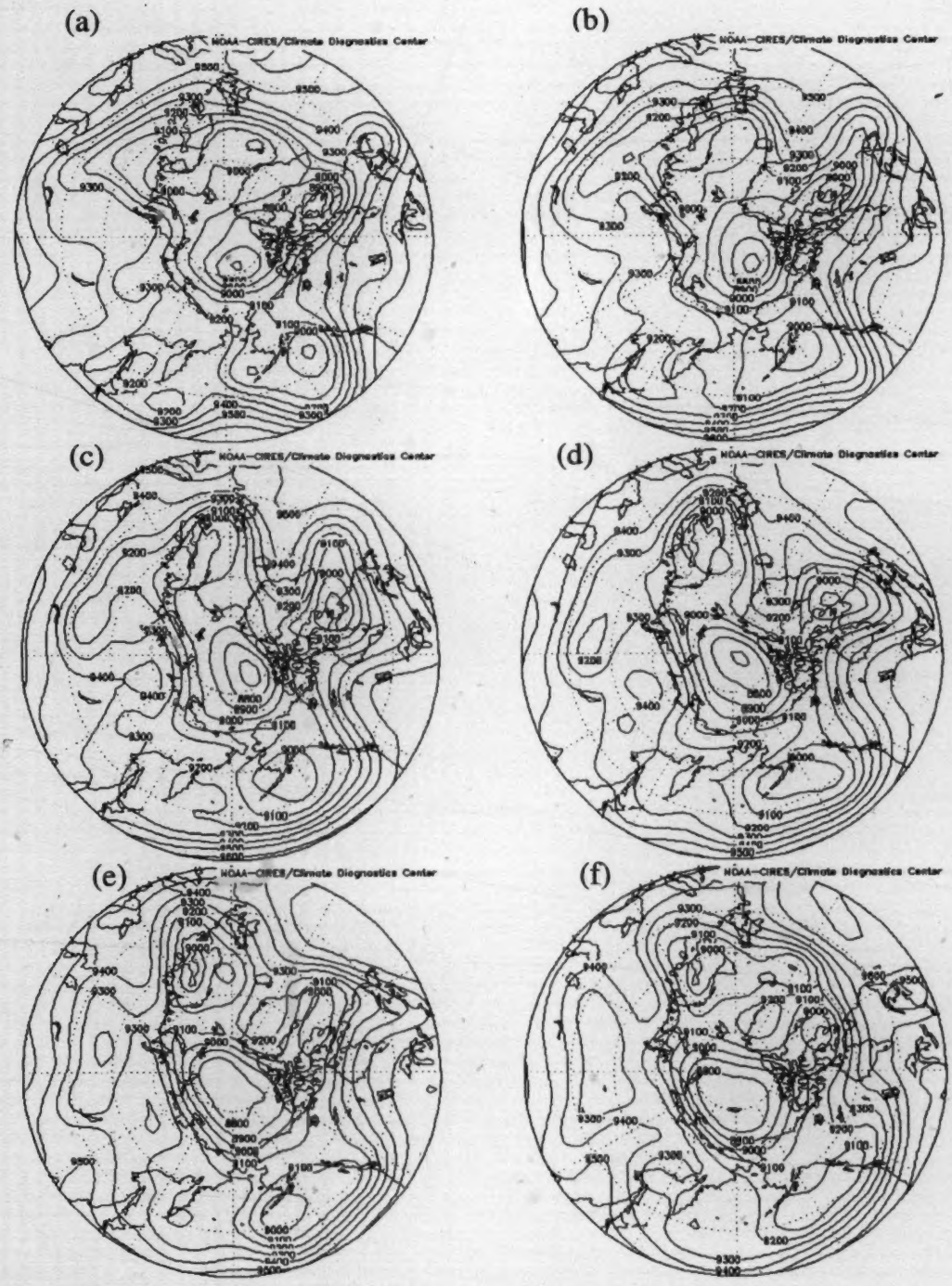

Figure 4.12. Daily mean geopotential height (m) at 300 hPa on June 25 (a); June 26 (b); June 27 (c); June 28(d); June 29 (e); and June 30 (f) of 2002 (day 176-181).

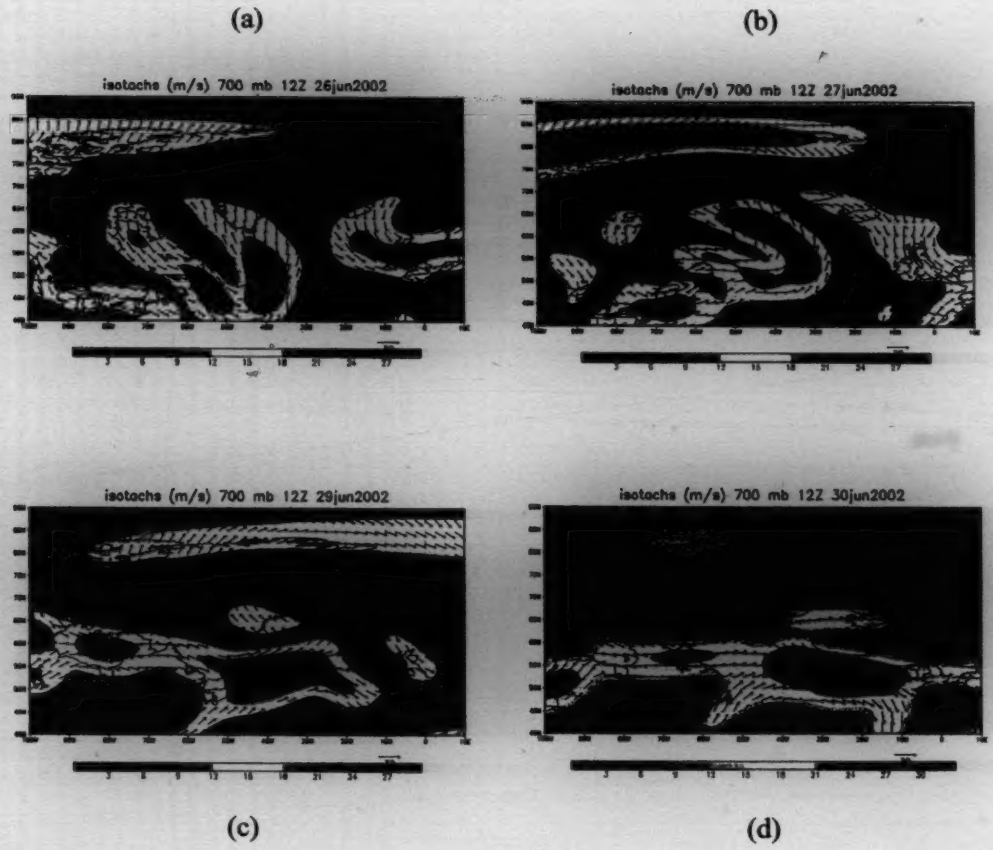

Figure 4.13. 700 hPa isotach maps for June 26 (a), June 27 (b), June 29 (c), and June 30 (d) of 2002.

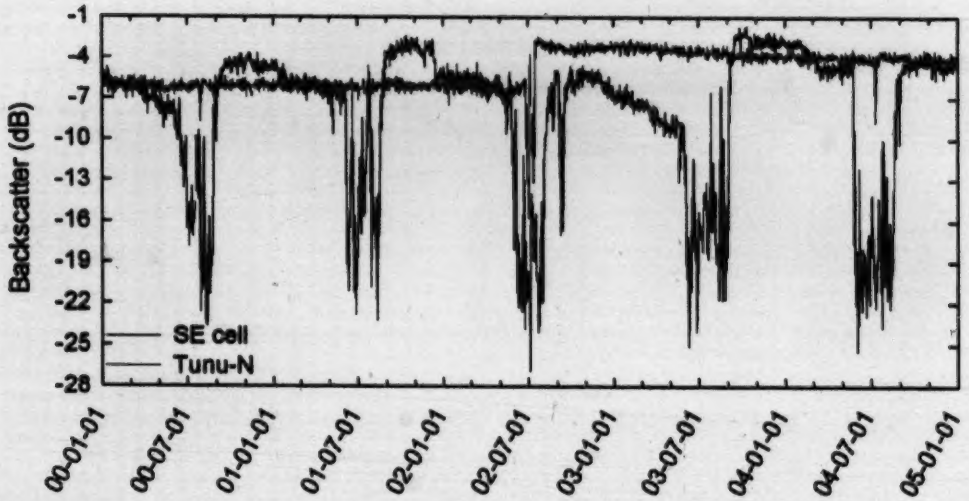

Figure 4.14. Time series of QSCAT σ^0 for Tunu-N and one cell in the southeastern (SE) corner of Greenland (see locations in Figure 4.1) during the 2000-2004 period.

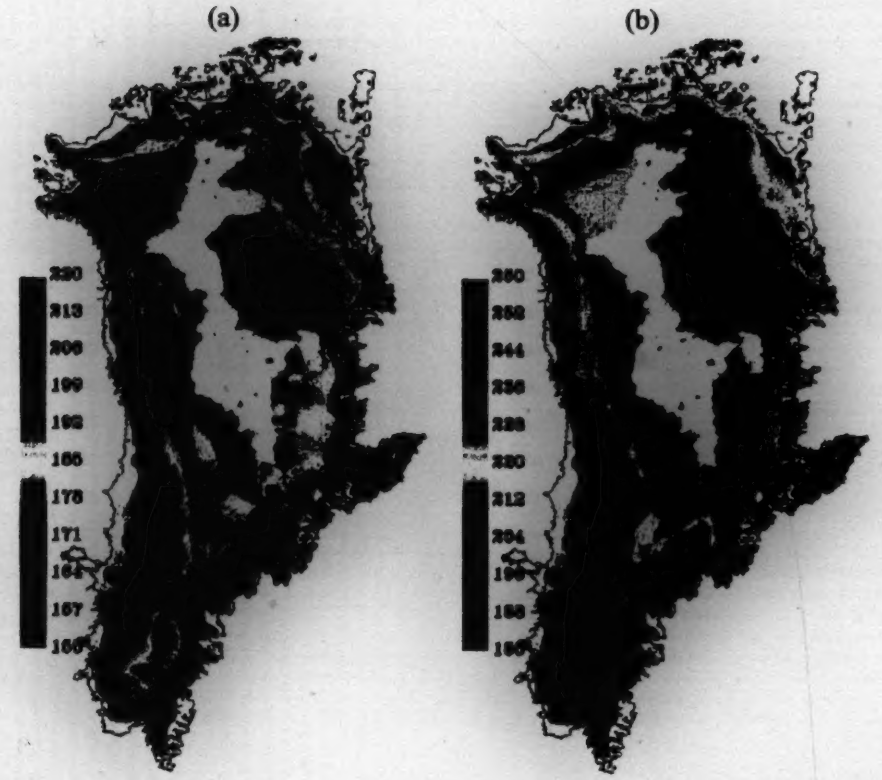

Figure 4.15. Average melt onset dates (a) and melt freeze-up dates (b) during the 2000 –2004 period.

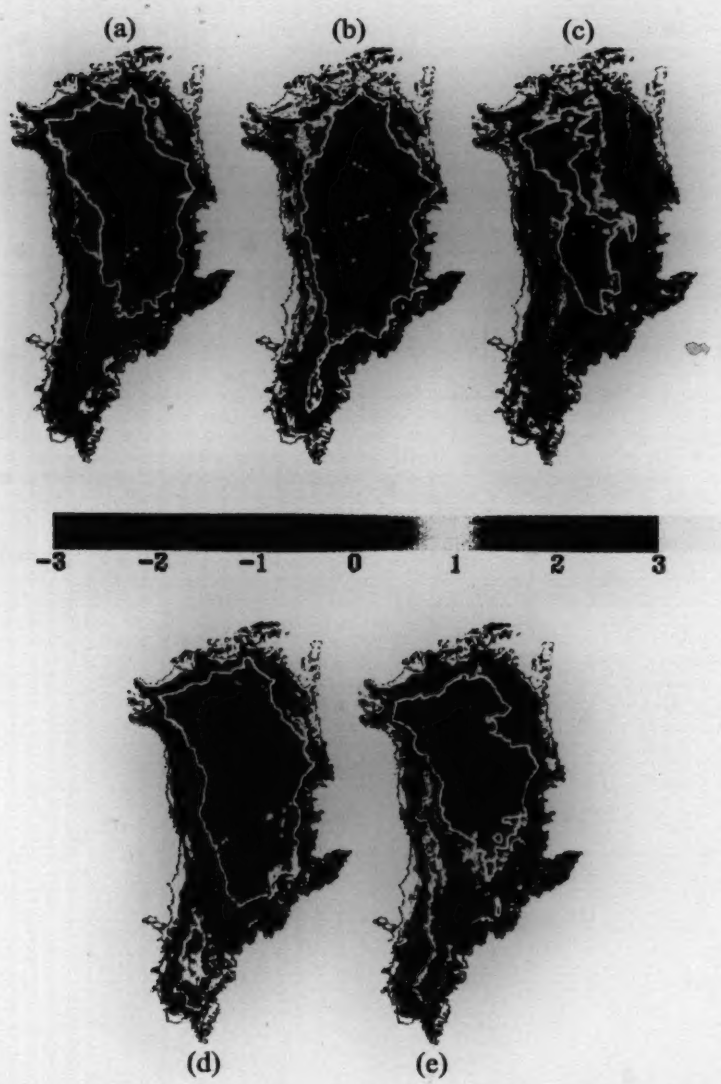

Figure 4.16. Changes in the biweekly averaged backscatter between the freeze-up periods in the current and the previous fall in 2000 (a), 2001 (b), 2002 (c), 2003 (d), and 2004 (e). The solid white and black contours represent the upper limits of melt for the current and the previous summers respectively.

CHAPTER 5.

SUMMARY AND CONCLUSIONS

5.1. Summary

This thesis has shown that satellite remote sensing is a powerful tool for mapping snow cover and snowmelt in the Arctic. In Chapter 2, an evaluation of the NOAA weekly snow cover dataset over the Canadian Arctic was conducted through comparisons with 4 other data sources, of which 3 are based on satellite data. In Chapters 3 and 4, time series of enhanced resolution QSCAT satellite images were used to detect the extent and duration of summer melt and changes in the distribution of ice layer formation on Arctic ice masses. The main findings are summarized below.

Relative to estimates of snow cover extent derived from AVHRR, SSM/I, Landsat TM browse images, and surface snow depth observations, the NOAA dataset showed delayed melt onset and overestimated snow cover during the melt period in all six selected springs (1981-2000) in a study area in the Canadian Arctic north of the tree line. The extent of the melt delay was different for each spring, ranging from 1 to 4 weeks. A number of factors that could potentially be responsible for the apparent delay in melt onset in the NOAA dataset were investigated. The most likely causes are the reduced availability of satellite data at higher latitudes, frequent spring cloud cover (which is not readily differentiated from snow in visible imagery), and the limited availability of surface observations. A change in the strategy used by analysts to record patchy snow cover may account for inter-annual differences in the magnitude of the apparent melt delay. These conclusions are also likely to apply to other regions of the Northern Hemisphere high latitudes.

A dynamic threshold method was used to detect the extent and duration of summer melt on ice caps in the QEI (Canadian high Arctic) from enhanced resolution QSCAT images for the 2000 – 2004 period. The method was justified by the good correspondence between the melt durations derived from QSCAT and from air temperature measurements on the Prince of Wales (POW) Icefield, Ellesmere Island. On average, melt onset dates ranged from late May to mid-July, and freeze-up dates ranged from mid-July to early September. Melt occurred all over the ice caps in warm summers, such as 2000, 2001,

and 2003, but did not occur in some high elevation areas in cold summers, like 2002 and 2004. In general, ice cap margins facing either Baffin Bay or the Arctic Ocean had significantly longer melt seasons than margins facing the interior of the QEI. Nearly 69% of the variance in the 5-year mean melt duration pattern over the whole QEI could be explained in terms of surface elevation and distance from Baffin Bay.

For the QEI as a whole, 2001 had the longest melt season (42.6 days) and 2002 the shortest (30.9 days). Inter-annual variations in the average melt duration over the larger ice caps were strongly positively correlated with local variations in the 500 hPa geopotential height, though the sign of melt duration anomalies in a given year may be opposite at high and low elevations on an ice cap. This appears to be linked to pressure-related variations in the vertical gradient of surface air temperature over the ice caps. This gradient was steeper in years with relatively low pressure than in years with relatively high pressure [Marshall et al., in review]. The results suggest that constant air temperature lapse rates assumed in most distributed temperature index models of glacier mass balance [e.g. Johannessen et al., 1995; Hock, 1999] may be problematic, and may not be suitable for ice caps in the Canadian high Arctic.

The temporal and spatial distribution of surface melt on the Greenland ice sheet was also detected from time series of enhanced resolution QSCAT images for the 2000 – 2004 period. On average, melt started in the middle of May, expanded from early June, and peaked in late June to mid-July. Refreezing began from mid-July, and most of the ice sheet refroze in late September, but melt may continue into October on southern Greenland in prolonged melt years like 2003. For the Greenland ice sheet as a whole, 2002 had the most extensive melt extent (79.7%) and the longest melt season duration (20.5 days), while 2001 had the least melt extent (44.2%) and the shortest melt season duration (14.3 days).

Nearly 86% of the ice sheet area experienced melt for at least one day during the study period. However, nearly 55% of the melt area experienced melt for less than 1 week each year, and about 76% of the melt area experienced less than 30 days of melt. Only 13% of the melt area experienced more than 60 days of melt. The distribution of the mean melt duration was largely a function of surface elevation and latitude, with shorter melt seasons in regions with higher mean elevations and at higher latitudes. In addition,

the melt seasons were shorter at a given latitude on the east side of the ice sheet than on the west side, which is consistent with the climatology of Steffen and Box [2001].

Regional differences in the extent and duration of surface melt over the Greenland ice sheet were examined by dividing the ice sheet into nine topographic regions. There is large variability in the mean melt season duration in each of the nine regions. Consistent with the multiple regression analysis of the mean melt duration for the ice sheet as a whole, the mean melt duration decreases from regions in the south to regions in the north, and the melt duration is longer for regions in west Greenland than for regions at similar latitudes in east Greenland. Region1, located in the southwest corner of Greenland, with a relatively low mean elevation (2035 m), had the longest mean melt duration (68.2 days) over the 5-year period. Region 7, which includes the highest regions of the ice sheet and has the highest mean elevation (2840 m) and the shortest mean melt duration (7.0 days). The standard deviation of the daily melt extent over the 5-year period is lowest in Region 1, where most pixels experience melt every summer; and highest in Region 6, where most pixels only experience melt in very warm years.

The mean melt extent in each region of the ice sheet is positively correlated with the local 300 hPa geopotential height at both daily and monthly scales. However, the monthly mean melt duration is more strongly correlated with the local geopotential height at all pressure levels than is the melt extent. Variations in the daily melt extent for the Greenland ice sheet as a whole and for each of the nine regions indicate that each melt season was characterised by up to 5 or 6 melt events of a few days duration. Extensive melt in the summer of 2002 was due to a single high melt event that lasted for only a few days. The most likely causes of that high melt event are the intrusion of a ridge over Greenland from the North Atlantic Ocean, bringing warm air to the west and north of the ice sheet, combined with adiabatic warming as this air descended on the lee side (northeast and east) of the ice sheet.

Inter-annual changes in the distribution of ice layer formation by melt water refreezing in the percolation zone of the ice sheet were mapped using the changes in the biweekly averaged backscatter between successive end of melt season periods for the 2000 – 2004 period. 2002 had extensive areas of ice layer formation in high elevation regions of west, east, and northeast Greenland, consistent with the unusually extensive

melt that occurred in these regions during that summer. In contrast, 2001 had lower than normal areas of ice layer formation in western and southern Greenland, where the melt duration anomalies were extremely negative during that melt season.

5.2. Discussion and Implications

Climate simulation models are extremely sensitive to parameterization of the Arctic sea ice and snow albedo on account of the impact of albedo on the surface energy budget [Johannessen et al., 2004; Dethloff et al., 2006]. Accurate Arctic snow and ice cover records are therefore essential to better understand climate change in the recent past and to project the future trend. As the longest spatially continuous dataset available for the Northern Hemisphere, the NOAA weekly snow cover product has been widely used in climate-related studies. However, an evaluation conducted in this thesis for a study area in the Canadian Arctic mainland indicated that the NOAA dataset shows delayed melt onset and overestimates snow cover extent during the spring melt period. Therefore caution should be exercised when using the NOAA dataset in any climatological study related to the timing of snowmelt in northern high latitudes. If the observed spring bias applied equally across the entire period of the NOAA dataset (and this may not be the case), trends in snow disappearance date would not be affected, but the bias would affect trend analyses of snow cover extent carried out on a monthly basis (e.g. trends attributed to April may actually be happening in March). The timing error would also affect correlations of monthly snow cover with other variables such as air temperature [e.g. Groisman et al., 1994] or indices of atmospheric circulation [e.g. Qian and Saunders, 2003; Schaefer et al., 2004].

The timing of snowmelt has effects on many high latitude processes, including the stability of permafrost [Osterkamp and Romanovsky, 1999], the length of the active growing season [Myneni et al., 1997] and the associated changes in the annual cycles of two important greenhouse gases, carbon dioxide [Keeling et al., 1996] and methane [Zimov et al., 1997]. Changes in the atmosphere concentration of these gases may have a feedback effect on climate. Consequent to these changes, plant and animal habitats may be impacted. Thus variations in the annual distribution of snow cover over high latitude land areas have far-reaching implications, both in the context of global warming and the

Arctic ecosystem. An accurate Arctic-wide snow cover product is required if a better understanding of anthropogenic climate forcing is to be gained. In April 1999, NOAA began to use an automated Interactive Multi-sensor snow and ice mapping System (IMS), which replaced the manual snow cover charting analysis [Ramsay, 1998]. Apart from optical sensors, passive microwave data were also used to provide an all weather capability. The IMS provides a daily snow and ice cover map for the Northern Hemisphere, and a pseudo-weekly chart has been created to maintain the continuity of the previous dataset. It is still unclear what impact this has had on the homogeneity of the data. However, due to known deficiencies of passive microwave sensors in detecting shallow, wet snow cover and snow cover in densely forested areas [Armstrong and Brodzik, 2001; Derksen et al., 2004], introducing passive microwave data to the IMS may not solve all the problems associated with high latitude snow cover mapping. Recent studies have shown that there are several advantages of using active microwave scatterometer data to detect snow cover, including the high sensitivity of these data to surface melt and the limited extent to which they are affected by vegetation cover [e.g. Nghiem and Tsai, 2001]. Combining the global-coverage of data from active and passive microwave sensors such as QuikSCAT and SSM/I, with data from optical sensors such as MODIS, may provide a more accurate and comprehensive snow cover dataset globally, and especially benefit studies of snow cover in Arctic regions, where frequent cloud cover and polar darkness hamper data acquisition by visible sensors.

General circulation models predict that anthropogenic climate warming will have the largest impact on Arctic regions [Houghton et al., 2001; Holland and Bitz, 2003]. So there is a strong interest in examining the Arctic for early indications of global warming. Given the good correspondence between melt season duration derived from microwave QSCAT images and from temperature measurements at field sites in both the QEI and the Greenland, routine mapping of melt season duration on the Arctic ice masses may be an effective and rapid way of detecting the spatial pattern of temperature variability during the summer melt season. Annual and inter-annual variations in melt season duration provide a clear picture of local climatic conditions on different ice masses. Extension of this approach to include all of the larger ice caps in the Arctic would provide the regional

scale variability in summer climate across the Arctic and may potentially be useful for us to better understand global climate change.

This thesis demonstrated that dates of spring melt onset and fall freeze-up, together with intermediate freeze-up periods within the melt season can all be detected from time series of daily QSCAT images. Thus transitions from dry to wet snow conditions and the corresponding changes in surface albedo can be closely monitored on a daily basis. This is especially useful for parameterization of the surface albedo in positive degree-day (PDD) mass balance models [Braithwaite 1995; Arendt, 1999]. Although melt duration in the ablation zone of Arctic ice caps and the Greenland ice sheet could not be determined from QSCAT due to difficulty in detecting the freeze-up date on bare ice surfaces, it may be possible to determine the timing (date) of complete snow melt – on which date the glacier ice is exposed, which could be validated if snow accumulation conditions are known on the ablation zone of the ice sheet. These are potentially very useful for validating the outputs of surface energy balance and regional scale climate models.

During the last two decades or so, many efforts have been made to retrieve changes in surface elevation of the ice sheets from satellite radar altimeters in order to estimate changes in ice volume and thus the mass balance of the ice sheets, and to improve the assessment of their contribution to sea level change [Zwally et al., 1989; 2005; Davis et al., 1998; 2000]. Several studies have focused on the development of retracking algorithms [Martin et al., 1983; Wingham et al., 1986; Davis, 1993; 1997], which are a key step in processing altimeter return waveforms to produce accurate surface elevation measurements. The shape of altimeter waveforms over an ice sheet is affected by both surface and subsurface backscattering [Ridley and Partington, 1988; Davis and Moore, 1993]. This complicated the development and implementation of retracking algorithms, because different facies/zones of the ice sheet are associated with different radar backscattering mechanisms. As described in Chapter 4, volume backscattering dominates in the dry snow zone, surface backscattering dominates in the ablation zone, and both surface and volume backscattering contribute to the radar return in the percolation/saturation zones. Davis [1997] suggested that different retracking thresholds should be used for different portions of the ice sheet. As demonstrated in Chapter 4 of this thesis, use of QSCAT images may be an effective way to map facies/zones on the

Greenland ice sheet and their changes over time. Inter-annual changes in the distribution of ice layer formation within the near surface snow and firn of the ice sheet can be detected from time series of QSCAT data. Extensive melt occurred at high elevations (above 2500 m a.s.l.) on the northeast of the ice sheet in 2002, and this resulted in a significant increase in ice layer formation relative to the previous years. In the northeast, melt seldom occurs above the 2000 m elevation contour, so before 2002 volume backscattering should have dominated the fine-grained dry snowpack. However, ice lenses and pipes formed during the extensive melt and refreezing in the summer of 2002 must have made both surface and volume backscattering important. At the same time, the density of the near surface firn affected by meltwater refreezing may have increased notably, and in the absence of an increase in snow accumulation, this could have decreased the surface elevation of the ice sheet in that region. If such a decrease in elevation were to be detected by altimeters, it could be interpreted as a densification induced elevation change and not necessarily as a result of a change in mass balance. Systematic mapping of changes in the boundaries of different facies/zones over ice sheets may therefore be very useful in the interpretation and retrieval of altimeter-derived measurements of changes in the surface elevation of the ice sheet.

5.3. Future work

It is apparent from the results of this thesis that further investigation of the following areas will be very important to further improve our knowledge of snow cover and snowmelt conditions in the Arctic and to better understand the interactions between the cryosphere and climate change at both regional and global scales.

(1) Further validate the NOAA snow cover dataset over other high latitude regions of the Northern Hemisphere. This is necessary to evaluate and finalize the conclusions drawn in this study. Since the primary datasets - the AVHRR Polar Pathfinder 5 km EASE-Grid Composites and the passive microwave SSM/I dataset, used to evaluate the NOAA dataset in the Canadian Arctic are available for the other high latitude regions, methods similar to those used in this thesis could be used to conduct the evaluation for other regions, such as northern Alaska and the Russian Arctic mainland north of the treeline. It is important to select a study area above the treeline to minimize the effects of

forest masking on both the AVHRR and the SSM/I data. As in this thesis, surface snow observations and Landsat TM browse images will be very helpful to establish and validate the thresholds used to derive snow cover extent from the AVHRR data. Unfortunately there are very few surface observations in these high latitude areas, even fewer than in the Canadian Arctic. Thus it may be helpful to examine the availability of Landsat TM browse images first and then choose a study area where there is good Landsat TM coverage. If the delayed melt onset found in the NOAA dataset over the Canadian Arctic was also found in other regions, it would be necessary to consider and pursue possible ways to improve the accuracy of this snow cover dataset.

(2) Explore the possibility of melt season duration detection on other ice caps or the Antarctic ice sheet. The enhanced resolution QSCAT scatterometer data are available globally, although at reduced temporal resolution at lower latitudes (3 day). It is therefore tempting to explore the possibility of melt detection on other ice caps or ice sheets. Since the highest spatial resolution available from the enhanced resolution QSCAT mages is about 5 km (slice-based), the method is only applicable to relatively large ice caps, such as those in the eastern Arctic (e.g. Svalbard and Novaya Zemlya), in South America (e.g. Patagonian icefields), in Asia (e.g. Tienshan), and the Antarctic ice sheet [Dyurgerov and Meier, 2005]. During this study, an attempt was made to detect melt season duration on the Barnes ice cap in Baffin Island in the Canadian Arctic. However, it was found that the dates of freeze-up over most parts of the ice cap cannot be determined reliably from time series of QSCAT images. This is probably due to the fact that superimposed ice is extensive on the ice cap [Hooke et al., 1987]. Dates of melt onset can, however, be detected over most of the ice cap. If melt season duration can be detected for other ice caps/ice sheets with the same QSCAT dataset, variability in global climate and atmospheric circulation during the summer could be investigated by comparing the annual and inter-annual variability in melt season lengths and timings at different ice caps or ice sheets.

(3) Investigate the relationship between melt season duration and mass balance. Given the good correlation between melt duration derived from QSCAT and the annual positive-degree-day (PDD) total at field sites over both the QEI ice caps and the Greenland ice sheet, it may be possible to use maps of melt duration to derive positive

degree-day fields that could be used to compute summer melt volume using temperature index melt models. In fact, this has been done on the Greenland ice sheet using passive microwave derived estimation of melt duration [e.g. Mote, 2000; 2003; Hanna et al., 2002], but the approach has not been tested for the ice caps in the QEI. Studies indicate that Ku-band backscatter is more sensitive to snow wetness than passive microwave brightness temperature and can detect snowmelt at an early stage [Nghiem and Tsai, 2001; Steffen et al., 2004]. In addition, the enhanced resolution QSCAT scatterometer images provide a higher spatial resolution (~8 km for egg-based SIR, ~5 km for slice-based SIR) than the passive microwave SMMR or SSM/I dataset (25 km). Synoptic melt mapping on ice caps in the QEI only became possible recently using the slice-based QSCAT SIR images [Wang et al., 2005]. Variations in summer melting are believed to be the main contributor to variations in mass balance on these ice caps [Dowdeswell et al., 1997; Koerner, 2002]. Therefore, further investigation of the relationship between the melt season duration derived from QSCAT and the summer melt volume on the QEI ice caps and the Greenland ice sheet is potentially very useful to gain an overall picture of the mass loss and thus mass balance of the ice caps and ice sheet.

(4) Investigate the relationship between the integrated summer reduction in backscatter and total PDD. PDD models have been widely used to estimate glacier mass balance. Although a close correspondence between melt season duration and PDD was found in this thesis, the integrated reduction in backscatter may provide a better estimate of melt intensity [Wismann, 2000]. Wismann [2000] found there was a good relationship ($r=0.98$) between temporally integrated PDD and the integrated reduction in backscatter during 8 summers at a single location on the Greenland ice sheet. Smith et al. [2003] further investigated this relationship and pointed out that scatterometer data may be used to estimate PDD for high elevation or high latitude glaciers where PDD do not exceed 500. During this study, the relationship between integrated reduction in QSCAT backscatter and PDD air temperatures recorded at 12 hobo sites during 2 summers in the Prince of Wales Icefields was examined. However, the relationship was poor. This may be due to the more complex surface topography of the QEI ice caps than the gentle-sloped Greenland ice sheet. In addition, the relationship between the integrated PDD and reduction in backscatter derived for single locations may not be used to extrapolate in

space. Grouping the hobo sites according to the surface and subsurface physical properties of snow and firn (different zones) may be helpful, but this solution could not be tested with the current limited field observations. It would therefore be valuable to further investigate the relationship between the integrated reduction in backscatter and PDD in combination with more field measurements of air temperature and snow/firn characteristics.

(5) Further investigate the relationship between synoptic conditions and the daily melt extent over both QEI and Greenland. The results in Chapter 4 indicates that each melt season on the Greenland ice sheet was characterized by up to 5 or 6 melt events of a few days duration, and the record melt extent in summer 2002 was due to a single melt event that lasted for only a few days. It would be very useful to further investigate if these melt events are associated with similar synoptic patterns in each region and determine the controls on the occurrence of synoptic patterns that promote melt in different regions. NCEP/NCAR Reanalysis data could be used to derive the histories of the synoptic patterns, extending our knowledge of the surface melt conditions on the Arctic ice masses back to late 1940s. One could also examine if there is any trend in the history of the synoptic patterns, especially during the late 1970s when the polar climate shifted from a cold to a warm phase. GCM simulations may be used to estimate the frequency of occurrence of high melt events in the future. This would provide a better understanding of the responses of the Arctic ice masses to climate change and improve prediction of the future trend.

5.4. References

Arendt, A. (1999), Approaches to modelling the surface albedo of a high Arctic glacier, Geografiska Annaler, 81a, 477- 487.

Armstrong, R. L., and Brodzik, M. J. (2001), Recent Northern Hemisphere snow extent: A comparison of data derived from visible and microwave satellite sensors, Geophysical Research Letters, 28, 3673-3676.

Braithwaite, R. J. (1995), Positive degree-day factors for ablation on the Greenland Ice Sheet studied by energy-balance modeling, Journal of Glaciology, 41, 153–160.

Davis, C. H. (1993), A surface and volume scattering retracking algorithm for ice sheet satellite altimetry, IEEE Transactions on Geoscience and Remote Sensing, 31, 811-818.

Davis, C. H., and R. K. Moore (1993), A combined surface and volume scattering model for radar altimetry, Journal of Glaciology, 39, 675-686.

Davis, C. H. (1997), A robust threshold retracking algorithm for measuring ice-sheet surface elevation change from satellite radar altimeters, IEEE Transactions on Geoscience and Remote Sensing, 35, 974–979.

Davis, C. H., C. A. Kluever, and B. J. Haines (1998), Elevation change of the southern Greenland ice sheet, Science, 279, 2086– 2088.

Davis, C. H., C. A. Kluever, B. J. Haines, C. Perez, and Y. T. Yoon (2000), Improved elevation change measurement of the southern Greenland ice sheet from satellite radar altimetry, IEEE Transactions on Geoscience and Remote Sensing, 38, 1367–1378.

Derksen, C., R. Brown, and A. Walker (2004), Merging conventional (1915-92) and passive microwave (1978-2002) estimates of snow extent and snow water equivalent over central North America, Journal of Hydrometeorology, 5, 850-861.

Dethloff, K., and 14 others (2006), A dynamical link between the Arctic and the global climate system, Geophysical Research Letters, 33, L03703, doi:10.1029/2005GL025245.

Dowdeswell, J. A., and others (1997), The mass balance of circum-Arctic glaciers and recent climate change, Quaternary Research, 48, 1 –14.

Dyurgerov, M. B., and M. F. Meier (2005), Glaciers and the changing earth system: A 2004 snapshot, Occasional Paper 58, Institute of Arctic and Alpine Research, University of Colorado, Boulder.

Groisman P.Y., T. R. Karl, R. W. Knight, and G. L. Stenchikov (1994), Changes of snow cover, temperature, and radiative heat balance over the Northern Hemisphere, Journal of Climate, 7, 1633-1656.

Hanna, E., P. Huybrechts, and T. Mote (2002), Surface mass balance of the Greenland ice sheet from climate analysis data and accumulation/runoff models, Annals of Glaciology, 35, 67-72.

Hock, R. (1999), A distributed temperature-index ice- and snowmelt model including potential direct solar radiation, Journal of Glaciology, 45, 101-111.

Holland, M. M., and C. M. Bitz (2003), Polar amplification of climate change in coupled models, Climate Dynamics, 21, 221 – 232.

Hooke, R. L., G. W. Johnson, K. A. Brugger, B. Hanson, and G. Holdsworth (1987), Changes in mass balance, velocity, and surface profile along a flow line on Barnes Ice Cap,1970–1984, Canadian Journal of Earth Sciences, 24, 1550–1561.

Houghton, J. T., Y. Ding, D. J. Griggs, M. Noguer, P. J. van der Linden, X. Dai, K. Maskell, and C. A. Johnson (Eds.) (2001), Climate Change 2001: The Scientific Basis, Cambridge University Press, New York.

Johannessen, T., O. Sigurdsson, T. Laumann, M. Kennett (1995), Degree-day glacier massbalance modelling with application to glaciers in Iceland, Norway, and Greenland, Journal of Glaciology, 41, 345-358.

Johannessen, O. M., L. Bengtsson, and M. W. Miles, et al. (2004), Arctic climate change: observed and modelled temperature and sea-ice variability, Tellus Series A, Dynamic Meteorology and Oceanography, 56, 328-341.

Koerner, R. M. (2002), Glaciers of Canada: Glaciers of the High Arctic islands, U.S. Geological Survey Professional Paper, 1386-J-1, 111 –146.

Marshall S. J., M. J. Sharp, D. O. Burgess, and F. S. Anslow (2006), Near-surface temperature lapse rates on the Prince of Wales Icefield, Ellesmere Island, Canada: Implications for regional downscaling of temperature, International Journal of Climatology, in review.

Martin, T. V., H. J. Zwally, A. C. Brenner, and R. A. Bindschadler (1983), Analysis and retracking of continental ice sheet radar altimeter waveforms, Journal of Geophysical Research, 88, 1608-1616.

Mote, T. L. (2000), Ablation rate estimates over the Greenland ice sheet from microwave radiometric data, Professional Geographer, 52, 322– 331.

Mote, T. L. (2003), Estimation of runoff rates, mass balance, and elevation changes on the Greenland ice sheet from passive microwave observations, Journal of Geophysical Research, 108, 4056, doi:10.1029/2001JD002032.

Myneni, R. B., C. D. Keeling, C. J. Tucker, G. Asrar, and R. R. Nemani (1997), Increased plant growth in the northern high latitudes from 1981 to 1991, Nature, 386, 698– 702.

Nghiem S. V., and W. Y. Tsai (2001), Global snow cover monitoring with spaceborne Ku-band scatterometer, IEEE Transactions on Geoscience and Remote Sensing, 39, 2118-2134.

Osterkamp, T. E., and V. E. Romanovsky (1999), Evidence for warming and thawing of discontinuous permafrost in Alaska, Permafrost Periglacial Processes, 5, 137– 144.

Qian, B., and M. A. Saunders (2003), Seasonal predictability of wintertime storminess over the North Atlantic, Geophysical Research Letters, 30, 1698, doi:10.1029/2003GL017401

Ramsay, B. (1998), The interactive multisensor snow and ice mapping system. Hydrological Processes, 12, 1537–1546.

Ridley, J. K., and K. C. Partington (1988), A model of satellite radar altimeter returns from ice sheets, International Journal of Remote Sensing, 9, 601-624.

Saunders, M. A., B. Qian, and B. Lloyd-Hughes (2003), Summer snow extent heralding of the winter North Atlantic Oscillation, Geophysical Research Letters, 30, 1378, doi:10.1029/2002GL016832.

Schaefer, K., A. S. Denning, and O. Leonard (2004), The winter Arctic Oscillation and the timing of snowmelt in Europe, Geophysical Research Letters, 31, L22205, doi:10.1029/2004GL021035.

Smith, L. C., Y. Sheng, R. R. Forster, and K. Steffen, et al. (2003), Melting of small Arctic ice caps observed from ERS scatterometer time series, Geophysical Research Letters, 30, 2034, doi:10.1029/2003GL017641

Steffen, K., and J. Box (2001), Surface climatology of the Greenland ice sheet: Greenland Climate Network 1995–1999, Journal of Geophysical Research, 106, 33,065-33,982.

Steffen, K., S. V. Nghiem, R. Huff, and G. Neumann (2004), The melt anomaly of 2002 on the Greenland ice sheet from active and passive microwave satellite observations, Geophysical Research Letters, 31, L20402, doi:10.1029/2004GL020444.

Wang, L., M. J. Sharp, B. Rivard, S. Marshall, and D. Burgess (2005), Melt season duration on Canadian Arctic ice caps, 2000–2004, Geophysical Research Letters, 32, L19502, doi:10.1029/2005GL023962.

Wingham, D. J., C. G. Rapley, and H. Griffiths (1986), New techniques in satellite altimeter tracking systems, in IGARSS '86 Symposium Digest, 1, 185 – 190, Zurich, Switzerland.

Wismann, V. R. (2000), Monitoring of seasonal snowmelt in Greenland with ERS scatterometer data, IEEE Transactions on Geoscience and Remote Sensing, 38, 1821–1826.

Zimov, S. A., Y. V. Voropaev, I. P. Semiletov, S. P. Daviodov, S. F. Prosiannikov, F. S. Chapin III, M. C. Chapin, S. Trumbore, and S. Tyler (1997), North Siberian lakes: A methane source fueled by Pleistocene carbon, Science, 277, 800– 802.

Zwally, H. J., A. C. Brenner, J. A. Major, R. A. Bindschadler, and J. G. Marsh (1989), Growth of Greenland ice sheet: Measurement, Science, 246, 1587–1589.

Zwally, H. J., M. B. Giovinetto, J. Li, H. G. Cornejo, M. A. Beckley, A. C. Brenner, J. L. Saba, and D. Yi (2005), Mass changes of the Greenland and Antarctic ice sheets and shelves and contributions to sea-level rise: 1992–2002, Journal of Glaciology, 51, 509-527.

APPENDIX A

Auxiliary materials in Chapter 3

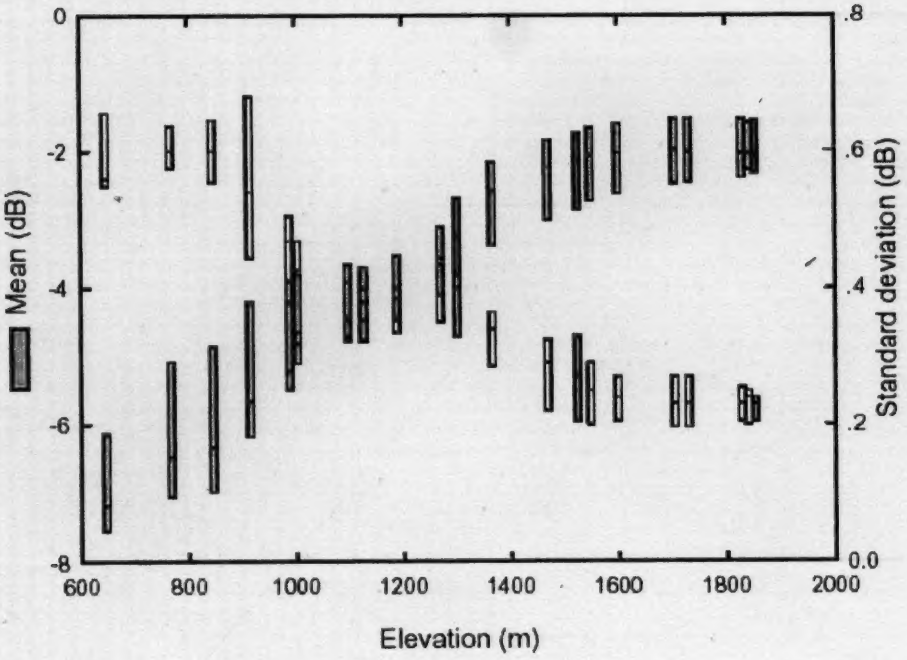

Figure 3.A.1. Mean and standard deviation of winter QSCAT σ^0 (1999-2003) along a transect over the Devon Ice Cap.

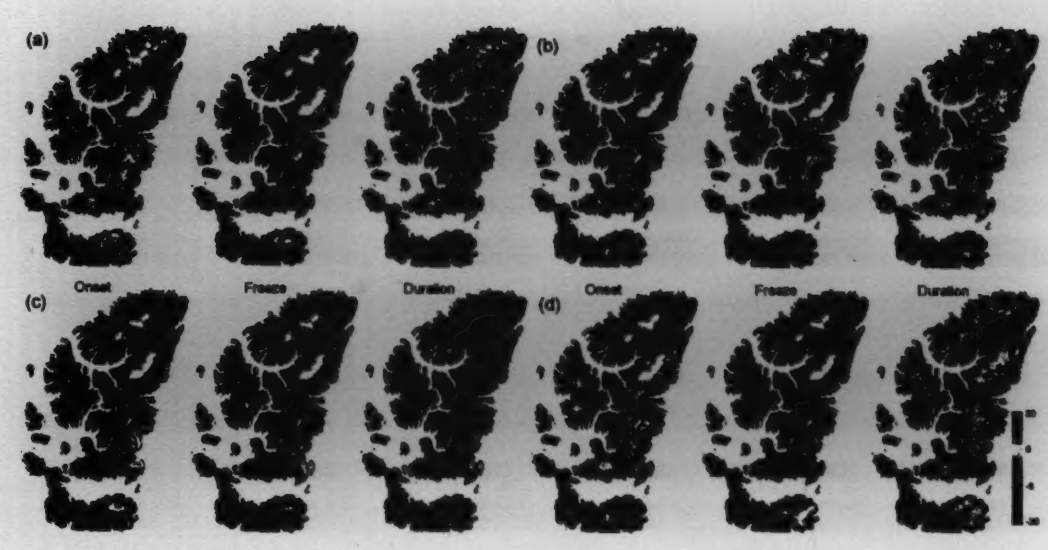

Figure 3.A.2. Melt anomalies (onset, freeze-up, and duration) relative to the climatology for 2000-2004 for the Queen Elizabeth Islands ice caps in the summers of 2000-2003: (a)2000; (b) 2001; (c) 2002; (d) 2003.